Physical-Layer Communications Using Direct Antenna Modulation

A THESIS SUBMITTED TO
THE DEPARTMENT OF ELECTRONIC AND ELECTRICAL ENGINEERING
THE UNIVERSITY OF SHEFFIELD
FOR THE DEGREE OF
DOCTOR OF PHILOSOPHY

By
HongZhe Shi
-2014-

ABSTRACT

Conventional wireless communications could be threatened by an eavesdropper with a sufficiently sensitive receiver and unlimited computational resources, or may reach the channel capacity in the near future. Recent research into a new digital modulation technique termed Direct Antenna Modulation (DAM) shows that DAM is a potential solution to the aforementioned problems. Direction-dependency, which describes the manner of signal transmission, is the most important attribute of a DAM system. Direction-dependent transmission can provide extra protection from a physical-layer source against security attack. Various transmission schemes are discussed in this work, and it is shown that accurate demodulation can be prevented from eavesdropping in the following two scenarios: first, when the angular separation between eavesdropper and intended recipient is very small; second, when one or two eavesdropping directions are pre-known. In addition, DAM system can be configured to have extra channel resources by introducing space as an additional domain for multiplexing. With the technique of space multiplexing, the transmitter can send independent data streams towards multiple receivers located at various transmission directions simultaneously. An algorithmic method is also presented to provide space multiplexing with a relatively low system cost.

ACKNOWLEDGEMENT

I would like to take this opportunity to express my sincere gratitude to my supervisor Dr Alan Tennant for his persistent support, encouragement and inspiration, during my long journey to be a self-confident Doctor of Philosophy.

I would also like to thank other academics and all my colleagues in Communications Group for the support throughout my doctorate study. Special thanks are given to Professor Richard Langley, Professor Tim O'Farrell, Dr Greg Cook and Dr Wei Liu for their guidance and valuable suggestions, and Dr Qiang Bai, Dr Shaozhen Zhu, Dr Qing Liu, Dr Bo Peng, Dr Jialai Weng and Dr Yizhen Tong for their help and inspiring discussions. Additionally I thank Professor Jennifer Bernhard and Dr Michael Daly from University of Illinois at Urbana-Champaign for their kindly responses towards a critical disputation in the field.

Finally, my deepest appreciation is given to my parents and parents-in-law for their unconditional support and sacrifices they have made in past years. In particular I thank my loving wife Yang Yu for her consistent encouragement and company at those tough days, which is beyond my words.

PUBLICATIONS

1. H. Shi and A. Tennant, "Simultaneous, Multichannel, Spatially Directive Data Transmission Using Direct Antenna Modulation," *IEEE Transactions on Antennas and Propagation,* vol. 62, no. 1, pp. 403-410, 2014.

2. H. Shi and A. Tennant, "Enhancing the security of communication via directly modulated antenna arrays," *IET Microwaves, Antennas & Propagation,* vol. 7, no. 8, pp. 606-611, 2013.

3. H. Shi and A. Tennant, "Covert Communication Using a Directly Modulated Array Transmitter," in *European Conference on Antennas and Propagation (EUCAP),* to appear.

4. H. Shi and A. Tennant, "Secure communications based on directly modulated antenna arrays combined with multi-path," in *Loughborough Antennas and Propagation Conference (LAPC)*, Loughborough, 2013

5. H. Shi and A. Tennant, "Secure physical-layer communication based on directly modulated antenna arrays," in *Loughborough Antennas and Propagation Conference (LAPC)*, Loughborough, 2012.

6. H. Shi and A. Tennant, "An experimental two element array configured for directional antenna modulation," in *European Conference on Antennas and Propagation (EUCAP)*, Prague, Czech, 2012.

7. H. Shi and A. Tennant, “Characteristics of a two element direction dependent antenna array,” in *Loughborough Antennas and Propagation Conference (LAPC)*, Loughborough, UK, 2011.

8. H. Shi and A. Tennant, “Direction dependent antenna modulation using a two element array,” in *European Conference on Antennas and Propagation (EUCAP)*, Rome, Italy, 2011.

Contents

List of Figures

List of Tables

Chapter 1

Introduction

1.1 Overview

Modern communications have developed rapidly over the past few decades. Besides the military and commercial applications, communication technology has now become an essential part of our daily lives. An interesting result was revealed by an investigation [1] on "the use and impact of modern media and technology in our lives" that: in the USA and China, more than half people now primarily prefer communicating using some sort of technology over communicating face-to-face. Due to the benefits from the good coverage of wireless (Wi-Fi/3G/GSM) networks, it is an inevitable trend that people begin to get used to communicating anywhere and at anytime via various techniques including (video) phone call, (instant) text message, e-mail and social networking sites etc. Another good supporting example is that Apple and Samsung have recently become two of the most successful technology companies because of their popular smart phones and tablets. However, underneath the prosperity, information security and limited channel capacity are also increasingly concerned. Information security (in wireless communication) is primarily threatened by the broadcast nature of conventional baseband modulation, i.e. the same baseband signals are sent to the whole space. To increase the security, candidate solutions include high-layer cryptography, phased arrays with sidelobe suppression and

artificial noise insertion. Channel capacity becomes limited because the number of users sharing the same information channel is increasing rapidly. In some scenarios, these users may be located at different transmission directions. However, due to the broadcast nature, these spatially separated users still have to multiplex the channel in the time domain or frequency domain. Therefore, one possible solution to improve the information security and channel capacity is modulating in a completely different way to have non-broadcast far-field signals. In this work, a new digital modulation technique termed by the author as Direct Antenna Modulation (DAM) is introduced and investigated. In DAM, far-field signals are direction dependent. Such a transmission system provides extra security in the physical-layer because the correct baseband signals are only sent to the desired recipient. Additionally, it can provide independent and simultaneous data transmission from transmitter to multiple receivers located at various directions.

1.2 Literature Review

In the 1950s, researchers began to consider the time domain as an additional variable to control antenna radiation characteristics[2]. Such an array system termed as, Time-Modulated (or time-switched) Arrays, can be accomplished by periodically switching on and off the array elements according to a predetermined time sequence. The time-modulation (TM) technique is usually employed to suppress the side-lobe levels of the antenna array [3-5] and to provide pattern synthesis [6-8]. This technique brings an insight that the array elements can be switched individually as a function of time to achieve a pattern design at system level. On the other hand, researchers are also interested in achieving signal modulation by directly changing antenna parameters. But the

implementation of direct signal modulation on a single antenna only provides a limited level of complexity of modulation, for example amplitude [9] and pulse modulation [10].

Intuitively, techniques move on to synthesize digital signals by directly switching parameters of array elements in a prescribed way, along with the radiation pattern. A very early study published in 1990 reported a communication scheme called "directional signal modulation" which can produce desired frequency shift keying (FSK) or phase shift keying (PSK) modulation by selecting the separation of discrete antennas in discrete time and/or space [11]. The essence of this approach is the control of overall amplitude and phase of the antenna array through independently switching the active/in-active states of array elements. Later, an array transmitter, reported in 2001, was designed to generate pulse-position modulation (PPM) to a broadside receiver by directly modulating the carrier wave with a two-state (0/π) phase shifter [12]. Although these two arrays are based on different configurations, both of them indicate a common transmission property that signals are dependent on the transmit angles.

In 2008, an amplitude- and phase-based modulation scheme termed by authors as Near Field Direct Antenna Modulation (NFDAM) was proposed by researchers from the California Institution of Technology (Caltech) [13] [14]. The transmitter is an array consisting of a single driven element operating at 60GHz and several, closely coupled, parasitic elements. By controlling the level of coupling between the driven and the parasitic elements, data modulation can be introduced at the element level in a process that the signal received at an intended direction is subject to the overall radiation pattern as a function of switching time. Signal patterns generated by this process are, therefore, dependent on transmission directions. A similar implementation of NFDAM operating at 2.45GHz has also been reported in [15]. Compared to previous work [11] [12], NFDAM

demonstrates the concept of direction-dependent transmission much more clearly by plotting complex signals received at different angles onto constellation diagrams. The use of parasitic elements provides sufficient choices of signal combinations at a relatively low system cost. On the other hand, it makes constellation diagram design very complicated. An optimization method called convex optimization is later suggested by researchers from Caltech to calculate the coverage area of the signal constellation diagram [16], and perform beamforming and sidelobe suppression[17].

A similar modulation concept was implemented on a different system configuration and termed Directional Modulation (DM) by researchers from University of Illinois at Urbana-Champaign in 2009 [18] [19]. The transmitter consists of a 4-element linear phased array, where digital phase shifters are employed to directly modulate baseband data. In this implementation the relative element phase is switched independently and actively to produce a far-field signal in a desired direction with a distinct modulation scheme. An important contribution this work [18] [19] is that the researchers set up a comparable traditional baseband array as a reference system so that the difference between DM and conventional baseband modulation can be analyzed and demonstrated from different aspects, including radiation patterns, constellation diagrams and bit error rate performance. Compared to the previously introduced NFDAM [14], the DM scheme reported in [18] [19] has an advantage that the relative element phase difference necessary to synthesize a digital symbol can be found via simple calculation. Therefore, it is more efficient to produce a desired constellation pattern for a desired receiver in DM. But the system cost is increased due to the use of expensive digital phase shifters. Other work on DM has reported the use of an array of reconfigurable, actively-fed elements to achieve beamsteering without using phase shifters [20]. Optimal signal pattern synthesis

is demonstrated by using a convex optimization method in [21] to achieve a better performance in providing a secure communication link.

Further works are reported by researchers from Nanjing University of Aeronautics and Astronautics (NUAA) and Queen's University Belfast (QUB) respectively [22-26]. Techniques reported by NUAA include utilising harmonic components via a time modulated linear array (TMLA) [22], adding artificial noisy beams via a monopulse cassegrain antenna [23] and individually controlling in-phase and quadrature baseband transmit beams [24]. The research group from QUB suggested two approaches: using phase conjugating lens (PCL) to provide additional phase shift [25], and using Fourier Rotman lens to synthesize radiation patterns with which the standard QPSK (Quadrature Phase Shift Keying) can only be received at selected communication direction [26].

1.3 Research Motivation

Existing techniques for implementing directly modulated antenna arrays developed recently are presented above. Although different system configurations are reported, but in principle, all these array systems are designed to operate the transmit array in a similar way: individually changing parameters of array element as a function of time. In this sense, regardless of techniques, the modulation *concept* is termed in this thesis as Direct Antenna Modulation (DAM). Initial investigation into DAM configured on a 2-element array system has been reported in [27] [28], and an experimental prototype DAM system using 4-bit phase shifters are presented in [29]. All the DAM schemes previously reported [11-29] have a common transmission property of *direction dependency*, regardless of what techniques or system configurations are used. With this property, directly modulated

array system shows its potential superior capability in providing physical-layer secure communications, and/or space multiplexing.

1.3.1 Physical-Layer Secure Communications

The security of wireless communications is challenged by the nature of conventional baseband modulation in that the antennas or antenna arrays broadcast the same information in every direction. A potential eavesdropper may be able to detect the same information as that received by the intended recipient at the desired direction.

Traditionally, high-layer cryptographic techniques are applied to provide security at the information level. The cryptographic methods can be divided into two categories: asymmetric and symmetric [30]. The encryption and decryption of information using symmetry cryptograph can be simple and efficient in the case that both the sender and receiver have pre-held identical keys. One famous symmetry cryptograph technique known as one-time pad was proved by Shannon in 1940s as theoretically impossible for an eavesdropper to decode the message without the key [31]. Therefore, it was termed as perfect secrecy. However, the practical use of this method is limited due to the difficulty of sharing the key between sender and receiver in a secure and secret way before the communication. To solve this problem, asymmetric cryptography, also known as the public-key method, was invented in 1976 [32] and demonstrated practically in 1978 [33]. With this method, the intended receiver generates a public key and private key following a certain mathematic algorithm, and broadcasts the public key only. The message encoded by sender with this public key can only be decoded by the private key which the receiver holds secretly. In communications today, asymmetric and symmetric methods are combined to provide both convenient key exchange and efficient encryption/decryption [30]. However, as the public key is mathematically related to the

private key, it is theoretically possible for an eavesdropper with enough computational resource to decode information, for example quantum computing.

The demand for high quality security in wireless communication drives the development of techniques providing keyless secure communications in the physical-layer. To evaluate the security degree, quantitative metrics were developed. For instance, “backscatter analysis” was used to quantify the prevalence of denial-of-service (DoS) activity on the internet [34], and “mean failure cost (MFC)” was proposed as a quantitative metric of cyber security [35]. However, the most suitable quantitative measurement for physical-layer cryptosystem is “secrecy capacity”, which is related to a strict notation of security termed “information theoretic security”. The initial work to discuss "information theoretic security" in the physical layer was reported by Wyner in 1975 [36]. In Wyner's wire-tap model, there is one transmitter (Alice), one legitimate receiver (Bob), and one wire-tapper (Eve). Eve's eavesdropping channel output is a degraded version of that from Alice to Bob. The secrecy of the transmission is measured by a quantity called "equivocation", which refers to the degree of uncertainty for the transmitted message. Wyner showed that when the main channel (between Alice and Bob) is probabilistically better than the wire-tap channel (between Alice and Eve), information can be securely transmitted at a positive rate, whose upper bound is termed the secrecy capacity. In the work reported in [37], Eve's channel is no longer a degraded version. Instead, they are connected to a single-input two-output broadcast channel. A non-zero secrecy capacity can be achieved if the main channel has better capacity or is less noisy than the eavesdropping channel. Further studies investigated the communication security on fading channels instead of additive white Gaussian noise (AWGN) channels. The secrecy capacity has been obtained in the presence of the quasi-static [38] and the ergodic [39] fading channels respectively. These work demonstrated that secure communication is achievable even when Eve has a

better signal-to-noise ratio (SNR) than Bob's on average. More recent techniques have looked at distorting eavesdropping channels by artificially inserting noise, while maintaining an AWGN main channel towards the desired receiver [40-42]. Artificial noise injection is also combined with MIMO/MISO (Multiple-input and multiple/single output) antennas to tackle the situation of multiple collaborating eavesdropping channels [43] [44].

Some other researchers worked on another important branch of low-level encryption schemes which can provide communication reliability and security simultaneously. The initial work of secure channel coding schemes dates back to a cryptosystem reported in 1978 [45], in which a public-key cryptosystem based on algebraic coding theory was proposed. Further studies were reported to improve the code rate [46] and shorten the key size [47] of this technique to make it practical. Recent works moved forward to capacity approaching codes including Turbo codes [48] [49] and Low Density Parity Check (LDPC) codes [50] [51], and low complexity linear block codes like Polar codes [52]. Pseudo-random [48] or AES [53] (Advanced Encryption Standard) based puncturing techniques have been proposed as the methods to insert the key to the codeword. By using secure channel coding schemes, the data can be transmitted efficiently, reliably and securely.

Recently, DAM schemes have been proposed by researchers as a potential method in providing a physical-layer secure communication link [12-29]. Unlike high-layer cryptography or artificial noise injection, in DAM schemes the antenna arrays or equivalent hardware platforms (like Fourier Rotman Lens, etc) are configured to generate signal patterns that are dependent on transmit angles. The direction dependent feature is a natural advantage for secure communication, in which case only the intended recipient

located at the desired direction can receive the correct constellation, while the signal patterns detected by eavesdroppers at unwanted directions have been scrambled. This property is demonstrated by on/off-beam PPM signals in [12], angular-dependent constellations in [13-15] [18-20] [23] [24] [27-29], and synthesized power & phase patterns in [26]. Therefore, the specific security threat that DAM potentially addresses is the eavesdropping from a non-legitimate receiver at non-desired transmit angles. For AWGN LoS channels having uniform SNRs, the information uncertainty of the eavesdropper channel is bigger than the main channel, because the "baseband" signal constellation detected by the eavesdropper is a scrambled version of the one received by the intended recipient. The eavesdropper is supposed to have more errors at demodulation than the legitimate receiver. Therefore, the communication security directly affected by using of DAM technique is usually statistically evaluated by its error rate performance [13] [14] [18-26].

Conventional DAM provides a general protection against eavesdropping from non-intended direction, but the protection is limited in the following scenarios: 1. the angular separation between eavesdropper and intended recipient is very small; 2. eavesdropper located at an angle receiving signals at a high power level. The author of the thesis reported three different methods to improve the performance of DAM technique under the above two scenarios respectively. The first method configured the DAM transmitter based on an array having larger element spacing and directive elements [54] [55], which is presented in section 4.4. The angular range of successful demodulation is reduced, so that special protection is given against the security threat in aforementioned scenario 1. The second method utilised the multi-level of the constellations existing in the DAM system [56], which is discussed in section 6.1. The mapping relationship is completely damaged by sending a low-level constellation containing less than half of the

distinguishable data points to the eavesdropper. This method can be very useful when the locations of potential eavesdroppers are pre-detected in the aforementioned scenario 2. The third method jointly considered the multipath channel and space multiplexing [57], which is demonstrated in section 6.2. The constellation received at the intended direction by using this method can be manipulated to be very different from those received at nearby angles. It can be used to tackle the security threat in the aforementioned scenario 1 too.

1.3.2 Space Multiplexing

To meet the increasing demand of high-speed wireless data transmission, traditionally multiple access methods, and techniques developed based on them are proposed as a solution [58]. Frequency Division Multiple Access (FDMA) and Time Division Multiple Access (TDMA) split bandwidth or time interval into non-overlapping components to provide an independent and permanent sub-channel for each user for entire period of communication. Code Division Multiple Access (CDMA) does not partition bandwidth or time interval but allocates a unique code signature for each user. Thus all the users share the same channel but information can be separated at the receiver by the assigned code. Nevertheless, these communication protocols mentioned above have to multiplex the existing channel in the frequency and time domain to improve the channel capacity.

A different line of thought aims to increase the transmission capacity by using MIMO techniques. The use of a MIMO communication system for capacity enhancement is achieved by sending data streams simultaneously through several independent transmission channels [59]. The capacity gain in respect of multiple antenna systems was also discussed earlier in [60]. With the rapid development of MIMO, such transmission algorithms, as those summarised in [61], was termed as spatial multiplexing. However as

pointed out in [61] [62], the differences of propagation conditions between the various transmit-receiver antenna pairs are very important for spatial multiplexing, so that a rich multipath environment is necessary and has to be dominant propagation mode. In addition, DSP (digital signal processing) modules are required at both transmit and receive sides to deal with the matrix formed by multiple propagating channels, so the computation complexity is also increased.

Space multiplexing is a concept termed by the author to describe a novel transmission scheme provided by the proposed DAM system. In this transmission scheme, data can be transmitted through multiple independent, LOS channels to recipients located in various directions. The idea of space multiplexing using DAM was first mentioned in [15], but the first practical implementation was demonstrated in [18]. The scheme reported in [18] illustrated the simultaneous transmission of two independent QPSK signals to receivers located at angles of ±30°, and a Genetic Algorithm (GA) is used to optimise the element phase combinations. However, to meet the system phase requirements, the phase shifters used in [18] were assumed to be lossless and continuous, resulting in an increased system cost.

Alternatively, the author of this thesis proposed an algorithmic method for space multiplexing, which is especially suitable for a DAM system configured using low-bit phase shifters [63]. Compared to the previous work, the biggest difference of this method is that it provides solutions to the required element phase combination based on system parameters of a given DAM array. The phase searching process is, therefore, simpler and exhaustive. The system designer can have a clear view of the system capability in space multiplexing, but as a tradeoff, the number of recipients who are able to receive independent data information is limited. Therefore, this method is more suitable to use in

scenarios that the number and locations of desired receivers are pre-known by the transmitter and do not change in real time.

1.4 Original Contributions

The following is a list of the original contributions of the thesis. The original contribution presented here is summarised based on the referred journals and conference papers listed on pages iii to iv of the thesis.

1. The characteristics of DAM system were explored on a simple 2-element linear phased array with 2-bit phase control. The most significant finding is a system property termed "signal convergence", which has not been reported before. Two very important applications were later developed based on this system property. Due to the benefit of using low-bit phase shifters, the transmission angles, where far-field signals will converge, can be predicted via simple mathematical relationship.

- **Direction dependent antenna modulation using a two element array [27].**

  In this work, we introduced a basic model of conventional DAM transmitter based on 2-element liner phased array. When compared to other techniques (NFDAM and DM), the use of 2-bit phase shifters provides a relatively low-cost but also reliable hardware platform. Besides the basic system property of direction dependence, an interesting phenomenon was illustrated in this paper that the far-field signal constellation regularly converges from a high order to lower order at specific angles.

- **An experimental two element array configured for directional antenna modulation [29].**

  In this work, we configured the prototype experimental system to examine the system properties discussed in an earlier paper [27]. Both "direction dependency" and "signal convergence" were validated.

2. The performance of DAM system was analysed under two specific security threats: 1) A potential eavesdropper receives signals from an angle which is very close to the desired transmission direction; 2) A potential eavesdropper receives signals at a position which is much closer to transmitter than desired recipient. These two scenarios have not been investigated before. System symbol error rates (SER) were calculated as a function of transmitting angles. An interesting finding is that, besides the power attenuations, DAM system provides extra safety in physical layer due to the baseband pattern distortion at non-intended directions.

- **Enhancing the security of communication via directly modulated antenna arrays [55].**

  In this work, one DAM transmitter and one traditional baseband modulation transmitter were modelled. To make them comparable, both transmitters were configured to send the same 8-PSK constellation as their baseband signal pattern to the intended recipient at broadside. With the increase of element spacing, or symbol to noise ratio (E_s/N_0), DAM system shows superiority against aforementioned threats.

3. We examined the potential of using a DAM system to send independent baseband symbols to multiple receivers located at different transmission angles simultaneously. Such a process has been termed as space multiplexing in this thesis. The main

contribution is that we took the advantages from "signal convergence" and found a completely new way to achieve space multiplexing. An algorithmic method was developed, which is different from the matrix-inverse method reported by others. The algorithmic method can provide exhaustive solutions based on the parameters of the existing phased array.

- **Simultaneous, Multichannel, Spatially Directive Data Transmission Using Direct Antenna Modulation [63].**

  In this work, DAM with the feature of signal convergence was demonstrated as an alternative solution to achieve space multiplexing. This paper presented the fundamentals of the technique, and provided an algorithmic method for phase searching. Several examples were given for illustration, including a scenario that a transmitter can send independent symbols through QPSK pattern towards three desired recipients located at 0° and ±30° respectively.

4. "Multi-level constellations" is an interesting attribute of DAM system, which has not been reported before. This attribute is based on the property of signal convergence. A low-level constellation has a reduced number of distinguishable symbol points, compared to the high-level one. By considering both distance and offset phase between array elements as changeable parameters, low-level constellation can be purposely oriented to two independent transmission angles.

- **Covert communication using a directly modulated array transmitter [56].**

  In this work, multi-level constellations were proposed to provide additional degree of security for wireless communication in physical layer. The constellation received by potential eavesdropper contains only half the number of

distinguishable symbols of the desired baseband pattern received by intended recipient.

1.5 Thesis Outline

The outline of this thesis is as follows:

Chapter 2 introduces the necessary background information needed by the reader before they move forward to subsequent chapters. The first part of this chapter introduces some fundamental antenna parameters, and the basic concept of a conventional linear phased array. Some examples of grating lobes are provided as the use of array with wider element spacing will be discussed in chapter 4. In addition, the concept of constellation diagram is introduced because it is an important tool to visualise the complex signals. The second part gives the reader a detailed theoretical background of the DAM technique through comparing it to the conventional baseband modulation. The mechanism of direction dependent transmission property is explained.

Chapter 3 demonstrates basic transmission properties of the DAM schemes on a 2-element array. A theoretical model of the DAM transmitter configured on an array with 2-bit phase control is discussed first. Then the transmission properties are reviewed as well. A special phenomenon termed “signal convergence” is observed and investigated on this DAM system. Finally, both “direction dependent” and “signal convergence” are validated by an experimental DAM transmitter.

Chapter 4 gives a general explanation of applying DAM in the area of secure communication. Firstly, symbol error rate is calculated statistically as a function of

transmission angles as a measurement of security level provided by a DAM transmitter. Then a concept called “error rate beamwidth” is introduced to describe the angular range within which signals can be demodulated at a given error rate. However, the DAM system may have the security threat when potential eavesdropper is monitoring from an angle which is very close to the intended transmit angle. In this chapter, an intuitive approach is suggested to narrow the error rate beamwidth at the intended direction. System error rate performance is also compared and analysed between the DAM system and an equivalent baseband modulated system.

Chapter 5 discusses another promising application area of DAM schemes in providing space multiplexing. With this technique, independent data streams can be simultaneously transmitted towards multiple spatial separated users. An algorithmic method is proposed in this chapter, which is developed based on the “signal convergence” property. The mathematical theory of the method is explained first, followed by simulation examples for various transmission scenarios. Finally, both advantages and limitations of the method are analysed.

Chapter 6 presents two optimised DAM schemes which can provide enhanced protection over the transmission link in some scenarios. The first scheme purposely sends two different levels of constellation to the intended recipient and potential eavesdropper respectively. The second scheme combines space multiplexing and a multipath channel to generate a well designed constellation at the intended direction, but at the same time, the constellation received at nearby angles is very different.

In chapter 7, the project is summarised and future work is discussed.

Chapter 2

Fundamental Background

This chapter introduces the necessary background information needed for a reader before they move forward to subsequent chapters. First of all, some very basic, but important, antenna parameters are introduced. Secondly, the concept of a conventional phased array is presented, followed by an analysis of grating lobes. Next, the concept of a constellation diagram is introduced because it is used as the main research method to visualise the complex signals. The last part of this chapter gives the reader a detailed theoretical background of a DAM scheme by comparing it with conventional baseband modulation. The mechanism of direction dependent transmission is also explained.

2.1 Antenna Parameters

2.1.1 Antenna Directivity, Efficiency and Gain

Directivity of an antenna is defined as "the ratio of the radiation intensity in a given direction from the antenna to the radiation intensity averaged over all directions."[64] Thus it is a parameter to describe how well the antennas focus the radiation in a given direction. A special case is if the antenna radiates equally in all directions, then its directivity is 1 in liner or 0 dB in dBs scale according to the definition. Normally, the

direction of directivity is referring to the direction of maximum radiation if not specified [64].

The total **efficiency** of antenna e_0 includes reflection efficiency e_r, conduction efficiency e_c and dielectric efficiency e_d, and it can be expressed as [64]:

$$e_0 = e_r e_c e_d \tag{2.1}$$

e_0 is caused by impedance mismatch between the transmission line and antenna. e_c and e_d are usually measured together as radiation efficiency e_{cd}, which is used to describe the loss caused by radiation of antenna [64]. To sum up, the efficiency of antenna is a parameter to describe the ratio of power finally radiated by the antenna over the power fed to the antenna.

Gain is one of the most commonly used parameter of antennas which is defined as "the ratio of the intensity, in a given direction, to the radiation intensity that would be obtained if the power accepted by the antenna were radiated isotropically."[64] The definition of gain is very close to directivity but it takes account the radiation efficiency. However, there is another gain termed as absolute gain which takes account the total radiation efficiency [64]. In practice, gain is measured by comparing the power level of target antenna to a reference antenna.

2.1.2 Radiation Pattern

Radiation Pattern is also called Antenna Pattern, which is defined as "a mathematical function or a graphical representation of the radiation properties of the antenna as a function of space coordinates."[64] Basically the antenna pattern is 3-dimensional. But 2-D plot is usually used in research for convenience. A well-known pair of 2-D plane for a

linearly polarised antenna is called **E-plane and H-plane**. The former one contains the electric field vector and the direction of maximum radiation, and the latter one contains the magnetic field vector and the direction of maximum radiation. In addition, radiation pattern can be specified to field pattern if it describes magnitude of electric (magnetic) field or power pattern if it shows power density [64]. A specific example of power pattern is illustrated in Fig. 2.1. The example antenna is an aperture antenna, whose length (orthogonal to E-plane) is 3λ, and width (parallel to E-plane) is 2λ. Fig. 2.1(a) and (b) are both calculated in decibels (dB) scale but plotted on Polar and Cartesian coordinates respectively, while (c) and (d) are in linear scale. They are the radiation patterns of the same 4-element linear array, but described in different ways. Polar coordinate shows the overall shape of pattern, while Cartesian coordinate is convenient when details (magnitude & transmitting angle) are concerned. The decibels scale is a logarithmic unit employed when it is necessary to accentuate the detail of those very small values in linear scale. The relationship between two scales is shown below:

$$\text{Gain}\ (\text{dBW/m}^2) = 10\log_{10}\text{Gain}\ (\text{W/m}^2) \tag{2.2}$$

$$\text{Gain}\ (\text{dBV/m or dBA/m}) = 20\log_{10}\text{Gain}\ (\text{V/m or A/m}) \tag{2.3}$$

Radiation lobes are defined as "a portion of the radiation pattern bounded by regions of relatively weak radiation intensity."[64] The pattern shown in Fig. 2.1 has different types of lobes. The major lobe, which is also called main beam, usually has the maximum power among all the lobes. The main beam of the antenna pattern in Fig. 2.1 is pointing at the broadside direction. Except the major lobe, all other lobes can be seen as minor lobes [64]. Two side lobes can be found for the E-plane pattern in Fig. 2.1 and four can be found for H-plane. If not stated specifically, the direction pointed by the main beam is the direction of the radiation. Finally, the lobe has approximately 180° offset with respect to

main beam direction is termed back lobe [64]. There is no back lobe in Fig. 2.1 because the pattern is ideal.

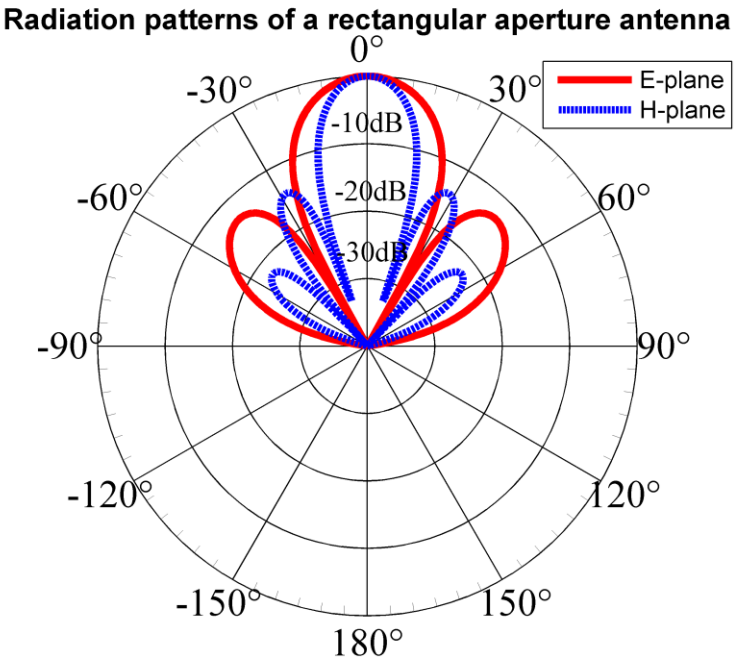

Fig. 2.1(a)

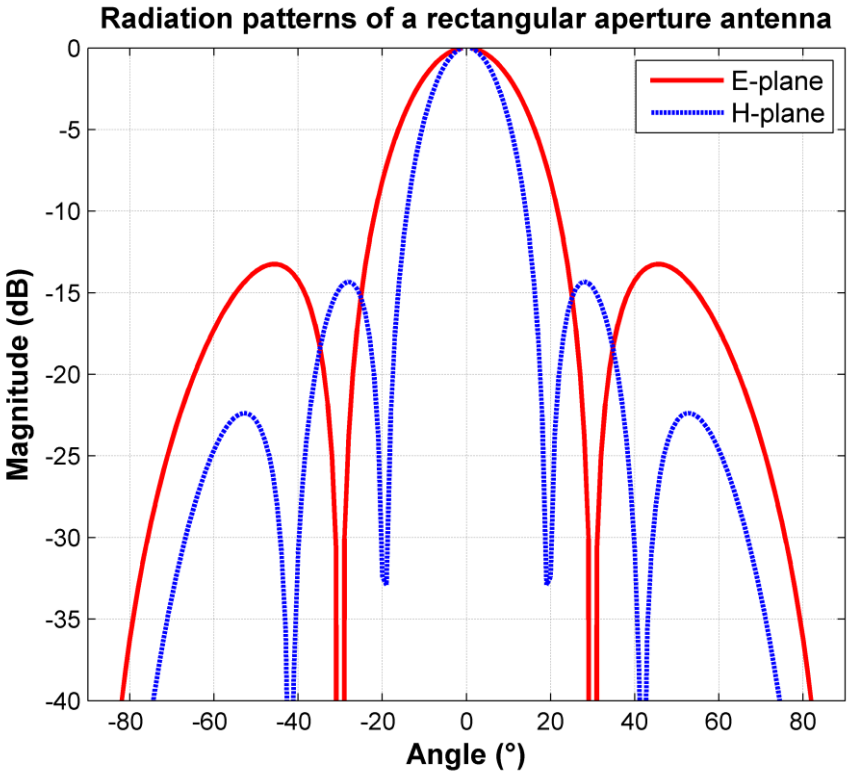

Fig. 2.1 (b)

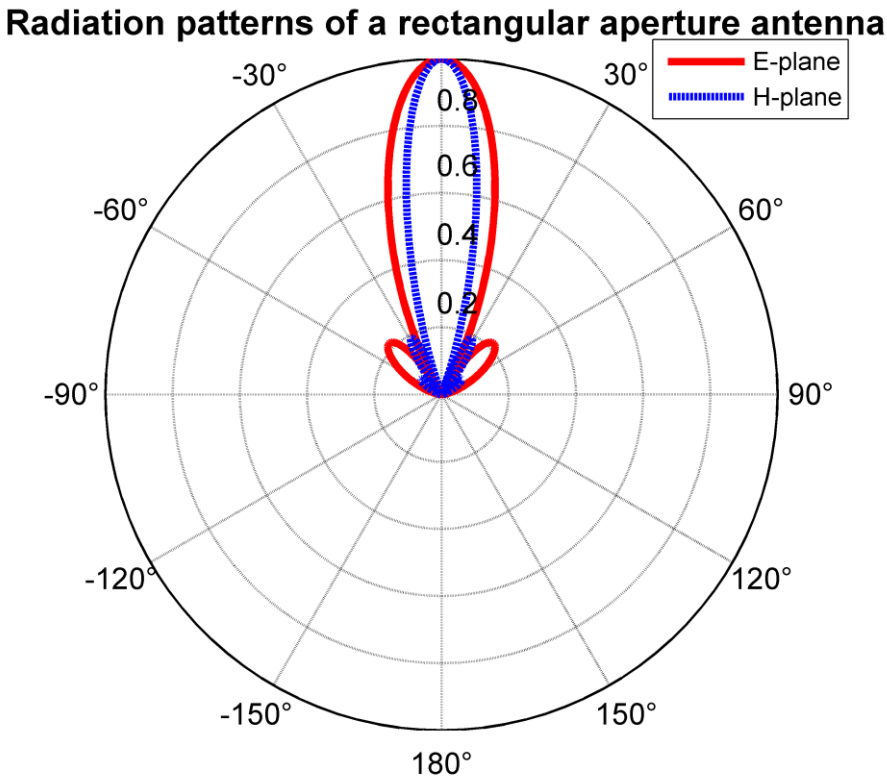

Fig. 2.1 (c)

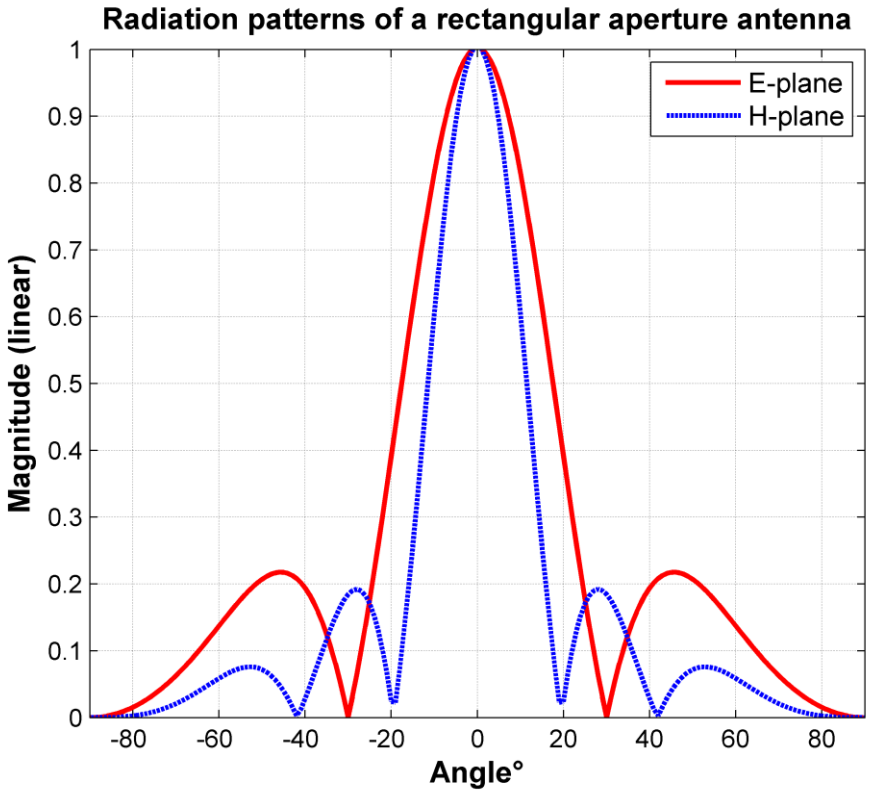

Fig. 2.1 (d)

Fig. 2.1 Radiation pattern of an aperture antenna with a dimension of 3λ x 2λ, plotted in dB scale on (a) Polar and (b) Cartesian coordinates and in linear scale on (c) Polar and (d) Cartesian coordinates.

2.1.3 Field Regions

Field regions refer to three regions of space surrounding an antenna. A typical classification of field regions is listed below:

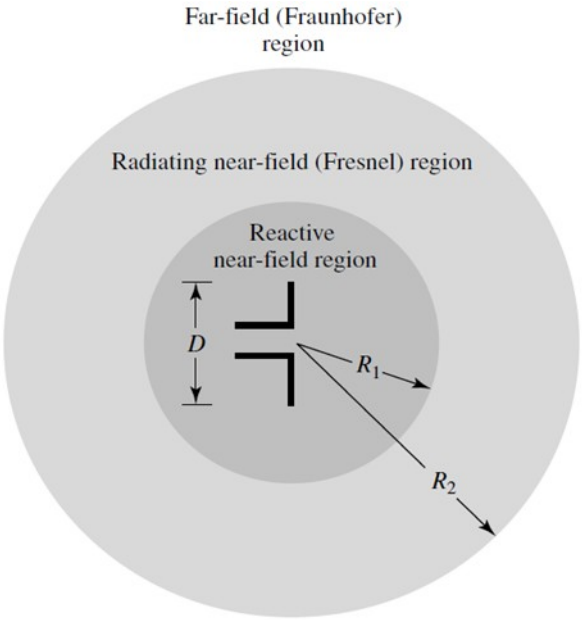

Fig. 2.2 Field regions of an antenna [64].

Reactive near-field region: $R_1 < 0.62\sqrt{D^3/\lambda}$

Radiating near-field region: $0.62\sqrt{D^3/\lambda} \leq R_2 < 2D^2/\lambda$

Far-field region: $R_3 \geq 2D^2/\lambda$

where D is the maximum dimension of antenna, and λ is the wavelength [64]. Normally, far-field region is the most interested. Fig. 2.3 shows a rough field calculation model of three antennas linearly positioned to illustrate the difference of far-field region and near-field regions. When observing in near-field region, three array elements have individual offset angles between the transmitting directions and the axis they are positioned. But in far-field region, these antennas are considered as radiating parallel to a given direction.

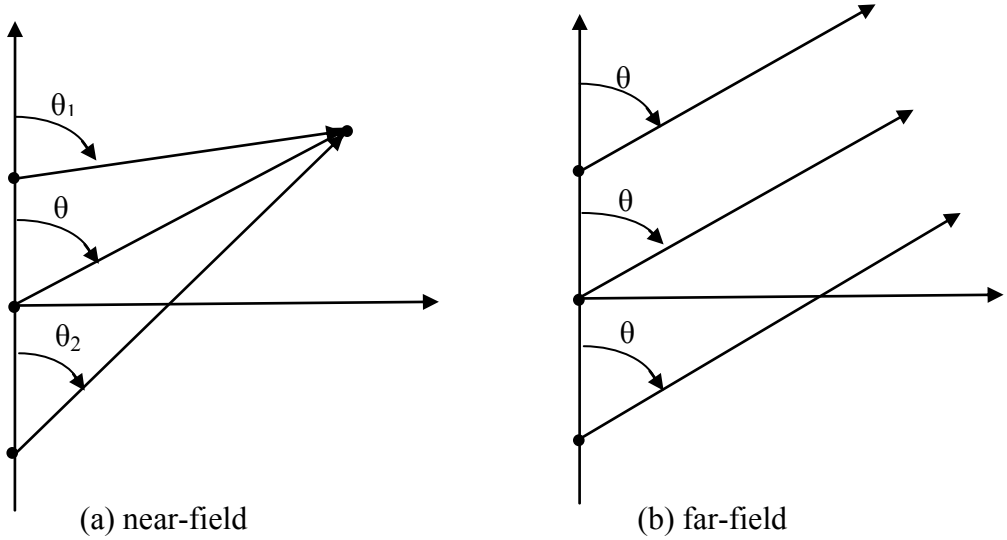

Fig. 2.3 Field illustration for an array in (a) near-field and (b) far-field [64].

2.2 Antenna Arrays

An antenna array is a concept that refers to multiple antennas in a desired electronic and geometrical configuration [64]. The overall field of array is the complex vector addition of all the element fields. The initial purpose of array design is to reinforce the radiation power in the useful direction through properly setting each element phase. In this section, the concepts of array factor, conventional phased array and grating lobe are explained respectively.

2.2.1 Array Factor

Array factor is defined as "… a function of the number of elements, their geometrical arrangement, their relative magnitudes, their relative phases, and their spacings" [64]. It is the most basic and important concept related to an antenna array. If the elements of the array are assumed to be identical and isotropic, the E-field can be described by a universal field vector $E_{element}$. According to the rule of "pattern multiplication" for arrays of identical element, the overall antenna pattern $E_{overall}$ can be described by:

$$E_{overall} = E_{element} \times AF \tag{2.4}$$

where AF is denoted as the array factor. The identical element fields $E_{element}$ can be further normalised to 1. In this sense, the overall field of antenna array, to a certain extent, can be simply represented by its array factor.

Recalling the definition of array factor mentioned at the beginning of last paragraph, there are five factors affecting the array factor: (1) number of elements; (2) geometrical arrangement; (3) relative magnitudes; (4) relative phases; (5) spacings. The geometrical arrangement of array can be linear, planner and circular etc. But this research only

investigates the linear array. Based on this condition, the geometry configuration of a linear array is illustrated by Fig. 2.4 (a). N infinitesimal antennas are linearly positioned along z-axis. Those element antennas are assumed to have uniform amplitude 1 and are equally separated by distance d. The last factor to define is the relative phases between elements. As shown in Fig. 2.4(a), assume the radiating direction has an offset angle θ with respect to z-axis. Then the radiation of n^{th} element is always arriving in advance of the $n\text{-}1^{th}$ ($1 \leq n \leq N$) element at far-field. Therefore, the relative phase difference caused by different propagation path length can be described as:

$$2\pi * \frac{d \sin \theta}{\lambda} = k * d \sin \theta \tag{2.5}$$

where $k = 2\pi/\lambda$. The relative phases can also be affected by introducing an initial phase at the feeding point of each array element to form a phased array (discussed in next section). Such an initial phase is usually identical for each array element, and is therefore termed as progressive phase β [64]. Finally, the array factor of a conventional N-element linear array with uniform amplitude and spacing can be expressed in [64]:

$$\begin{aligned} &“AF = 1 + e^{j*(k*d*sin\,\theta+\beta)} + e^{j*2*(k*d*sin\,\theta+\beta)} + \cdots + e^{j*(N-1)*(k*d*sin\,\theta+\beta)} \\ &= \sum_{n=1}^{N} e^{j*(n-1)*(k*d*sin\,\theta+\beta)} \\ &= \sum_{n=1}^{N} e^{j*(n-1)*\psi} \qquad \psi = k*d*sin\,\theta+\beta\,” \end{aligned} \tag{2.6}$$

The overall array factor defined by (2.6) can also be graphically illustrated by Fig. 2.4(b).

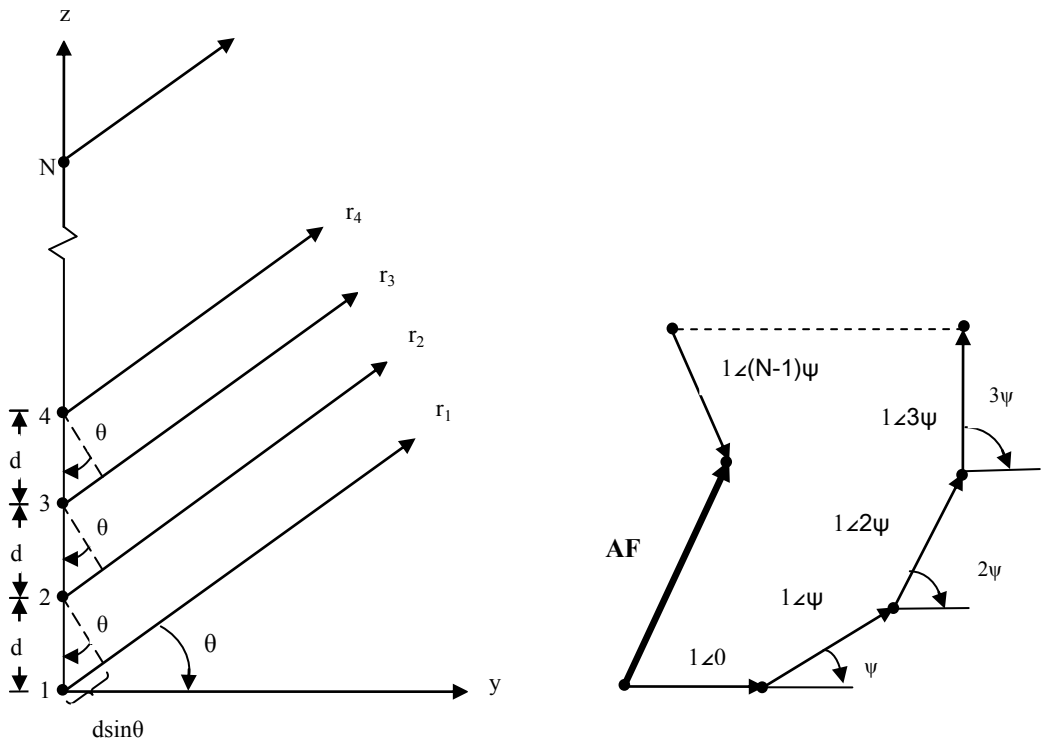

(a) Geometry (b) Phasor diagram

Fig. 2.4 The far-field geometry and phasor diagram of N-element array of isotropic sources positioned along the z-axis [64].

2.2.2 Conventional Phased Array

A conventional phased array is usually designed for reinforcing radiation at an intended direction [64] [65]. Before analysing the mechanism of phased array, three terms need to be explained first. "Broadside direction" usually refers to the special direction which is normal to the linear array, while "Endfire" refers to the direction along the array axis. "Intended direction/observation angle" is used in this thesis to describe the direction the desired receiver locates or the incident/scattering angle concerned.

In basic terms, phased array uses the progressive phase β to compensate the relative phase difference caused by different propagating paths. Fig. 2.5 illustrates the use of progressive phase based on a simple 2-element array with element spacing of $\lambda/2$. If the

array is radiating to a receiver positioned in broadside direction as shown in Fig. 2.5(a), then the radiating waves of both array elements will arrive together. In this case there is no propagation phase difference. Next as shown in Fig. 2.5(b), signal waves arrived at far-field receiver located at 30° will have a phase difference of π/2 according to equation (2.5). In this case, the signal waves are not completely in-phase so that the radiation received by recipient at 30° is not the maximum. Finally as shown by Fig. 2.5(c), by adding a progressive phase –π/2 at the feeding of element 2, the phase offset caused by the path difference is compensated.

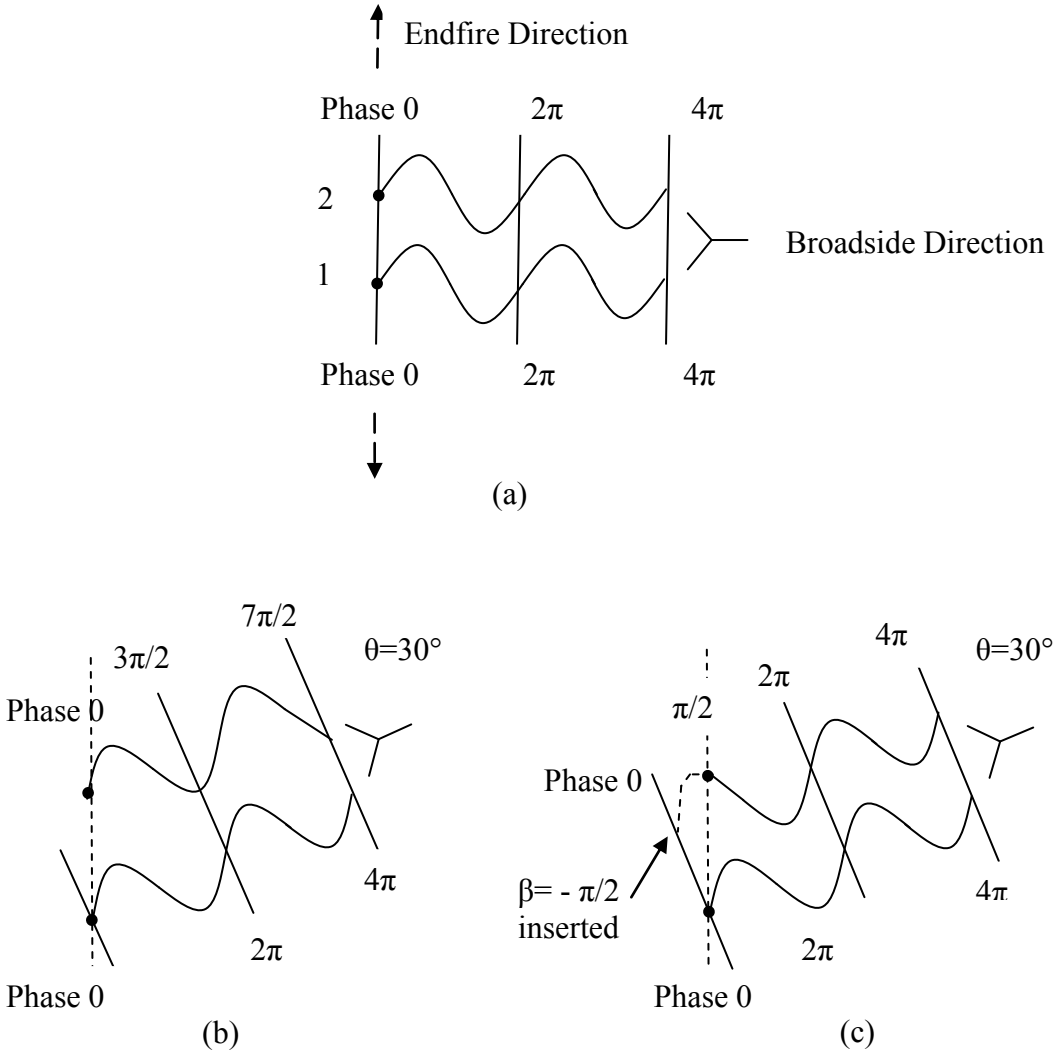

Fig. 2.5: Graphic illustration for the use of progressive phase β when the 2-element array is: (a) transmitting to broadside; (b) transmitting to 30° without β; (c) transmitting to 30° with β.

A mathematical demonstration is given in the following. For the case illustrated by Fig. 2.5(a), N = 2, θ = 0°, d= λ/2, k = 2π/λ and β=0, according to equation (2.6):

$$AF_{(a)} = 1 + 1 = 2 \tag{2.7}$$

Next, for the case illustrated by Fig. 2.5(b), N = 2, θ = 30°, d= λ/2, k = 2π/λ and β=0, according to equation (2.6):

$$AF_{(b)} = 1 + e^{j\frac{\pi}{2}} = 1 + j \tag{2.8}$$

Finally, for the case illustrated by Fig. 2.5(c), N = 2, θ = 30°, d= λ/2, k = 2π/λ and β = -π/2, According to equation (2.6):

$$AF_{(c)} = 1 + 1 = 2 \tag{2.9}$$

For a 2-element array with uniform amplitude 1, the maximum array factor is 2. By setting $\beta = -k * d * sin\,\theta_0$, theoretically the maximum radiating power can be achieved at any intended direction ($\theta = \theta_0$) whatever θ_0 is.

Finally, array factor of 10-element array with uniform amplitude and element spacing is calculated as a function of observation angle for illustrative purpose. As shown in Fig. 2.6, the x-axis is the observation angles from -90° to 90°, and the y-axis is the normalised magnitude of array factor in decibel scale. The main beam is steering to -30°, 0°(broadside) and 45° by adding progressive phase $\beta_1 = -kdsin60$, $\beta_2 = -kdsin90$ and $\beta_3 = -kdsin135$ respectively. Therefore, by controlling the progressive phase of the array, the radiation power can be optimised to the intended direction.

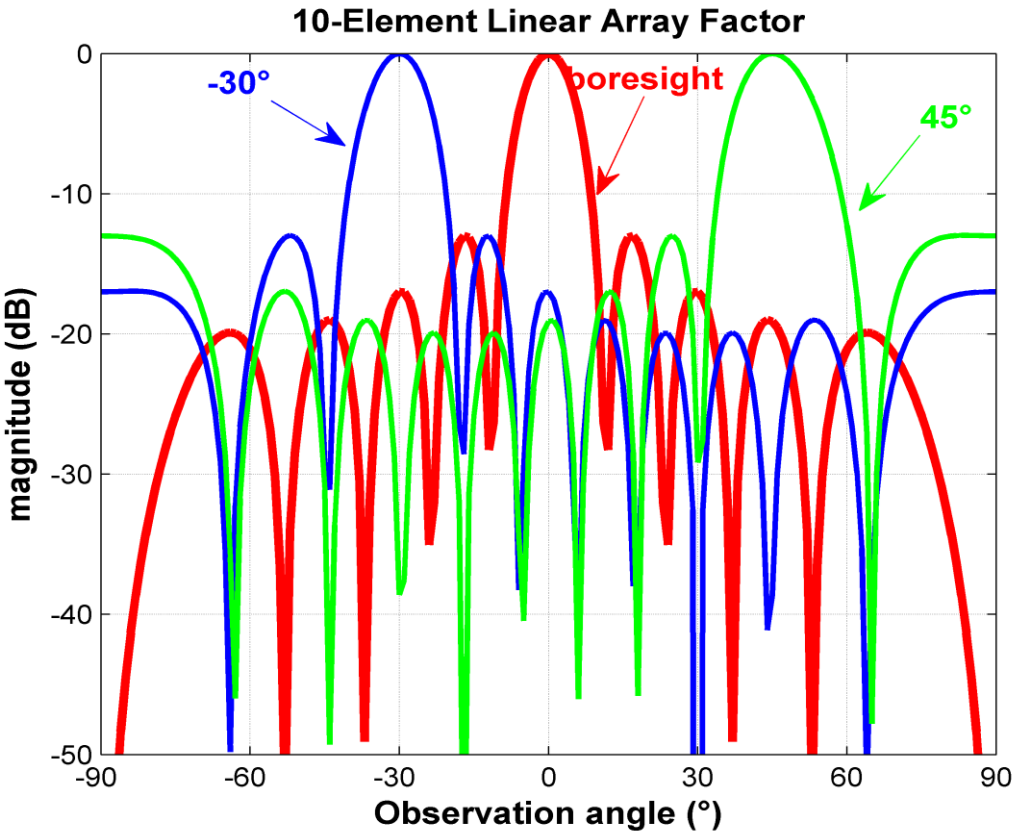

Fig. 2.6 Simulation result of array factor with the change of intended radiating angle.

2.2.3 Grating Lobes

A grating lobe is defined as "a lobe, other than the main lobe, produced by an array antenna when the inter element spacing is sufficiently large to permit the in-phase addition of radiated fields in more than one direction" [64]. A simple example is shown in Fig. 2.7. The spacing between these two elements is set to one wavelength. Therefore, when the field radiated by one element arrives at the other, there is no relative phase difference, which is also called in-phase addition. There are two grating lobes existing at angle -90° and 90° according to Fig. 2.7.

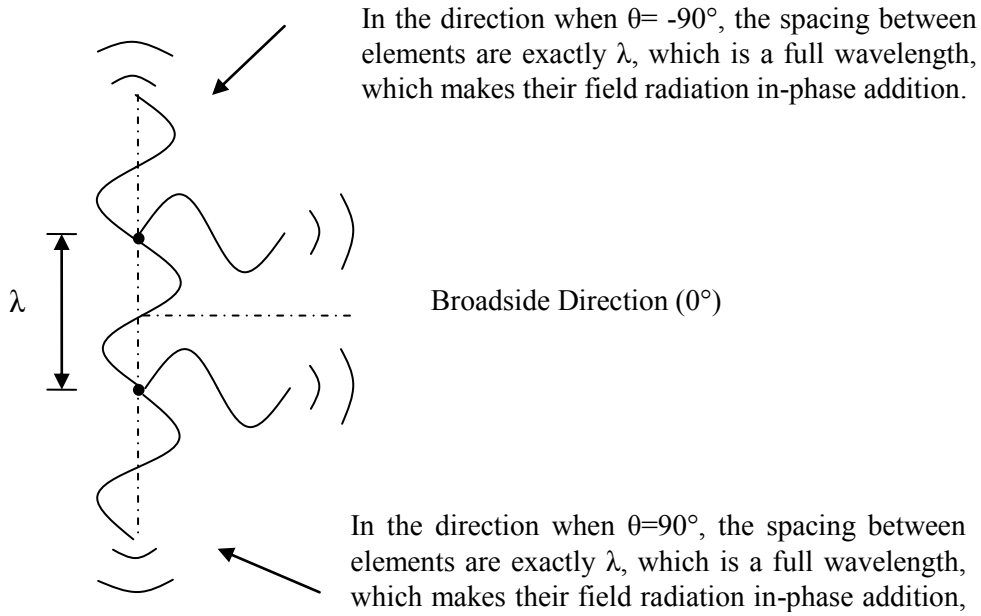

Fig. 2.7 Graphical illustrations to the generation of grating lobes.

In the far-field, the grating lobes can be seen as a replica of mainlobe. When the radiating element is omi-directional, the grating lobes have the same power as mainlobe. A few more examples are shown by Fig. 2.8 and Fig. 2.9. Fig. 2.8(a) shows the simulated array factor on Cartesian coordinate of example illustrated by Fig. 2.7. Fig. 2.9 shows a group of simulated results about grating lobes in polar diagram. Diagrams from (a) to (d) demonstrate the generating of grating lobes with the increase of spacing d. Diagrams (e) and (f) show the results of changing progressive phase β. Combining d and β, number and directions of the grating lobes are flexible.

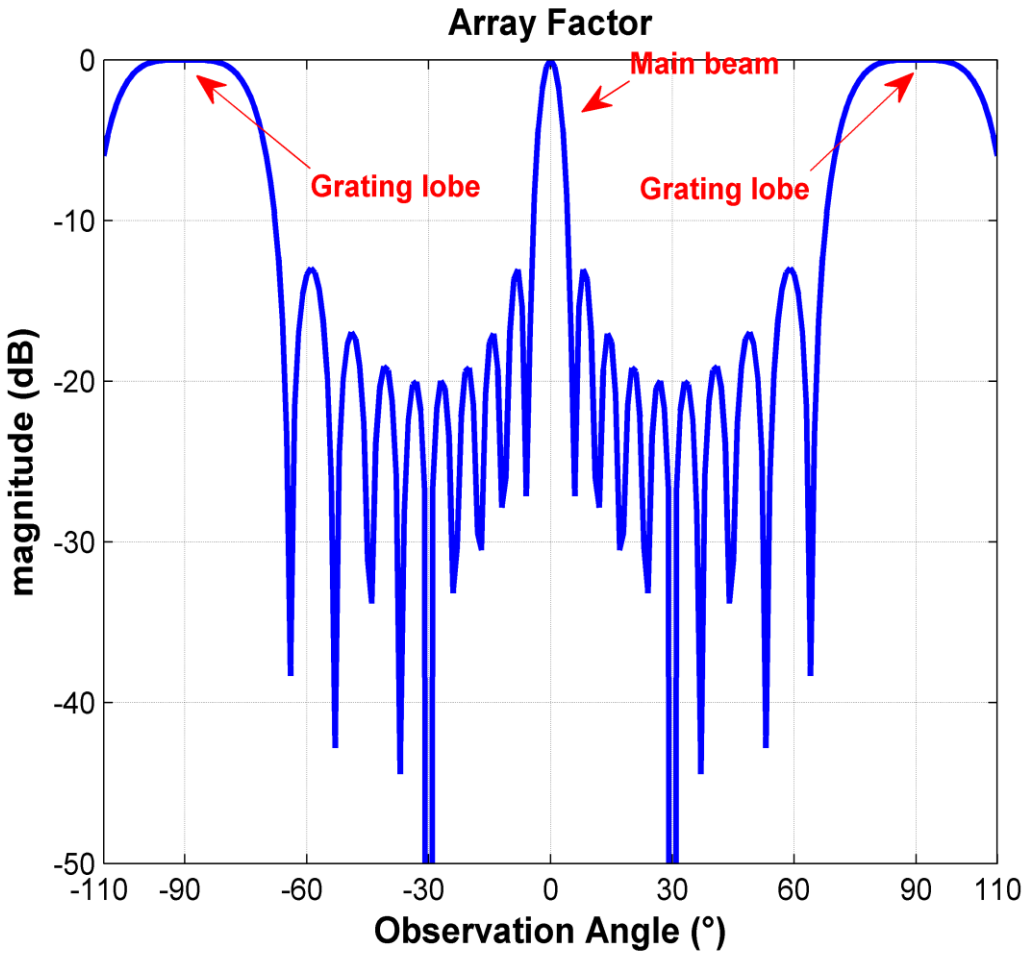

Fig. 2.8 Illustration of grating lobes on Cartesian coordinates.

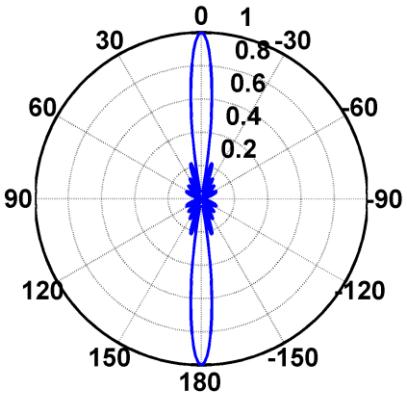

(a) d= λ/2, radiating to 0°

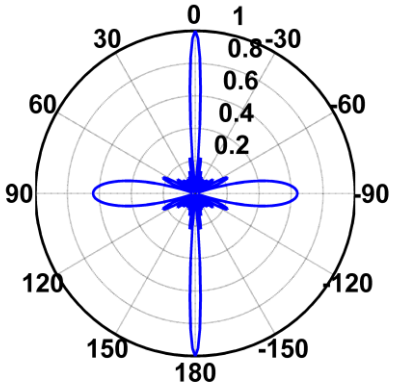

(b) d= 0.95λ, radiating to 0°

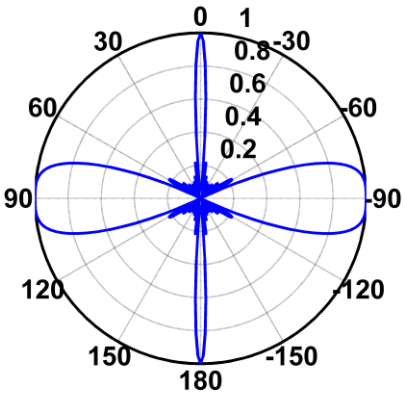

(c) d= λ, radiating to 0°

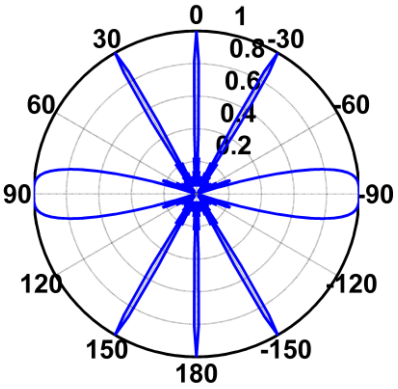

(d) d= 2λ, radiating to 0°

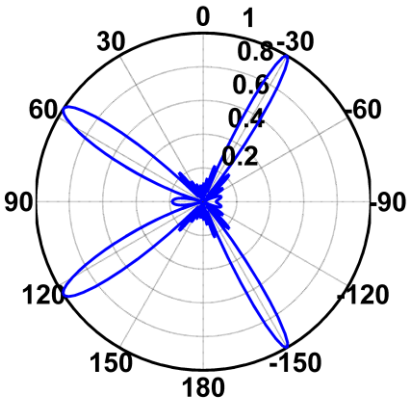

(e) d=0.75λ, radiating to -30°

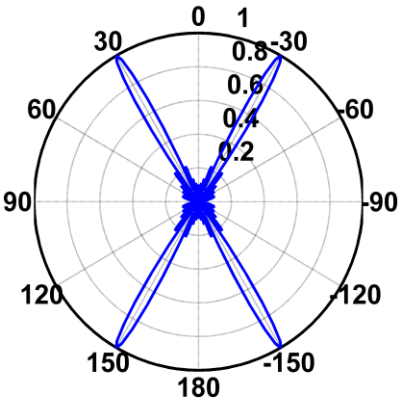

(f) d=λ, radiating to -30°

Fig. 2.9 Illustration of grating lobes in Polar coordinates.

2.3 Constellation Diagram

A constellation diagram is also called I/Q diagram or real-imaginary diagram. The signals radiated by antennas or arrays are complex, which contains real and imaginary parts. For a complex signal, real part is referred to as the in-phase (I) component, while the imaginary part is the quadurature (Q) component. During one transmission period, complex signals are sent by the transmitter one by one. At the receiver, these received signals can be resolved as signal points on the diagram to form a certain constellation pattern. As reported in [66-68], receiver is able to automatically recognise the entire constellation pattern. Therefore, the constellation diagram is employed as the main investigation tool to visualise the complex signals by the author in his research. With the constellation diagram, the researchers can have a clear view of relative relationship of the signals from two aspects: magnitude and phase. For illustrative purpose, assume a transmitter sends 4 signals to far-field receiver. The real-imaginary expressions of these signals are 1+j, -1+j, -1-j and 1-j. By converting them into exponential form, they have the same magnitude of $\sqrt{2}$, and equally separated phases of 45°, 135°, 225° and 315°. With the aid of constellation diagram shown by Fig. 2.10, the above math relationship is clearly visualised.

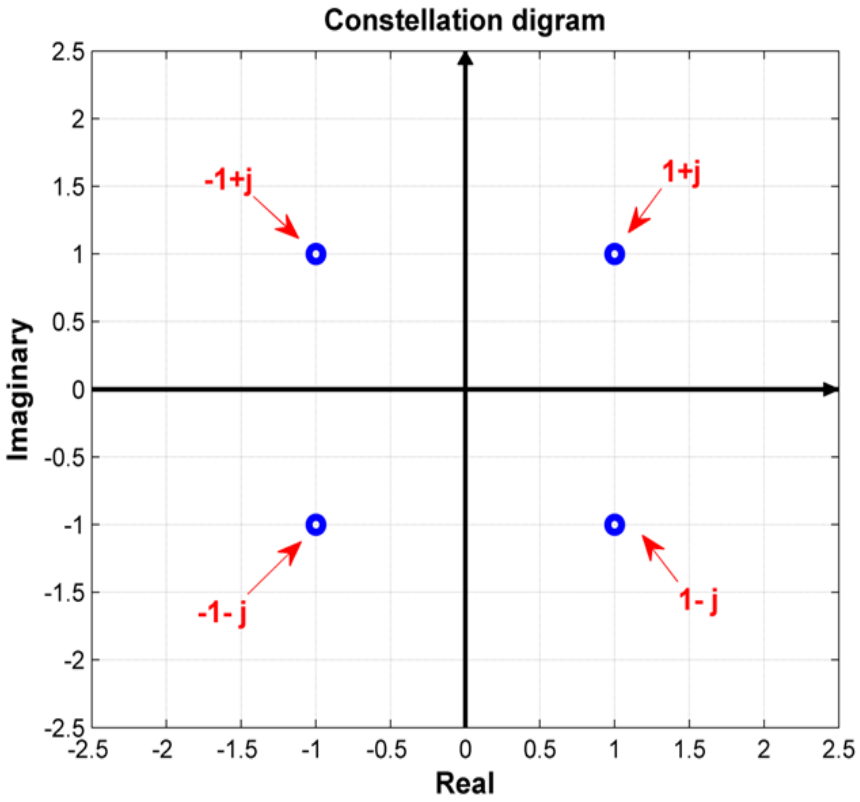

Fig. 2.10 Illustration of a QPSK constellation.

2.4 Background Theory of DAM

In section 1.2, literature about direct antenna modulation (DAM) was summarised and analysed. The most important property of DAM is the direction dependency of far-field signals. To demonstrate this property, a comparison between DAM and conventional baseband modulation is given in the following sections.

2.4.1 Baseband Modulation

In conventional radio transmission, signal patterns that carrying information are modulated at the baseband and then up-converted to radio frequency (RF), and finally amplified and transmitted by antenna or array [18] [69]. A schematic diagram of conventional baseband modulation is illustrated by Fig. 2.11. In such a transmission system, baseband information pre-modulated at the transmitter is broadcasted to every direction in the space. For a line-of-sight transmission system, the received signals only vary at the scale of magnitude and phase difference due to different propagation path lengths. In this case, an eavesdropper with sufficient sensitive receiver located at undesired direction can obtain the same baseband signals as the desired receiver.

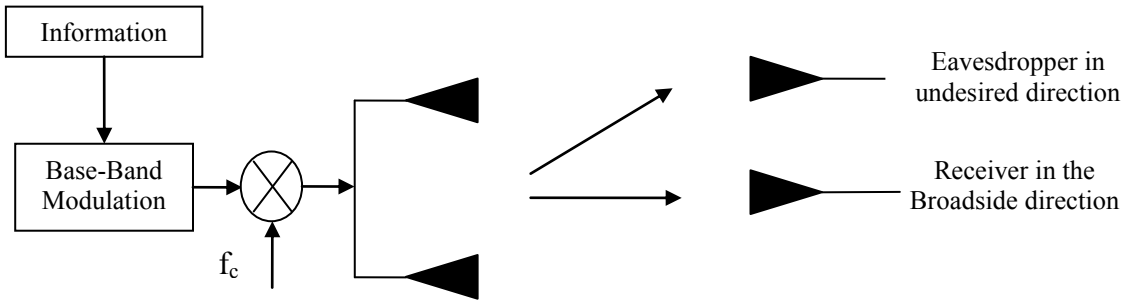

Fig. 2.11 Illustration of traditional baseband modulation system [18].

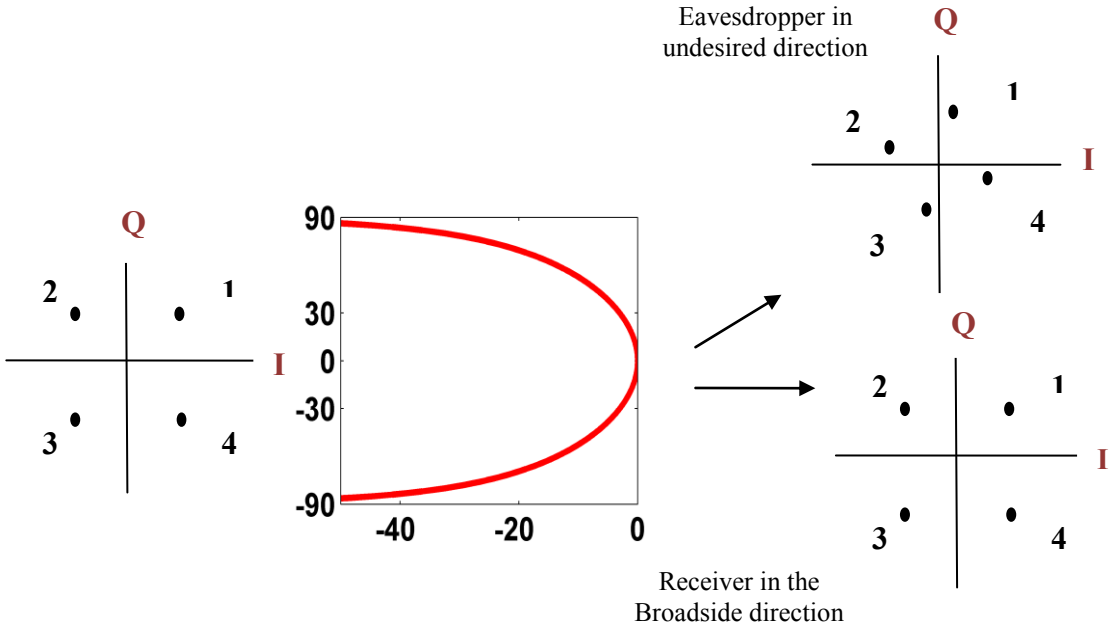

Fig. 2.12 A possible transmission scheme in conventional baseband modulation.

For illustrative purpose, a mathematical description of a possible transmission scheme in conventional baseband modulation is given below. Assume the baseband signals form a standard QPSK constellation pattern as shown by Fig. 2.12. These four signal points can be represented by complex numbers: 1+j, -1+j, -1-j and 1-j. Also, they can be expressed in the form of $Ae^{j\alpha}$, where $A = \sqrt{2}$, and the data set of α includes 45°, 135°, 225°, 315°. Then the signal is up-covert to RF ω that:

$$S(t) = Ae^{j\alpha} * \cos(\omega t) \tag{2.10}$$

After transmission, the received signals vary with directions due to path difference:

Broadside Receiver: $$S_1(t) = A_1 e^{j(\alpha+\beta_1)} * \cos(\omega t + \varphi_1) \tag{2.11}$$

Eavesdropper: $$S_2(t) = A_2 e^{j(\alpha+\beta_2)} * \cos(\omega t + \varphi_2) \tag{2.12}$$

At Demodulator:

$$S_1'(t) * \cos(\omega t) = A_1' e^{j(\alpha+\beta_1)} * \cos(\omega t + \varphi_1) * \cos(\omega t)$$

$$= A_1' e^{j(\alpha+\beta_1)} * \frac{1}{2}[\cos(2\omega t + \varphi_1) * \cos(\varphi_1)] \quad (2.13)$$

$$S_2'(t) * \cos(\omega t) = A_2' e^{j(\alpha+\beta_2)} * \cos(\omega t + \varphi_2) * \cos(\omega t)$$

$$= A_2' e^{j(\alpha+\beta_2)} * \frac{1}{2}[\cos(2\omega t + \varphi_2) * \cos(\varphi_2)] \quad (2.14)$$

After low-pass-filter:

$$S_1''(t) = \frac{A_1' \cos(\varphi_1)}{2} e^{j(\alpha+\beta_1)} \quad (2.15)$$

$$S_2''(t) = \frac{A_2' \cos(\varphi_2)}{2} e^{j(\alpha+\beta_2)} \quad (2.16)$$

Signals shown by equations (2.15) and (2.16) only differ from scale of magnitude and phase caused by propagation delay. As displayed in Fig. 2.12, the constellation pattern received at undesired angle has a power attenuation and overall rotation, compared to the one received at broadside. However, the pattern can be still recognised as a standard QPSK. This example demonstrated a fact that baseband data pattern is broadcasted in a conventional transmission system.

2.4.2 Direct Antenna Modulation

There were several different approaches to achieve DAM as introduced in "literature review" in chapter I. For convenience, the example system illustrated below only individually controls the element phase of the array. Such a system configured on a 2-

element array is shown by Fig. 2.13. In Fig. 2.13, there is no baseband modulation unit. Instead, each arm of the array is connected to a phase shifter. In DAM, the mechanism of signal generations is different from conventional baseband modulation. Signals are modulated directly through changing the relative phase (and amplitude) at element level, so that the radiation pattern of the array is changing at the symbol rate. The changing radiation patterns result in the direction-dependent signals. By properly configuring the element phases, a desired constellation pattern can be generated for the recipient at an intended direction. At the same time, constellation patterns generated for other directions are corrupted.

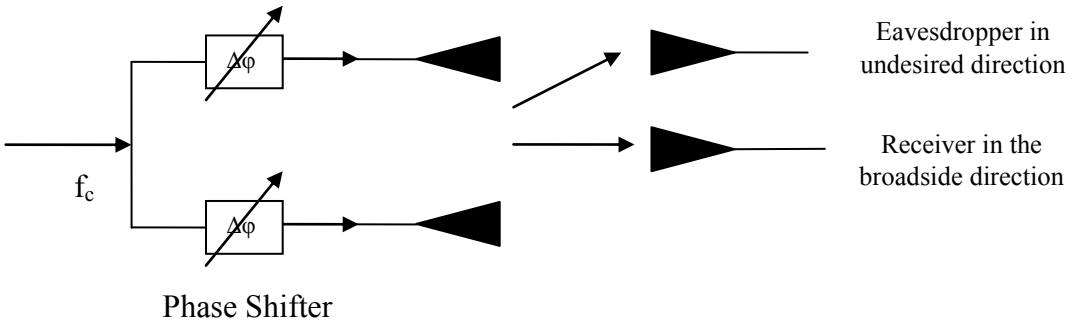

Fig. 2.13 Illustration of DAM array system based on a 2-element phased array [18].

To demonstrate the process described above, a mathematical illustration of a possible transmission scheme is given below. In Fig. 2.14, the "baseband signal" is still the standard QPSK used in section 2.4.1. They can still be expressed by 1+j, -1+j, -1-j and 1-j, but this time they are modulated individually by controlling the element phase pairs as shown in Fig. 2.14. Assume that the element spacing is half a wavelength and the progressive phase β is zero, then according to equation (2.6) the array factor is:

$$AF = 1 + e^{j(\pi \sin\theta)} \tag{2.17}$$

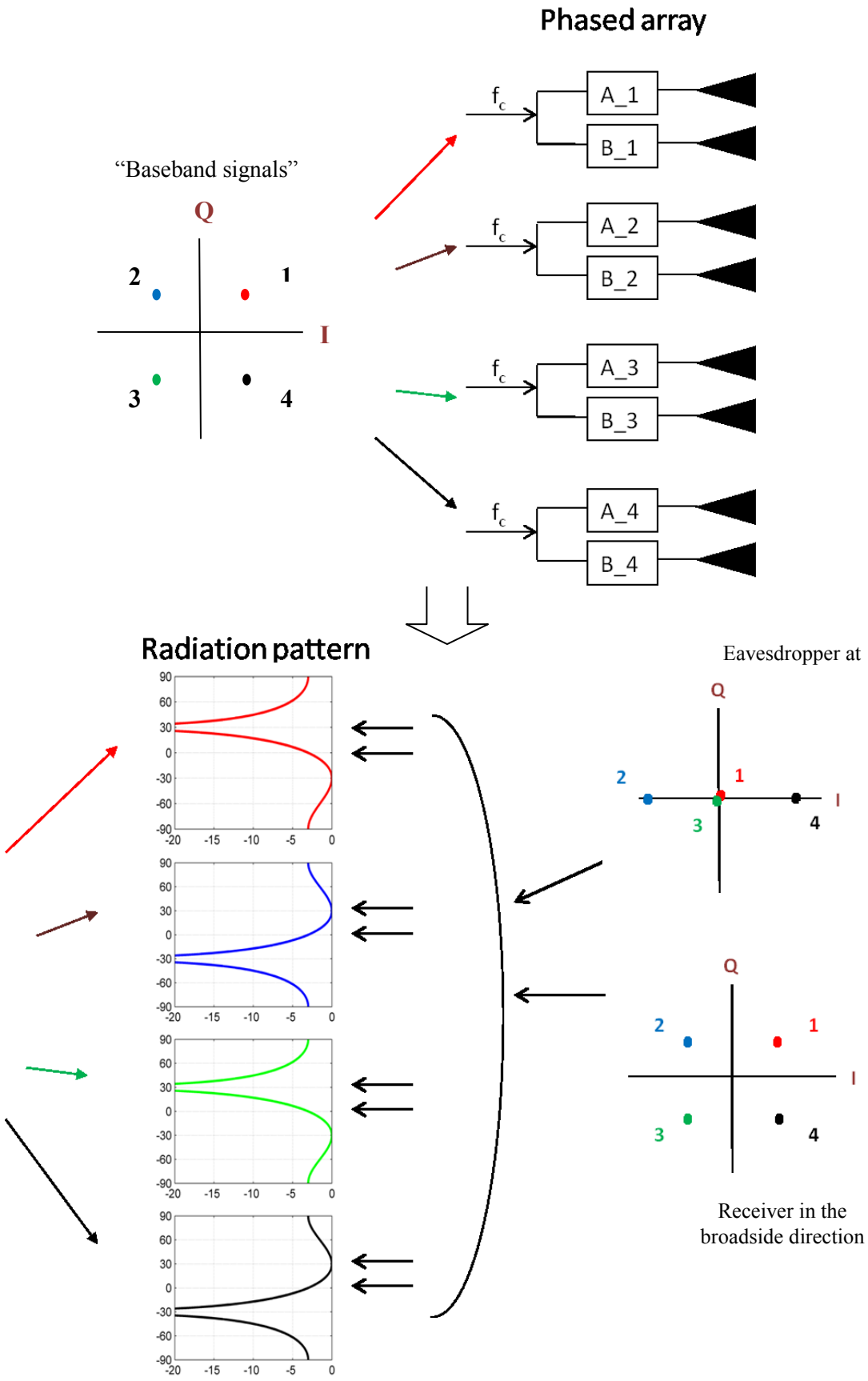

Fig. 2.14 A possible transmission scheme in directly modulated transmitter system.

In Fig. 2.13, two phase shifters are added to the array. Assuming the additional phase shifts provided by them are e^{jA} and e^{jB} respectively, then the array factor in this configuration is:

$$AF' = e^{jA} + e^{j(\pi\sin\theta+B)} \tag{2.18}$$

By substituting [A_1, B_1] = [0^o , 90^o], [A_2, B_2] = [180^o , 90^o], [A_3, B_3] = [180^o , -90^o] and [A_4, B_4] = [0^o , -90^o] into (2.18), the transmitter system has four different array factors (if the array element is identical, the radiation patterns can also be represented by these array factors):

$$AF'_1 = e^{j0} + e^{j(\pi\sin\theta+90)} = 1 + j * e^{j(\pi\sin\theta)}$$

$$AF'_2 = e^{j180} + e^{j(\pi\sin\theta+90)} = -1 + j * e^{j(\pi\sin\theta)}$$

$$AF'_3 = e^{j180} + e^{j(\pi\sin\theta-90)} = -1 - j * e^{j(\pi\sin\theta)}$$

$$AF'_4 = e^{j0} + e^{j(\pi\sin\theta-90)} = 1 - j * e^{j(\pi\sin\theta)}$$

First, we calculate 4 signals received at the broadside direction (θ=0°):

Point1: $AF'_1 = 1 + j * e^{j(\pi\sin0)} = 1 + j$

Point2: $AF'_2 = -1 + j * e^{j(\pi\sin0)} = -1 + j$

Point3: $AF'_3 = -1 - j * e^{j(\pi\sin0)} = -1 - j$

Point4: $AF'_4 = 1 - j * e^{j(\pi\sin0)} = 1 - j$

As illustrated in Fig. 2.14, the intended recipient at broadside can receive the desired QPSK constellation pattern. This QPSK pattern can be considered as “baseband signals” in the DAM system. Then, we calculate 4 signals received at 30°:

Point1 sent to 30°: $AF''_1 = e^{j0} + e^{j(\pi \sin 30 + 90)} = 1 - 1 = 0$

Point2 sent to 30°: $AF''_2 = e^{j180} + e^{j(\pi \sin 30 + 90)} = -1 - 1 = -2$

Point3 sent to 30°: $AF''_3 = e^{j180} + e^{j(\pi \sin 30 - 90)} = -1 + 1 = 0$

Point4 sent to 30°: $AF''_4 = e^{j0} + e^{j(\pi \sin 30 - 90)} = 1 + 1 = 2$

As shown in Fig. 2.14, when the observation angle moves from 0° to 30°, signal points 1 and 3 go to the origin, while signal point 2 and 4 keep 180° phase difference. In this case, the overall signal pattern becomes a BPSK (Binary Phase Shift Keying). The migration of the constellation points on the constellation diagram is also illustrated by Fig. 2.15. The results show that "baseband signals" sent to 30° are completely different from those sent to 0°.

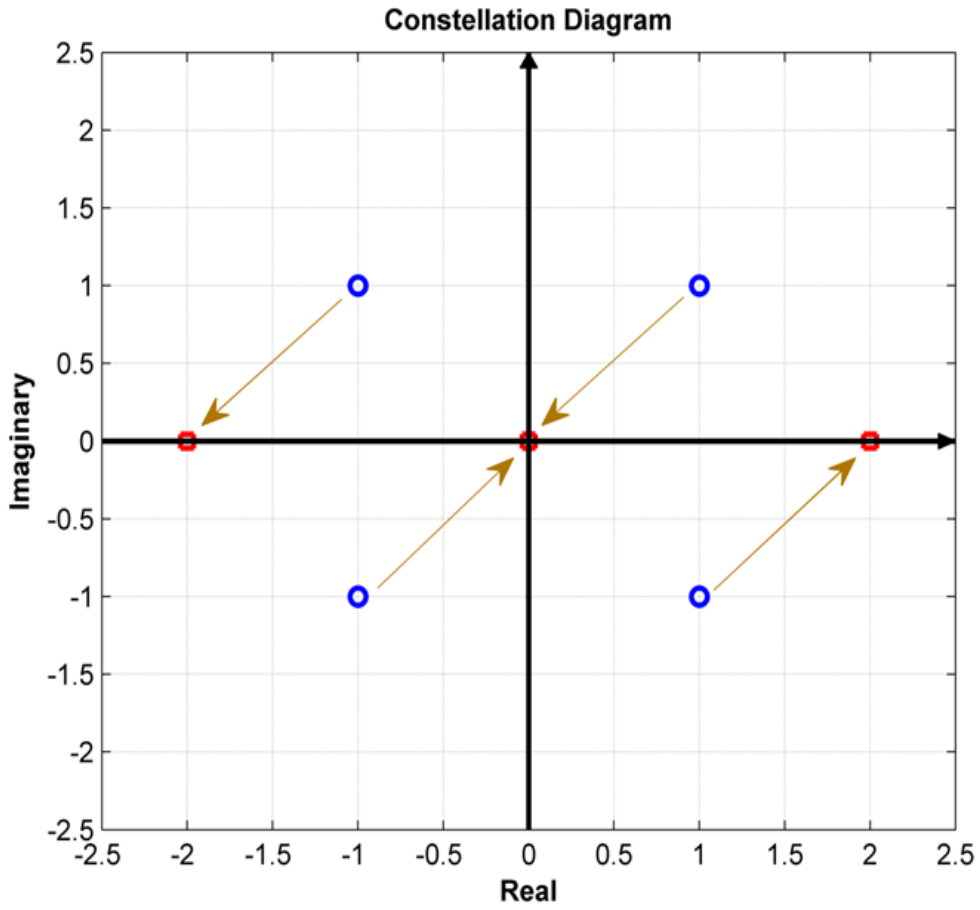

Fig. 2.15 The distribution of points 1-4 on constellation diagram when observation angle moves from 90° (circles) to 60° (squares).

2.4.3 Potential Benefits of DAM

The first advantage brought by DAM is its potential application in secure communication. The changing constellations ensure there is only one direction at which the desired "baseband" signal pattern can be recognised. At all other directions, the eavesdroppers need to pay extra effort for accurate demodulation from a corrupted constellation pattern. Additionally, the technique can be optimised to purposely prevent successful decoding from a few pre-know eavesdropping angles.

The second interesting application of DAM is introducing space as an extra domain for channel multiplexing. With proper configuration, in DAM, the signal constellation sent to one direction can be completely independent from that sent to another direction. Therefore, the transmitter can simultaneously send independent data streams towards recipients located at various directions.

2.5 Summary

In this chapter, the basic theory of antenna and phased arrays was introduced. Then the constellation diagram was introduced as it is the important research tool used to visualise complex signals. Finally a detailed comparison between conventional baseband modulation and direct antenna modulation is given, including the existing application potentials of DAM.

Chapter 3

Characteristics of Direct Antenna Modulation

Among the different, existing, approaches to configure DAM (as summarised in the literature review), the technique demonstrated by the researchers from the University of Illinois at Urbana-Champaign is relatively efficient and flexible compared to other methods. Nevertheless, the system cost is also significantly increased due to the required continues phase shifters. In this chapter, a DAM model configured on an array with 2-bit phase control is investigated. The direction dependent property is validated by both simulation and experiment. The primary reason of using low bit phase control is to reduce the system cost. It also results in a loss of system flexibility. However, the fixed bit phase control brings an interesting feature termed by author as “signal convergence”. It is demonstrated by simulation, and validated in an experiment. Moreover, the applications based on this feature will be further discussed in Chapter 5 & 6.

3.1 Theoretical Model of a DAM Transmitter

One possible schematic structure of a DAM transmitter is shown by Fig. 3.1. The transmitter system consists of an N-element linear array with independent 2-bit phase control. The array is fed directly without a baseband modulation unit, and the power is equally split by a divider. According to section 2.2.1, the conventional expression of the array factor for this linear phased array is:

$$AF(\theta) = \sum_{n=1}^{N} e^{-j\left[(n-1)\frac{2\pi}{\lambda}dsin\theta+\beta\right]}$$

$$n = 1,2,\cdots N \tag{3.1}$$

where λ is the wavelength in free space, d refers to the distance between elements, θ is the transmission angle (0° is normal to the array), and β is the progressive phase. However, as the 2-bit phase shifters are independent to each other, it is more convenient to replace β

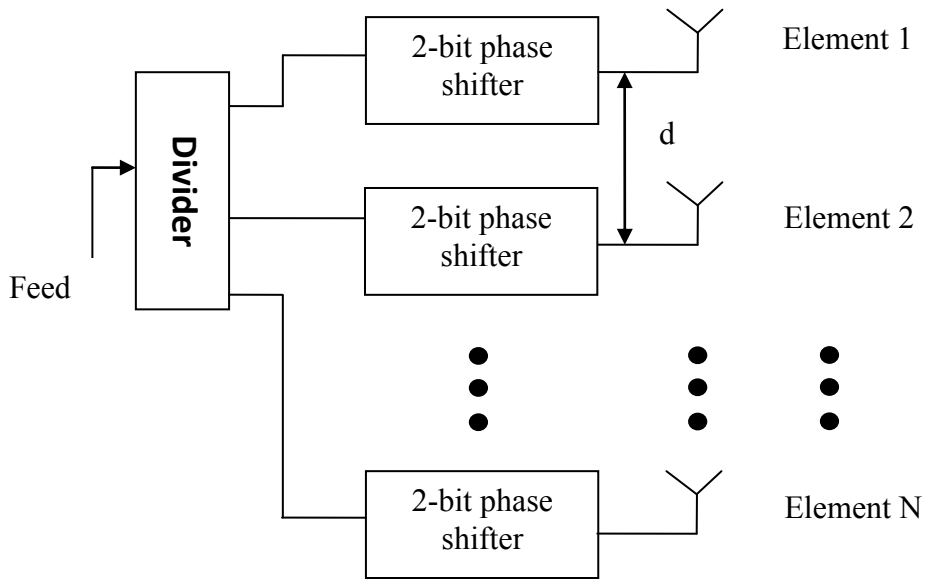

Fig. 3.1 Schematic structure of the DAM transmitter consisted of an N-element array with 2-bit phase control.

with a time dependent phase shift φ(t). With this change, the array factor of this DAM transmitter can be expressed as:

$$AF(\theta, t) = \sum_{n=1}^{N} e^{j\varphi_n(t)} \times e^{-j\left[(n-1)\frac{2\pi}{\lambda} d sin\theta\right]}$$

$$n = 1,2, \cdots N \tag{3.2}$$

Assume the antenna elements are omi-directional and identical, then the far-field signals generated by such an N-element DAM transmitter can be represented by the above equation, which simplifies the computation.

3.2 Characteristics Investigation

In this section, the basic system characteristics of the 2-bit DAM transmitter are investigated.

3.2.1 System Description

With 2-bit phase control, there are four phase states available for each antenna element. For illustrative purpose, the schematic structure of this 2-element DAM array can be shown as Fig. 3.2. Units "D_1, D_2, D_3, D4" are used to represent the phase states {0°, 90°, 180°, 270°} respectively. Only one phase state can be selected each time by the single-pole-4-throw (SP4T) switches. Unit "D" could be a possible common phase offset between two arms of the array, or the additional phase shift added to one element antenna. According to Fig. 3.2 and equation (3.2), the array factor of this 2-element transmitter can be expressed as:

$$AF(\theta, t) = e^{j\varphi_A(\mathrm{t})} + e^{j(\varphi_B(\mathrm{t})+\varphi_D - \pi \sin\theta)} \tag{3.3}$$

where $\varphi_{\mathrm{A}}(\mathrm{t})$ and $\varphi_{\mathrm{B}}(\mathrm{t})$ are the standard phase states (i.e. {0°, 90°, 180°, 270°}) selected by element antenna A and B at time t, φ_{D} is the additional phase offset between two arms of the 2-element array. The phase offset φ_{D} (∠D is used to denote the phase offset in degree) is not time-dependent here because we assume it is a fixed value in a particular data transmission. However, it will be an adjustable parameter when considering different data transmissions. According to Fig. 3.2, there are 16 element phase pairs available for a certain value of ∠D. They are listed in Table 3.1.

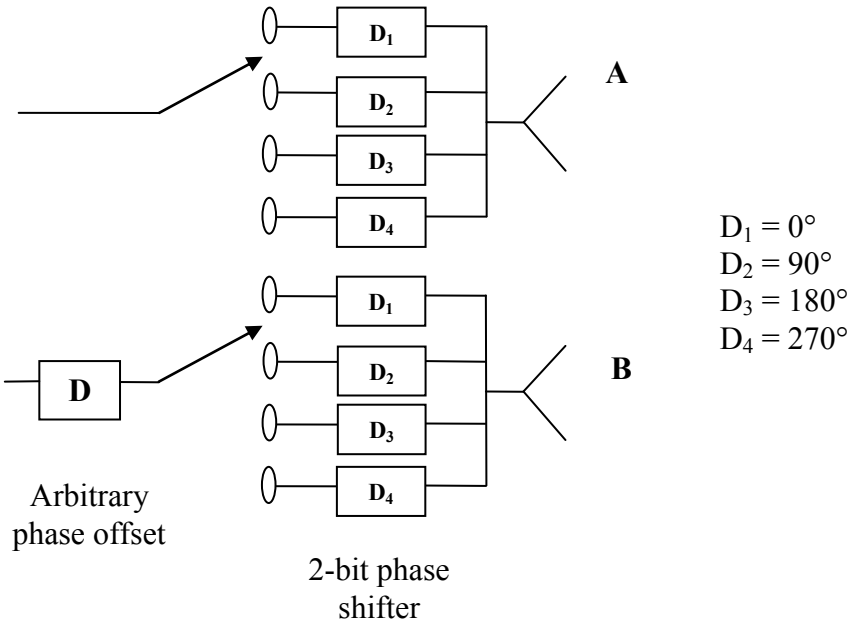

Fig. 3.2 Example of a 2-element DAM transmitter with 2-bit phase control.

Table 3.1 All the possible phase combinations

Phase combinations	[Element A Element B]	Phase combinations	[Element A Element B]
1	[0° 0°+∠D]	9	[180° 0° +∠D]
2	[0° 90° +∠D]	10	[180° 90° +∠D]
3	[0° 180° +∠D]	11	[180° 180° +∠D]
4	[0° 270° +∠D]	12	[180° 270° +∠D]
5	[90° 0° +∠D]	13	[270° 0° +∠D]
6	[90° 90° +∠D]	14	[270° 90° +∠D]
7	[90° 180° +∠D]	15	[270° 180° +∠D]
9	[90° 270° +∠D]	16	[270° 270° +∠D]

3.2.2 “Baseband” Signal Pattern Generation

The generation of “baseband” signals in a DAM system is different from conventional baseband modulation. It modulates signals directly through configuring the relative element phase (and amplitude) at the symbol rate. Next, we demonstrate the procedure based on the 2-element array mentioned in section 3.2.1.

By substituting different phase combinations from Table 3.1 into equation (3.3), the transmitter can ideally modulate up to 16 unique far-field signals for a certain offset phase φ_D. An example is shown in Fig. 3.3 that full constellation of the far-field signals is generated by the array transmitter in the boresight direction when offset phase $\angle D$ is 31°. The offset phase 31° is chosen for illustrative purpose that 16 distinct signals can be generated. The numerical numbers (1-16) in the diagram are 1-to-1 mapping to the phase combination numbers in Table 3.1. Therefore, the constellation shown by Fig. 3.3 can be seen as "baseband" signals modulated by this transmitter for boresight recipient.

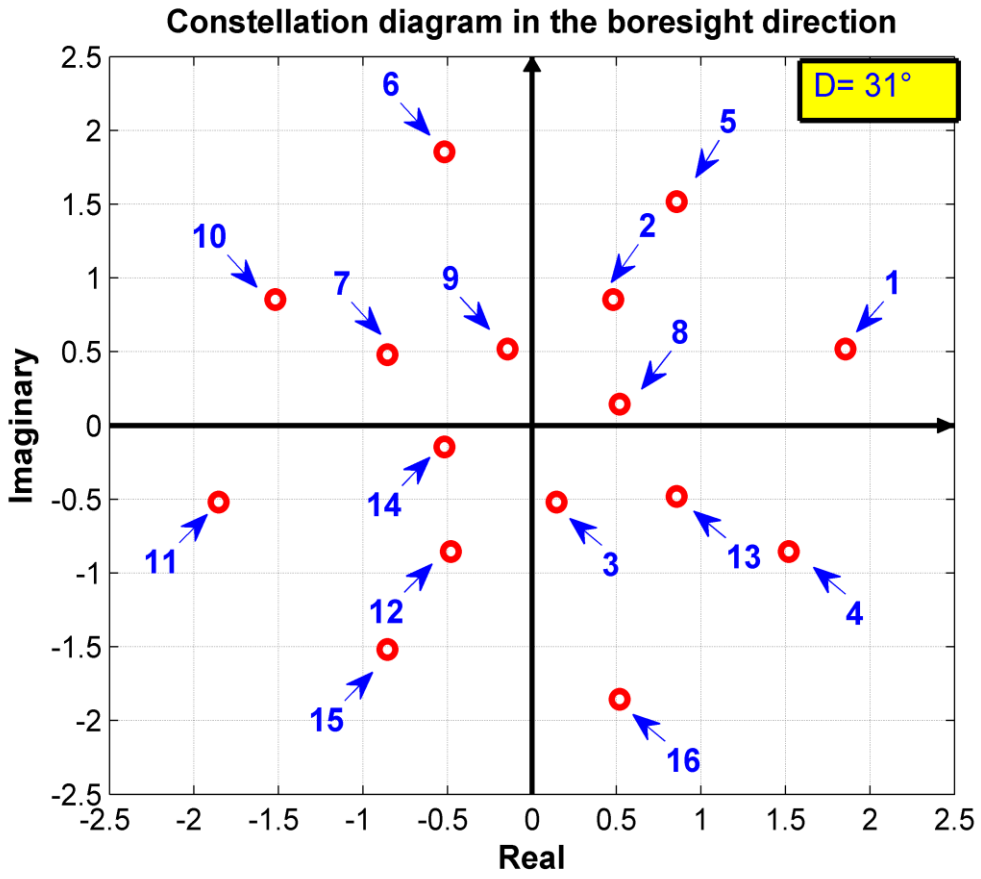

Fig. 3.3 Constellation generated by the DAM transmitter in the boresight direction when the offset phase is set to 31°.

The mathematical calculation of the partial "baseband" signals is illustrated below:

Constellation point 1: $\varphi_A = \varphi_B = 0,\ \varphi_C = 31°, \theta = 0°$

$$AF_1(0,1) = e^{j0} + e^{j(0+31-\pi \sin 0)}$$

$$= 1 + cos31 + jsin31 = 1.86 + 0.52j$$

Constellation point 5: $\varphi_A = 90°,\ \varphi_B = 0,\ \varphi_C = 31°, \theta = 0°$

$$AF_2(0,5) = e^{j90} + e^{j(0+31-\pi \sin 0)}$$

$$= j + cos31 + jsin31 = 0.86 + 1.52j$$

Constellation point 14: $\varphi_A = 270°,\ \varphi_B = 90°,\ \varphi_C = 31°, \theta = 0°$

$$AF_2(90) = e^{j270} + e^{j(90+31-\pi \sin 0)}$$

$$= -j + cos121 + jsin121 = -0.52 - 0.14j$$

It is demonstrated in this section that the "baseband" signals are successfully generated by the proposed DAM transmitter configured on a 2-element array. When the intended recipient has the knowledge of how the original data was mapped on to the constellation diagram, the information imposed on the signals can be decoded. In this sense, this DAM transmitter is shown to be able to encode and transmit information to the desired recipient by directly modulating the relative phase difference between array elements.

3.2.3 Direction Dependency

As the most important attribute of the DAM system, direction dependency is explained in detail in this section. The constellation shown in Fig. 3.3 is for broadside. Now we move the transmitting angles from -90º to 90º by observing constellation "point 1" only. The simulated result is shown in Fig. 3.4. The blue dotted circle is the movement track of constellation point 1 when observation angle θ shifts from 0° to 180°. Comparing it with Fig. 3.3, the positions of constellation point 1 at boresight are exactly the same. But when angle changes from -90° to 90°, they form a standard circle centred at point (1, 0) with uniform radius 1 on the constellation diagram. It can be easily derived by substituting $\varphi_A = 0°,\ \varphi_B = 0°,\ \varphi_C = 31°$ into equation (3.3):

$$AF(\theta, 1) = e^{j0} + e^{j(0+31-\pi \sin\theta)}$$

$$= 1 + e^{j(-\pi \sin\theta+31)} \tag{3.4}$$

Where $\left|e^{j(\pi \cos\theta+31)}\right| = 1$, so it forms a unit circle on Re/Im diagram; and the component $e^{j0} = 1$, which shifts the centre of the unit circle from origin to (1, 0).

The moving path shown by Fig. 3.4 is a circle with radius 1. But considering all 16 constellation points have their own moving paths, the migrations of overall signal pattern can be complicated. Fig. 3.5 shows two constellations received from 0º and 20º respectively when the offset phase is still 31º. At the first glance, the pattern formed by red circles is just rotated a certain degree compared to the pattern formed by blue diamonds. Then those signals modulated by the same phase pairs are connected by dotted lines. Apparently, these two constellations are completely different.

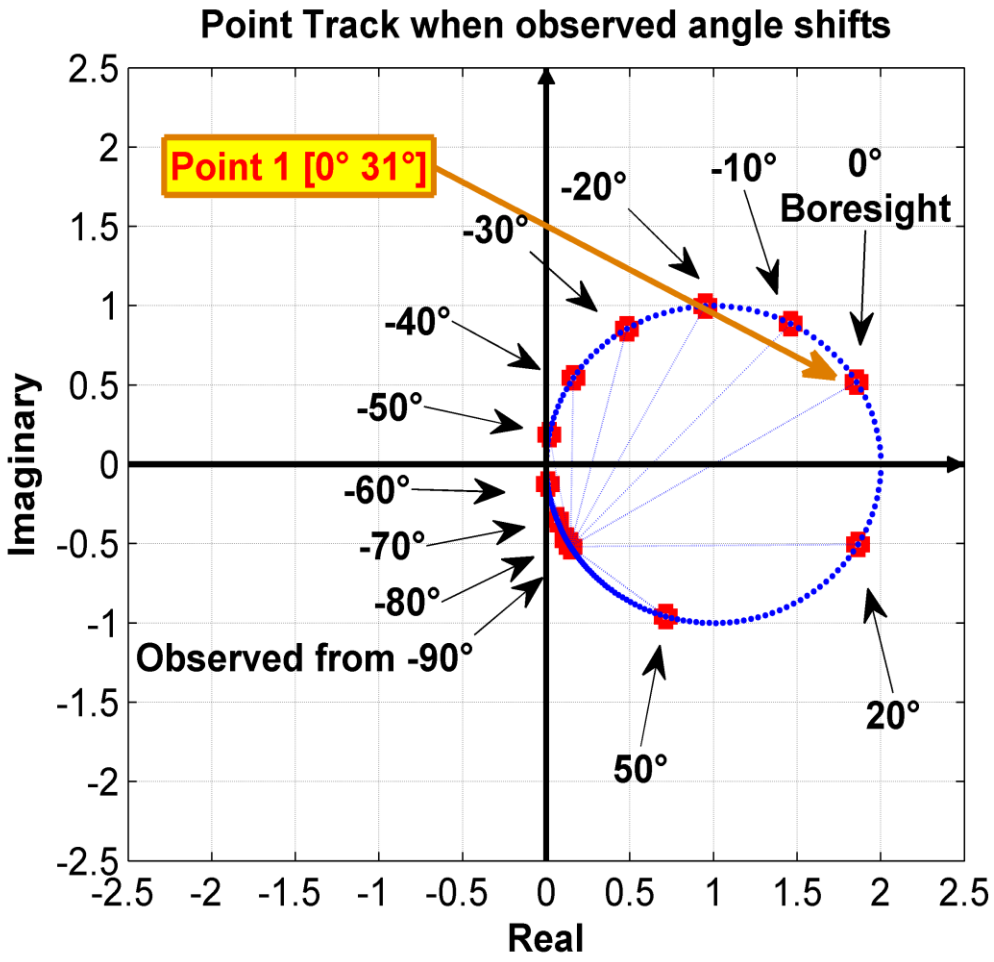

Fig. 3.4 Track of constellation point '1' when observation angle shift from 0° to 180°.

The mathematical demonstration for constellation point 1 is given below by substituting θ= 0º and θ=20º into equation (3.4) respectively:

At 0º, the blue diamond: $AF(0,1) = 1 + e^{j(-\pi \sin 0 + 31)} = 1.86 + 0.52j$

At 20º, the red circle: $AF(20,1) = 1 + e^{j(-\pi \sin 20 + 31)} = 1.86 - 0.51j$

Fig. 3.5 is a good demonstration for the property "direction dependency". In DAM, the "baseband" signals are not in the same distribution any more. The locations of signal points on the constellation diagram vary with the transmitting angles.

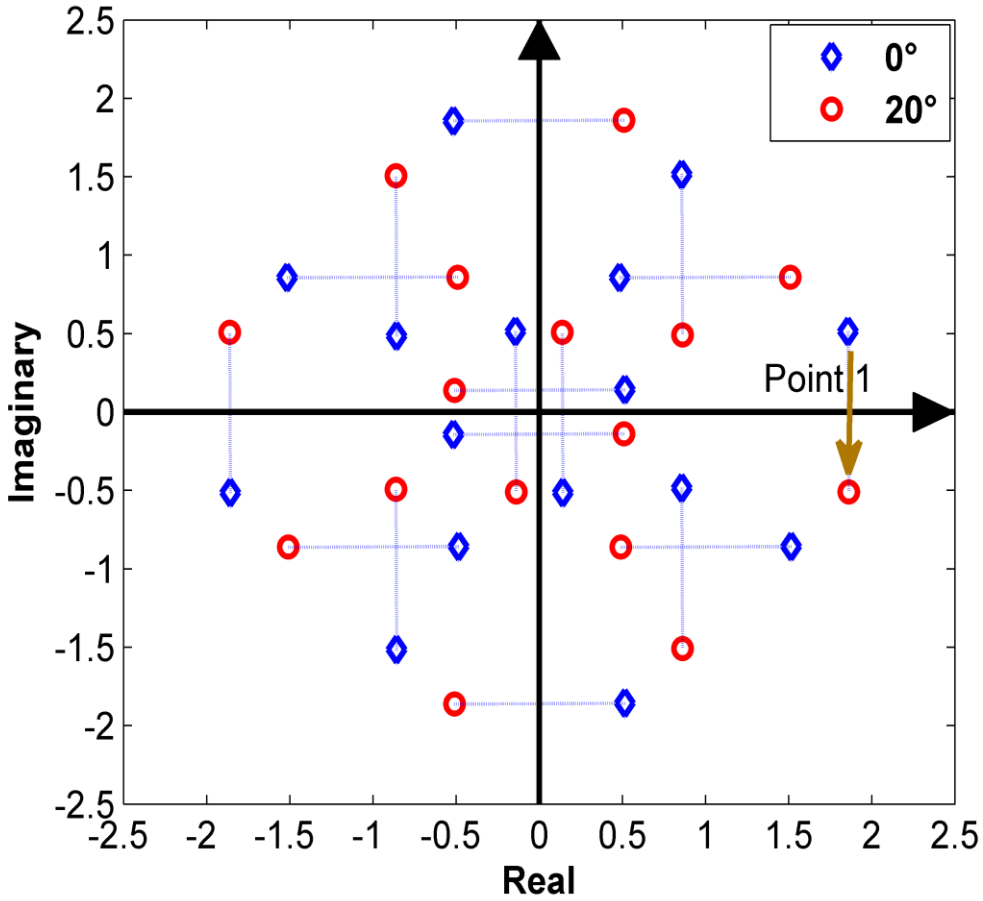

Fig. 3.5 Migration of constellations when observation angle moves from 0° to 20° (the same DAM transmitter as Fig. 3.3).

3.2.4 Signatures of the Transmission

The transmitter and the intended recipient should have common knowledge of how the original information is encoded onto the data points in the received constellations. Therefore the key point of a successful transmission is to ensure the recipient can receive a constellation with desired "baseband" signal pattern. In this sense, the constellation with a correct signal pattern becomes the signature of the transmission.

Traditionally, the signature (signal pattern) is pre-defined at baseband. One may change it by generating different baseband signals. In DAM, the signatures can be directly modified by the offset phases. In equation (3.3), the offset phase, φ_D, is a constant. But when considering the entire constellation, all the 16 constellation points have been modulated. In this case, $\varphi_D$is the only variable which can change the distribution of the entire constellation at a particular transmitting angle θ. In the example shown by Fig. 3.6, the transmitting angle is fixed at 0º. Two different constellations differed by red circles and blue diamonds are generated by setting the offset phase at 45º and 23º respectively.

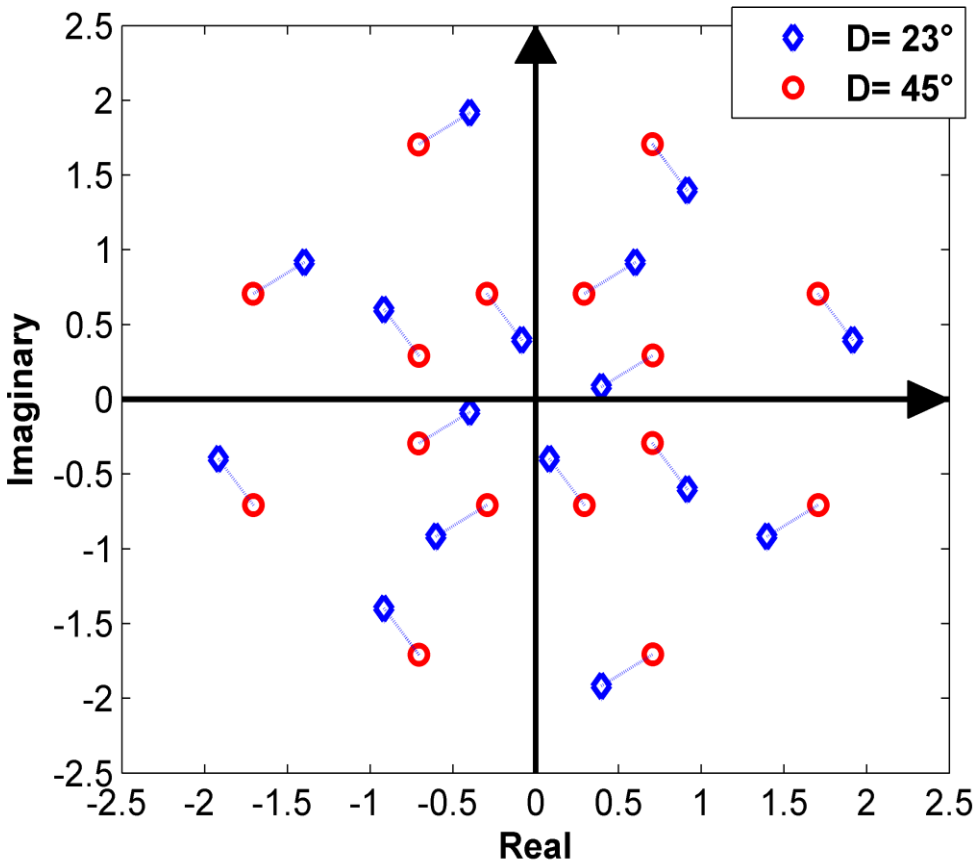

Fig. 3.6 Constellations received at broadside when offset phase is set to 23º and 45º respectively.

3.2.5 Signal Convergence

As mentioned at the beginning of this chapter, a special phenomenon called signal convergence can be observed in this 2-bit DAM transmitter system. This phenomenon can be described as: signals converge to the same constellation locations at some special transmitting angles. To demonstrate this property, the offset phase φ_D is set to zero. In Fig. 3.7, two signal patterns received at 0° and -10° are plotted on the constellation diagram. The pattern received at -10° contains 16 discrete data points (blue diamond). But at 0°, some of them move to the same positions. The pattern only contains 8 distinct data points (red circles). As illustrated in Fig. 3.8, the phenomenon can be regularly observed at following transmitting angles: -90°, -30°, 0°, 30° and 90°.

In fixed bit DAM transmitter system, this property is important because the phenomenon of signal convergence is predictable. The mathematical conditions of this property are given in Chapter 5. One application of the property is to provide multi-directional, independent & simultaneous data transmission to recipients located at various directions, which is discussed in Chapter 5. Another application of the property is to prevent accurate demodulation from up to two pre-know eavesdropping angles, which is discussed in Chapter 6.

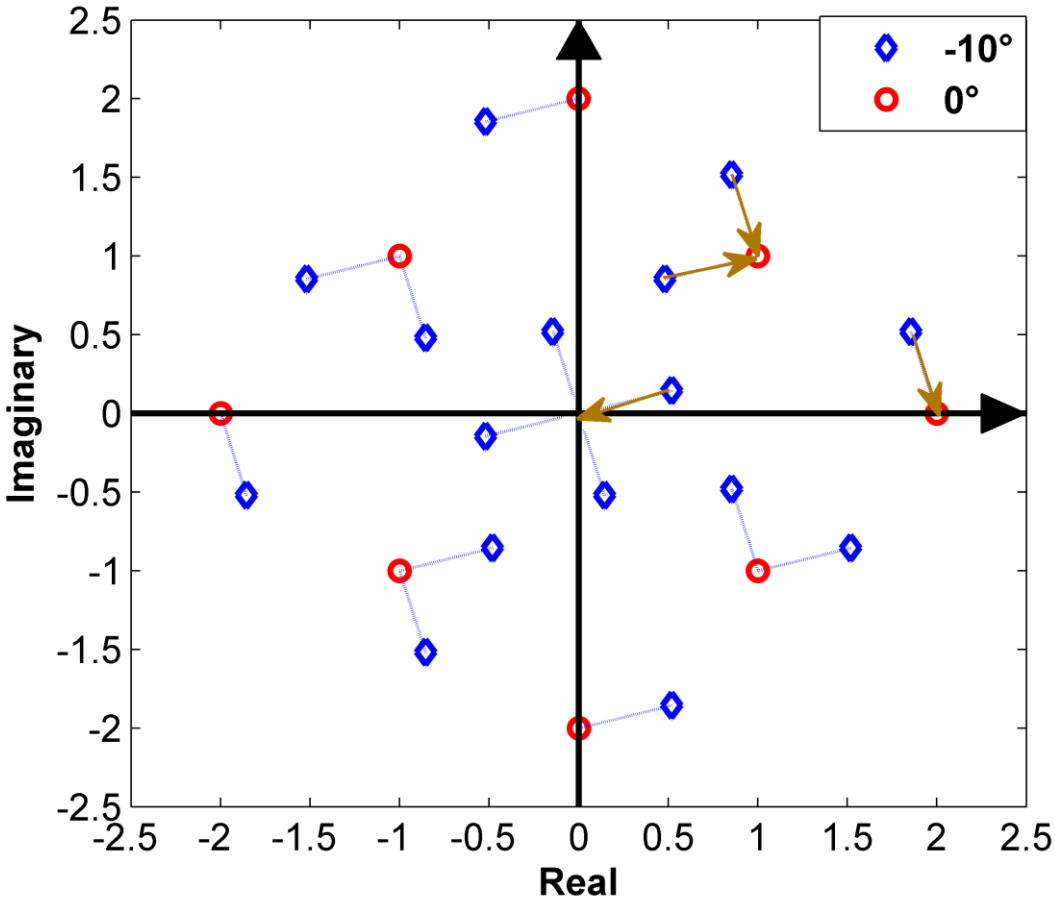

Fig. 3.7 Illustration of signal convergence when observation angle changes from -10° to 0° (offset phase is set to zero).

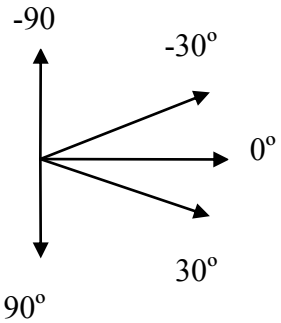

Fig. 3.8 Directions of reduced constellation (8 points) when offset phase is set to zero.

3.3 Experimental Validation

A prototype DAM transmitter is configured and measured for validation. Experimental constellations are given in this section and compared to simulated ones.

3.3.1 Measurement System Preparation

The experiment was carried out in the anechoic chamber. The anechoic chamber is an indoor space as shown in Fig. 3.9. Its walls, ceiling and floor are fully covered by absorbers to reduce the interference and reflection. Fig. 3.10 shows the schematic structure of NSI-800F-10 antenna measurement system [70]. Inside the anechoic chamber, it contains two components: antenna under test (AUT) and source antenna. As shown in Fig. 3.9, on the right side, there is a wideband horn antenna as the source antenna. On the

Fig. 3.9 Photograph of indoor anechoic chamber.

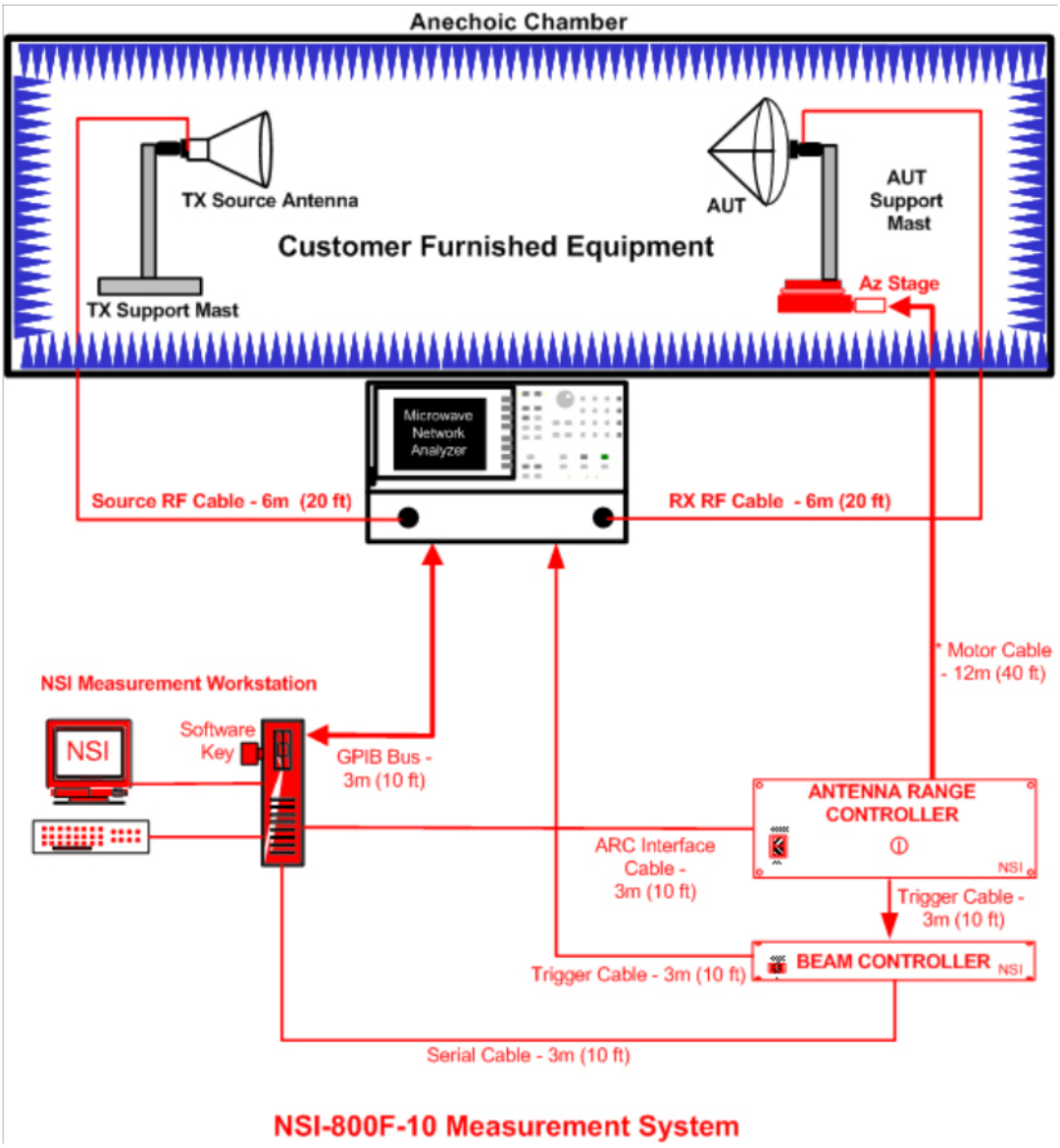

Fig. 3.10 NSI-800-10 measurement system [70].

left side, AUT is positioned on the turn table for measuring. The turn table can be rotated 360° in the azimuth plane. Outside the anechoic chamber, the measurement system contains an antenna ranger controller, a beam controller, a workstation and a network analyzer [70]. The measured data can be seen and analysed on the workstation. The data can also be exported. The network analyzer can be used independent from the measurement system. The series of network analyser used in the measurement is E5071C ENA. It is manufactured by Agilent Technologies and designed for evaluating RF

components and circuits for frequency up to 20 GHz [71]. The network analyzer has various powerful functions. In antenna measurement, the network analyzer is usually used to determine the resonant frequency of the antennas.

3.3.2 Experimental DAM Transmitter

As the very first step, we use the network analyzer to determine the working frequency of the antennas. The antenna used in the experiment is half-wavelength dipole antenna formed on a ceramic substrate. Two dipoles are chosen from many sample antennas as they have very similar resonant frequency at 8.3GHz. The second step is to test the phase shifters. The phase control is provided by two 4-bit digital diode phase shifters (series number is 8360-4XD and manufactured by Microwave Associates Inc). Each of them has 16 different phase states. But in our experiment, only 4 states are needed: -90°, 0°, 90° and 180°. After connecting the phase shifter to the dipole antenna, we can use the network analyzer to record the radiated complex signals at different phase states. The purpose of this step is to find the two most identical combinations of antenna & phase shifter. The measured data are listed in Table 3.2. These two combinations have relatively steady power level and accurate phase shift states compared to others.

The experimental DAM transmitter is then configured based on these selected components. The selected combinations of dipoles and phase shifters consisted of a 2-element phased array. A 3dB power splitter is connected to both arms of the array, whose series is ML17941 and branded by the same company as phase shifter. The schematic diagram of such a 2-element array is illustrated by Fig. 3.11. Fig. 3.12 is a photograph of the experimental transmitter inside the chamber. The dipoles are vertical polarised, and positioned in a horizontal row. The distance between them is set to 0.55λ.

Table 3.2 Parameters measured for two pairs of combined phase shifter and dipole

Theoretical phase states (º)	Power level measured (dB)	Phase measured (º)	Power level normalised (linear)	Phase normalised (º)
Phase shifter 026 & dipole antenna 01				
0	-51.4	-62	1	0
-90	-51.9	-153	0.8913	-91
180	-52	122	0.8710	184
90	-51.8	33.8	0.9120	95.8
Phase shifter 025 & dipole antenna 52				
0	-51.9	-82	0.8913	0
-90	-51.7	-169	0.9333	-87
180	-52.3	100	0.8928	182
90	-51.9	14	0.8913	96
Data recorded at radiating frequency 8.3GHz phase shifter is fed by +1.5V & -5V direct voltages				

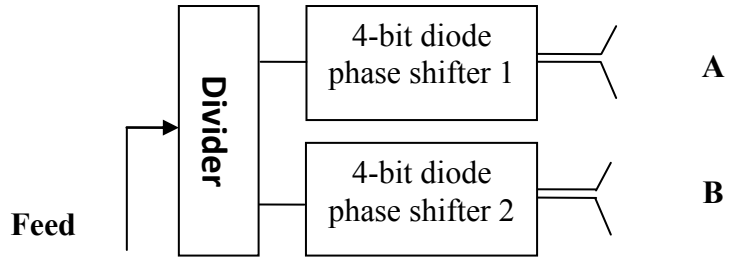

Fig. 3.11 Schematic diagram of the experimental DAM transmitter.

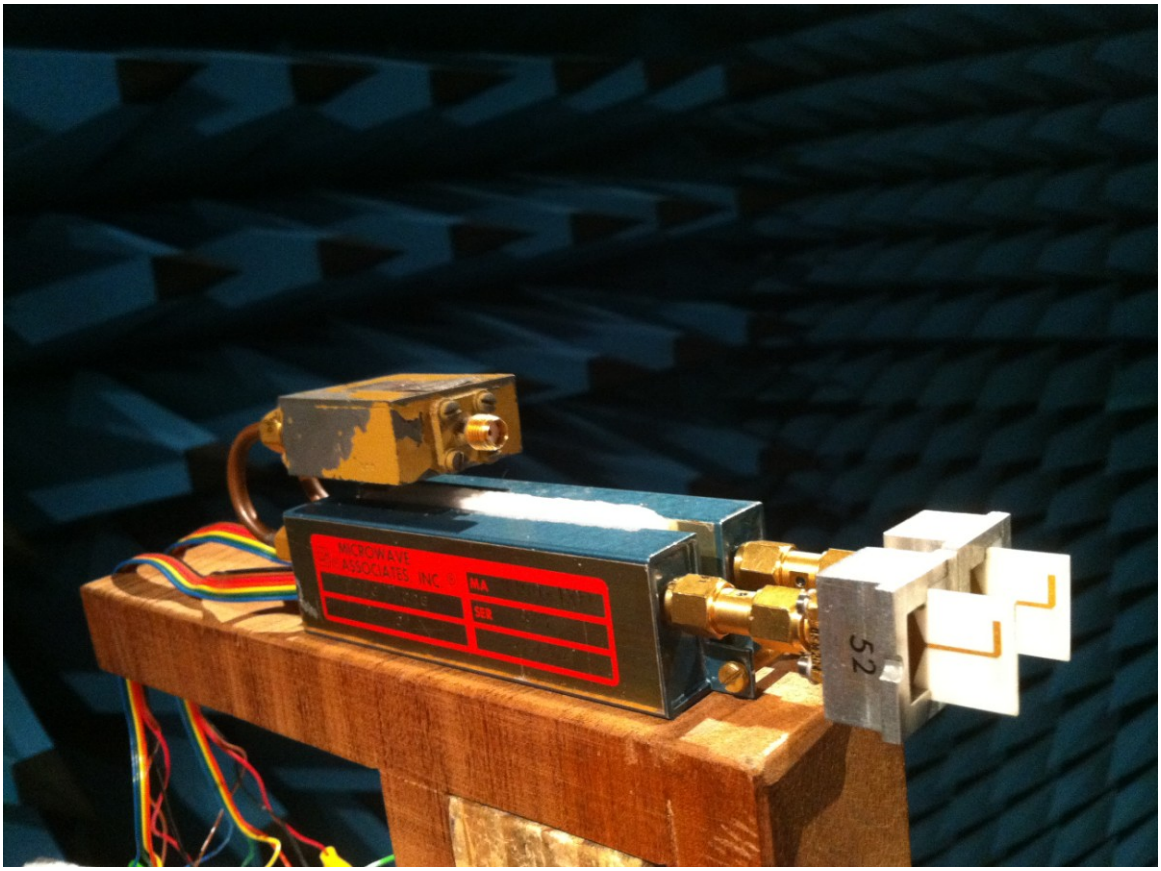

Fig. 3.12 Photograph of the experimental system.

3.3.3 Measured Experimental Constellation

The experimental DAM transmitter is used to validate the theoretical model suggested in section 3.2.1. Therefore, the structure shown in Fig. 3.11 is very similar to that shown in Fig. 3.2. The only difference is the offset phase between two arms of the array is zero in the experiment. Phase shifters in the experiment system are controlled according to phase combination shown in Table 3.3. Then the measured signals can be plotted onto an I/Q diagram at each discrete transmitting angle. Fig. 3.13 shows the constellation received in the broadside of the array.

Table 3.3 Phase pairs provided by phase shifters in measurement

Phase pairs	[Element A Element B]	Phase combinations	[Element A Element B]
1	[0° 0°]	9	[180° 0°]
2	[0° -90°]	10	[180° -90°]
3	[0° 180°]	11	[180° 180°]
4	[0° 90°]	12	[180° 90°]
5	[-90° 0°]	13	[90° 0°]
6	[-90° -90°]	14	[90° -90°]
7	[-90° 180°]	15	[90° 180°]
8	[-90° 90°]	16	[90° 90°]

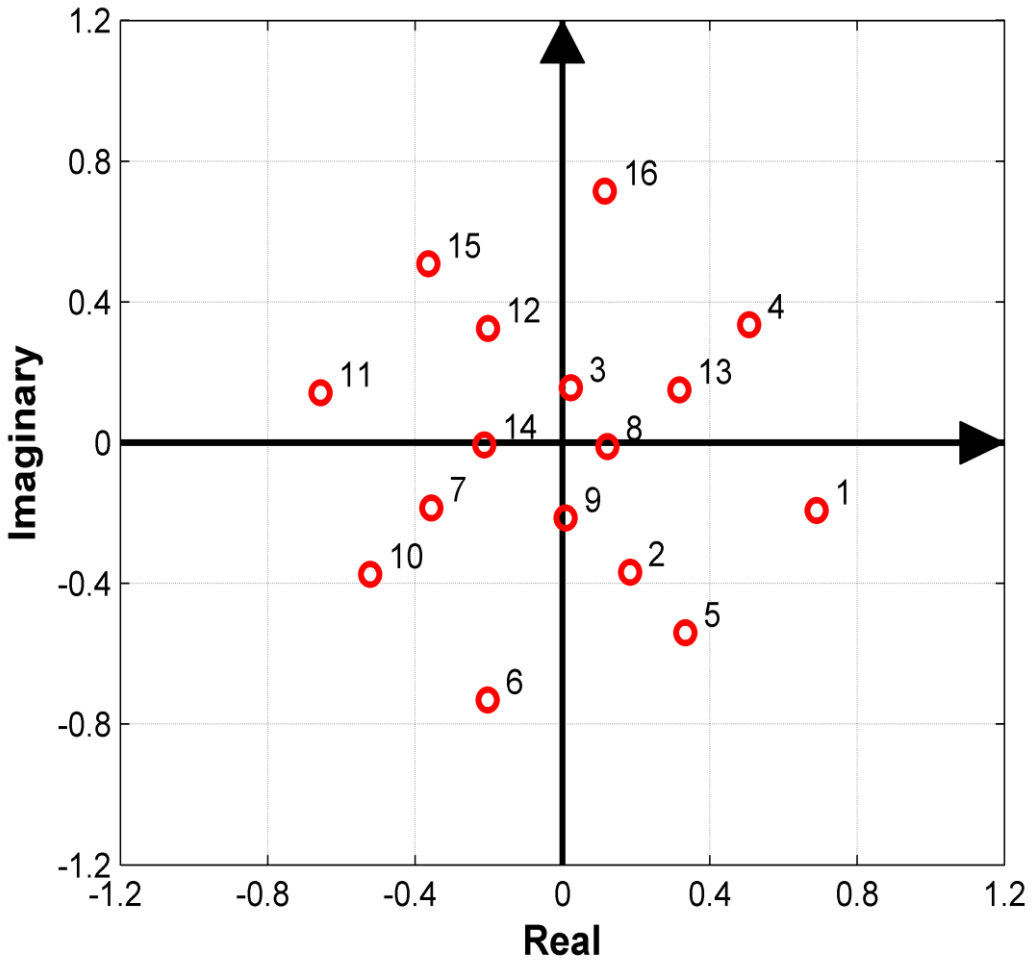

Fig. 3.13 Constellation of signals generated by the experimental DAM transmitter in the boresight direction.

To verify the correctness of the constellation, we simulate the theoretical model (equation (3.3)) by substituting the phase pair relationship according to Table 3.3. Then the comparison between the measured and simulated constellations at broadside is shown by Fig. 3.14. Unfortunately, they look completely different. The mismatch can be caused by following three reasons. Firstly, the experimental DAM transmitter is working at 8.3GHz. The distance between dipole antennas in the prototype system is 0.55λ at this frequency, which is constrained by their physical dimensions. But the element spacing in theoretical model is 0.5λ. Secondly, in the theoretical model, the length of propagating path is assumed to be a number, which is equal to multiple integer of wavelength. But in the measurement, an extra phase rotation could be caused. Thirdly, two arms of the array are assumed to be identical in the theoretical model. But according to the measured data in Table 3.2, two arms of the experimental array are not identical. There is an unexpected offset phase existing in this DAM transmitter. Therefore, the measured data needs calibration.

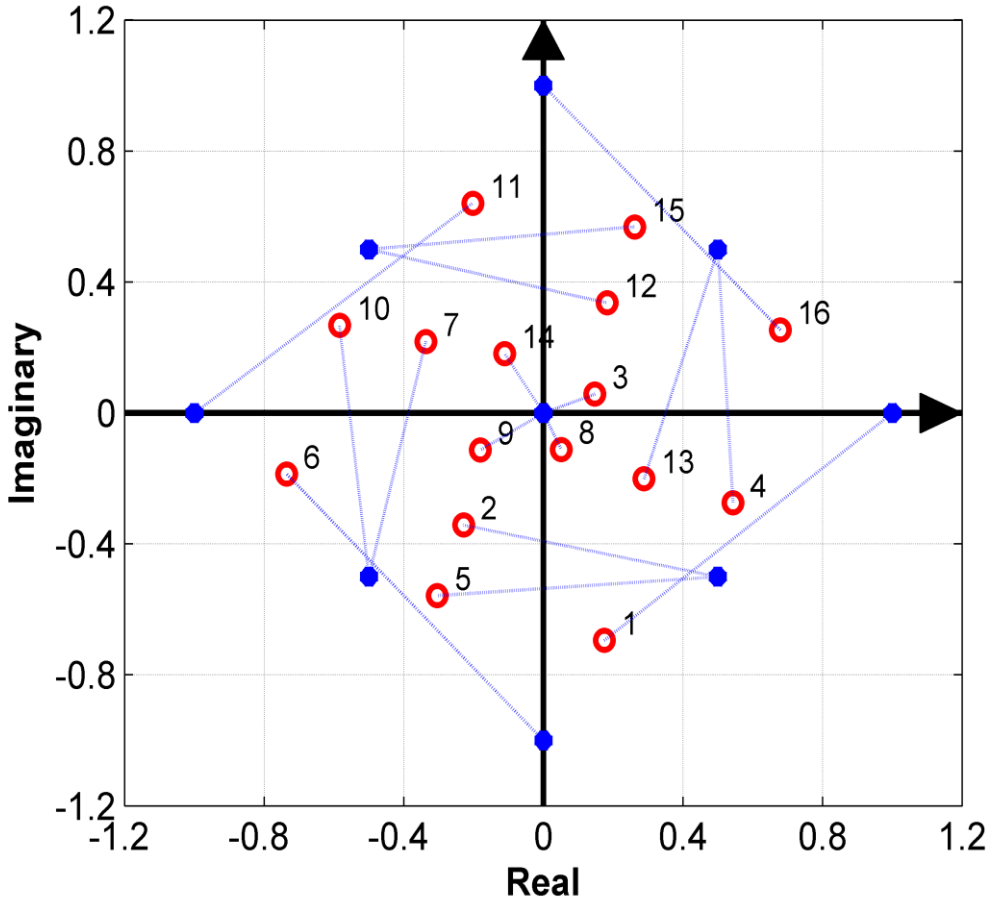

Fig. 3.14 Comparison between simulated (dots) and initial experimental (circles) constellations received by broadside receiver.

3.3.4 Calibration

The mismatch of constellation in Fig. 3.14 includes two parts: i) the red circles are supposed to converge to 8 discrete locations as predicted by blue dots; ii) a phase rotation is observed in which the red pattern is rotated clockwise on the diagram compared to the blue pattern.

The first mismatch is caused by the unexpected phase offset between two arms of the DAM transmitter. For this purpose, the reference case mentioned in section 3.2.5 is referred to. In the theoretical simulations, directions "0º, ±30º, ±90º" are found where only 8 distinct signals can be detected. If the experiment is successful, the same

phenomenon will be observed as well. Therefore, an exhaustive search among the experimental constellations from -90° to 90° is carried out to find and record all the reduced ones (8 points). The directions, where the signal convergence can be observed, are displayed in Fig. 3.15. Several steps are designed to find the unexpected offset phase between array elements. As shown in Table 3.4, step 1 is a reference case for the theoretical prediction of signal convergence. Step 2 takes the experimental element spacing of 0.55λ into theoretical model, and the angles are getting closer. In step 3, the theoretical model is modified again by considering the experimental parameters of the DAM transmitter. The amplitude and phase shift states of each arm of the array are substituted according to Table 3.2. In the new simulated model, the angles are not symmetrical to the broadside angle. In step 4, φ_D = -20° is chosen as the unexpected offset phase because it makes the angles found in simulated model as similar as possible to the ones observed in experiment (illustrated by step 5). The first mismatch has been calibrated, and both simulated and measured constellation diagrams received at -7° are shown in Fig. 3.16.

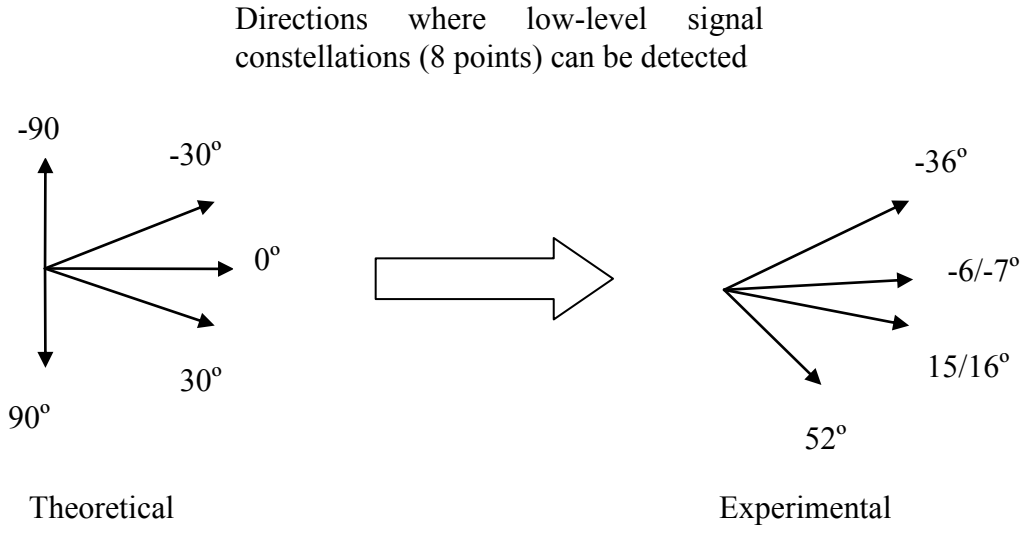

Fig. 3.15 Graphic illustration of directions where low-level signal constellations can be received theoretically and experimentally.

Table 3.4 Steps taken for calibrating the mismatch caused by unexpected phase offset between arms of the DAM transmitter.

Step	Data type	Parameter	Directions (°) of reduced constellation (8 points)				
1	Theoretical	$\varphi_D = 0$ $d = 0.5\lambda$	-90	-30	0	30	90
2	Theoretical	$\varphi_D = 0$ $d = 0.55\lambda$	-68	-28	0	28	68
3	Simulated	$\varphi_D = 0$ $d = 0.55\lambda$	-68	-28	0	25	64
4	Simulated	$\varphi_D = -20°$ $d = 0.55\lambda$	-71	-36	-7	18	52
5	Experimental	Aim of calibration	none	-36	-7	16	52

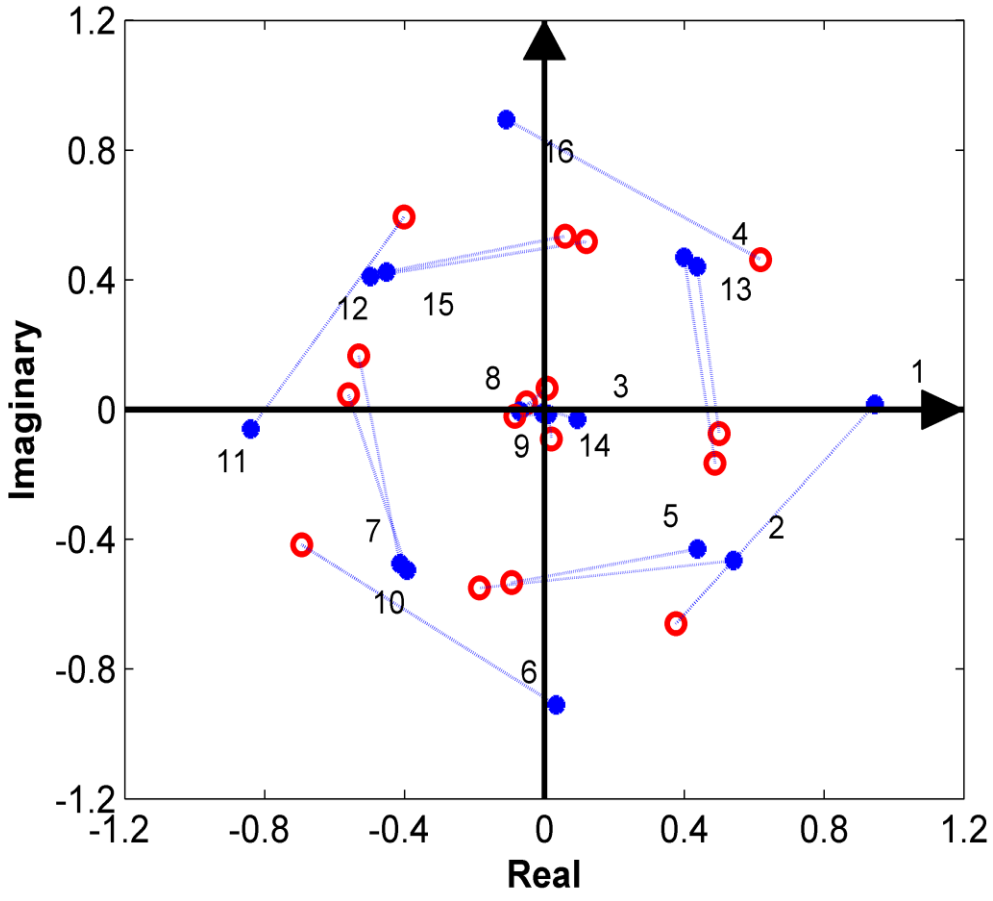

Fig. 3.16 Simulated (blue dots) and measured (red circles) constellations received at -7° after the first calibration.

The problem remaining in Fig. 3.16 is the overall phase rotation between two patterns. This mismatch is caused by the difference of the propagation paths (theoretical vs measurement). To calibrate, a general phase shift, 60°, is added to rotate the measured constellation to the predicted location. As shown in Fig. 3.17, the simulated and measured constellations received at -7° are now very similar.

In general, the practical DAM transmitter has three differences from the theoretical model. By changing the element spacing from 0.5λ to 0.55λ, adding an unexpected offset phase $\varphi_D = 20°$ and general phase shift of 60°, the measured constellation is matched with the prediction.

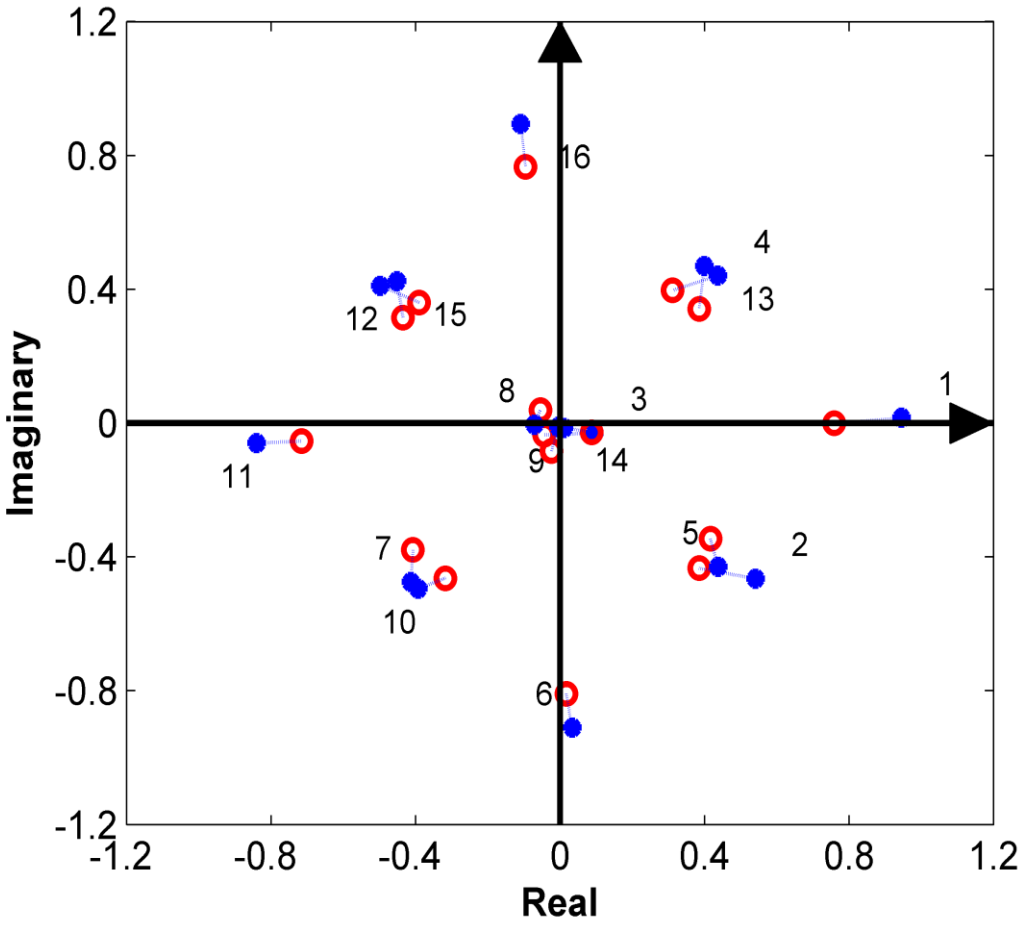

Fig. 3.17 Simulated (blue dots) and measured (red circles) constellations received at -7° after the second calibration.

3.3.5 Experimental Validation of the Properties of DAM System

The purpose of the experiment is to validate two most important properties of DAM transmitter: direction dependency and signal convergence.

A simulated constellation diagram containing signal patterns received from -7° and 0° is shown by Fig. 3.18. Both properties are illustrated. First, the signal pattern formed by red circles and blue dots are obviously different, which means the constellations are direction dependent. Second, with the moving of observation angle from -7° to 0°, only 8 signals can be distinguished. That means some signals converge to the same locations on the diagram.

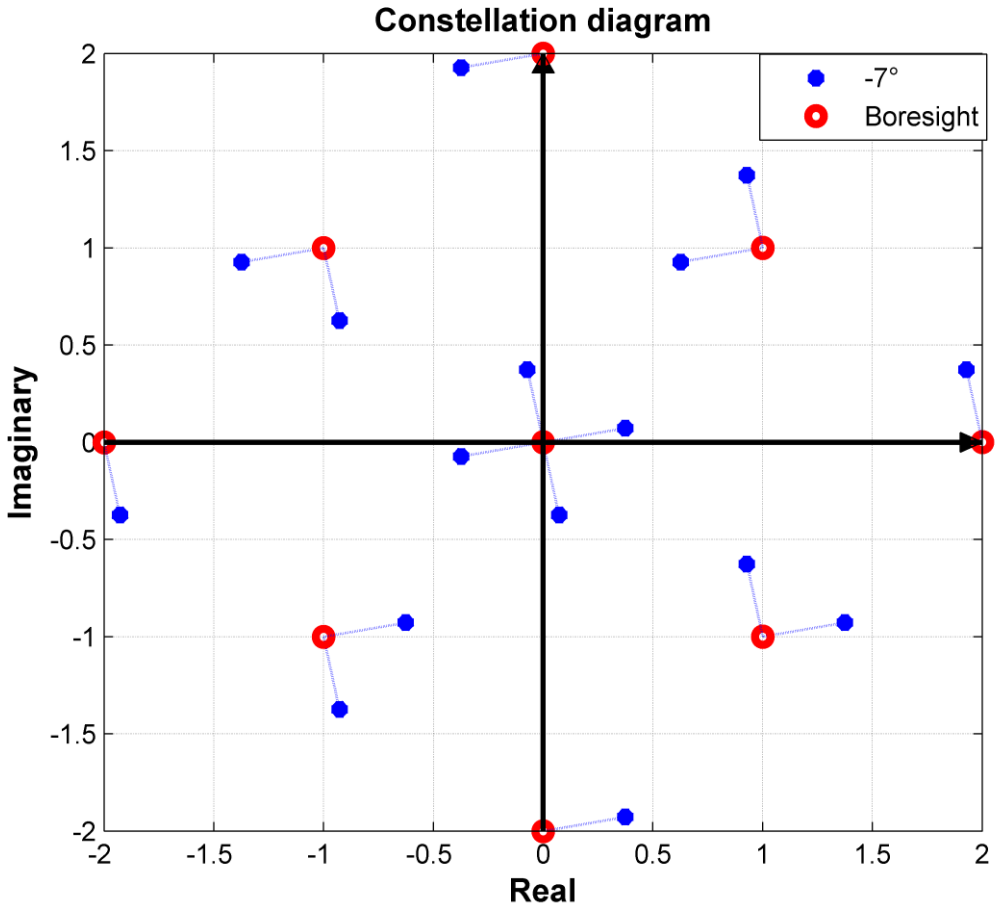

Fig. 3.18 Constellations received at 0° and -7° predicted by theoretical model.

The measured constellations received at -7° and 0° are plotted in Fig. 3.19 as a comparable result with the predicted constellations shown in Fig. 3.18. First, the constellations received at -7° and 0° are also different from each other as predicted, which validates the direction dependency property. Second, the overlapping of signals is not ideal in the measurement, but the basic trend has been clearly observed in Fig. 3.19, which, to a certain extent, validates the signal convergence property.

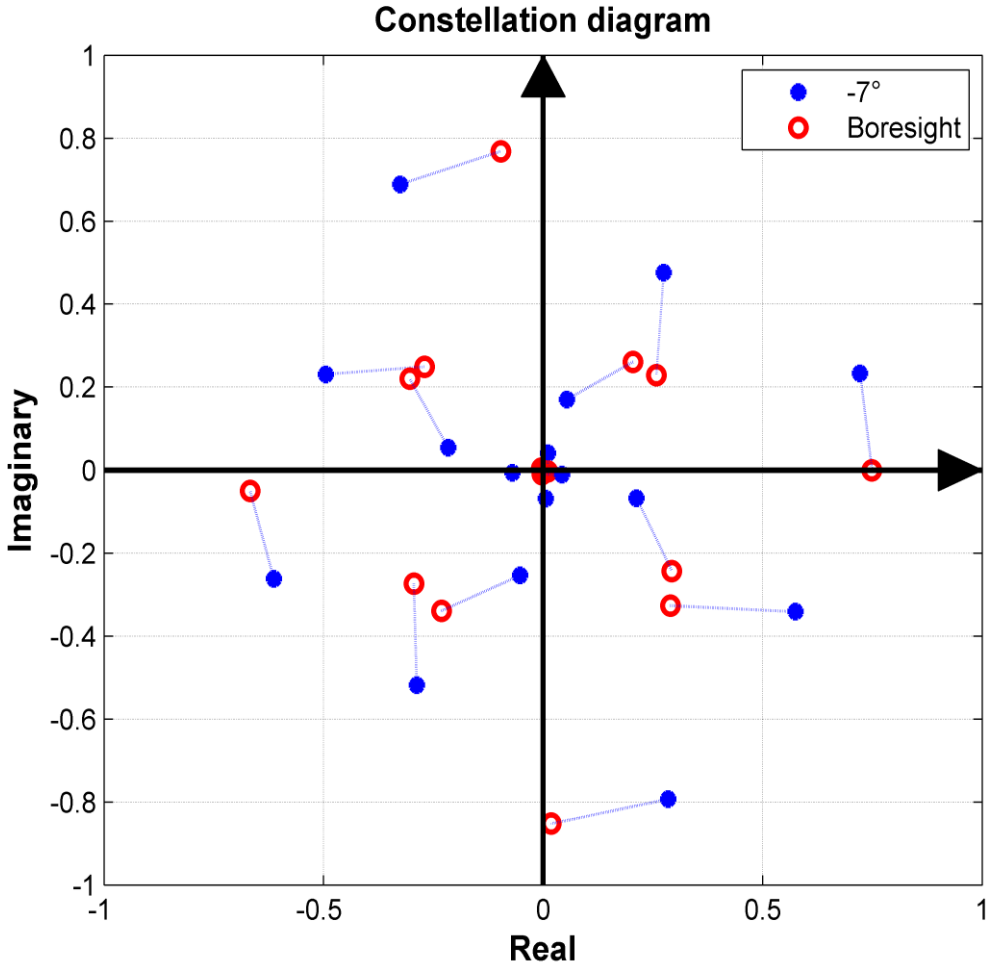

Fig. 3.19 Measured constellations received at -7° and 0°.

3.4 Summary

In this chapter, a theoretical model of a DAM transmitter based on a 2-element phased array was developed. Although only 2-bit phase control was employed, the property of direction dependency was still clearly demonstrated by the system. In addition, a phenomenon of signal convergence was noticed in the system. Finally, an experimental DAM transmitter was constructed for validation purpose. After a comprehensive calibration procedure, the measured data were shown to be very close to the theoretical prediction. Also, the prescribed system properties, direction dependency and signal convergence, were successfully validated experimentally.

Chapter 4

Communication Security Provided by the DAM Transmitter

The property of direction dependent modulation provides an extra degree of security in the physical-layer for wireless communication. To demonstrate this, symbol error rate is calculated statistically as a function of transmitting angle in the presence of Additive White Gaussian Noise (AWGN). The security level provided by the conventional DAM scheme is limited at angles which are very close to the intended transmitting direction. To overcome this weakness, the spacing between array elements is increased, and directive antennas are employed to reduce the grating lobes. The results show a superiority of DAM system in providing communication security compared to a conventional baseband system.

4.1 Reference Constellation Recognition

The reference constellation is defined as a constellation diagram containing "baseband" signals, which are recognised by both transmitter and recipient. Traditionally, the transmitter may send training signals containing pilot symbols for the desired recipient to "learn" the reference constellation. In time-varying channels, the pilot symbols may be sent periodically. Therefore, each time the pilot symbols are sent, there will be a chance for all the receivers to re-estimate the accuracy of the reference constellation. A security threat in conventional baseband modulation system is: the broadcast nature means that the same reference constellations can be received by both desired recipient and potential eavesdroppers at un-wanted directions (assuming they are perfectly recovered from channel distortion).

The situation is different in DAM system. The "baseband" signal pattern in DAM system is direction dependent, which means it changes with transmitting angle. Thus the reference constellation received by an eavesdropper located at a different transmitting angle will be different from the one received by desired recipient at the intended direction. However, in this case (solely using DAM transmitter), the security provided by DAM scheme against eavesdropping is still limited. That is because the reference constellation detected by eavesdropper is also "correct" for the signals transmitted at that direction. The decoding task may be not that difficult unless some of reference constellation points are very close to each other or even overlapping (such transmitting scenario will be illustrated in Chapter 6).

In the following sections we propose an operation scheme for reference constellation recognition, which may mislead eavesdroppers to decode information based on a wrong

reference constellation. All the subsequent simulated results presented in this chapter are based on it. In this scheme, there will be two parallel positioned transmitters, as shown in Fig. 4.1. One is configured with conventional baseband modulation, and another is a DAM transmitter. The conventional transmitter is used to broadcast pilot symbols periodically to all the receivers in space, including potential eavesdroppers. Therefore, eavesdroppers will have the same reference constellation as the one received by desired recipient, but the data information is actually transmitted by the DAM transmitter. Since the signal pattern generated by DAM transmitter at intended direction is exactly the same as the reference constellation broadcasted by conventional transmitter, the desired recipient is able to decode information as normal. In contrast the signal patterns generated by DAM transmitter at eavesdropping directions will be different from the reference constellation, which leaves a considerably difficult task for eavesdroppers to demodulate the correct information.

The success of this transmitting scheme lies with the eavesdropper's behaviour. To make eavesdroppers recognise the broadcasted pilot symbols as the reference constellation, there will be some constrains: 1, the eavesdropper should not be aware of the existence of the DAM transmitter; 2, the pilot symbols have to be repeated at a proper frequency to make the eavesdropper believe the reference constellation they received is the correct one; 3, the shorter the transmission, the lower possibility that eavesdroppers can find out that they are mislead in reference constellation recognition.

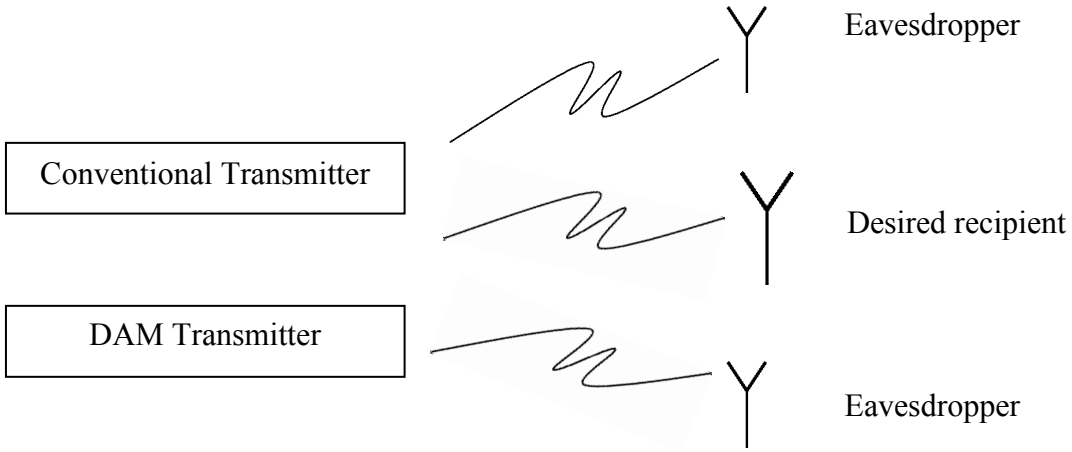

Fig. 4.1 Schematic structure of proposed reference constellation recognition transmission scheme

4.2 Decoding Algorithm

The reference constellation in DAM scheme is not always the standard signal pattern like 16-QAM or 64-QAM etc. That is because high-order pattern synthesis in DAM involves an increase of array elements, as well as continuous phase shifters and linear amplitude control. The system cost is much higher in DAM than that in conventional method. Therefore, the distribution of the constellation points generated by DAM transmitter could be pseudo-random. In this case, the minimum distance decoding is chosen as the decoding algorithm. The term “minimum distance” refers to the Euclidean distance between points on the constellation diagram. The selected decoding algorithm is adaptive, because the only rule it follows is the minimum distance from the received signal to all the other reference positions of baseband signals [18] [72]. To illustrate the above algorithm, we model a standard 2-element DAM transmitter with 2-bit phase control. The offset phase between two arms is set to 45°. Fig. 4.2 shows the boresight signal constellation received in the presence of Additive Gaussian White Noise (AWGN). Such

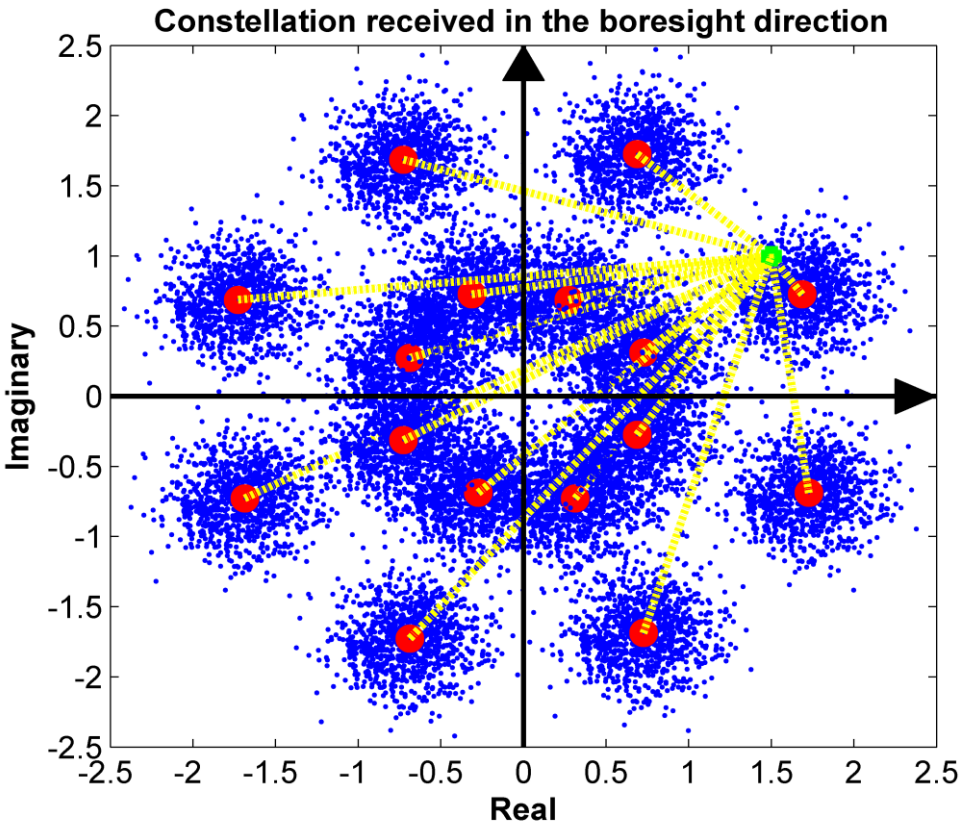

Fig. 4.2 Boresight signal constellation in the presence of Additive Gaussian White Noise (AWGN) for illustrative purpose.

a constellation contains 16 distinct symbol points. The big red circles show the reference position of baseband signals. The blue dots in the diagram are simulated signals in the presence of AWGN. The green square pointed out by the arrow is an example signal received by boresight receiver. According to minimum distance decoding, the assignment of this example signal depends on the minimum Euclidean distance from this green square to all the 16 red circles. Fig. 4.3 shows the same constellation as Fig. 4.2 without AWGN. In Fig. 4.3, the assignment of the received signal can be easily judged that it is mostly possible sent as signal point 1. If the transmitter did send a signal point 1, the reception is correct, otherwise, the error occurs.

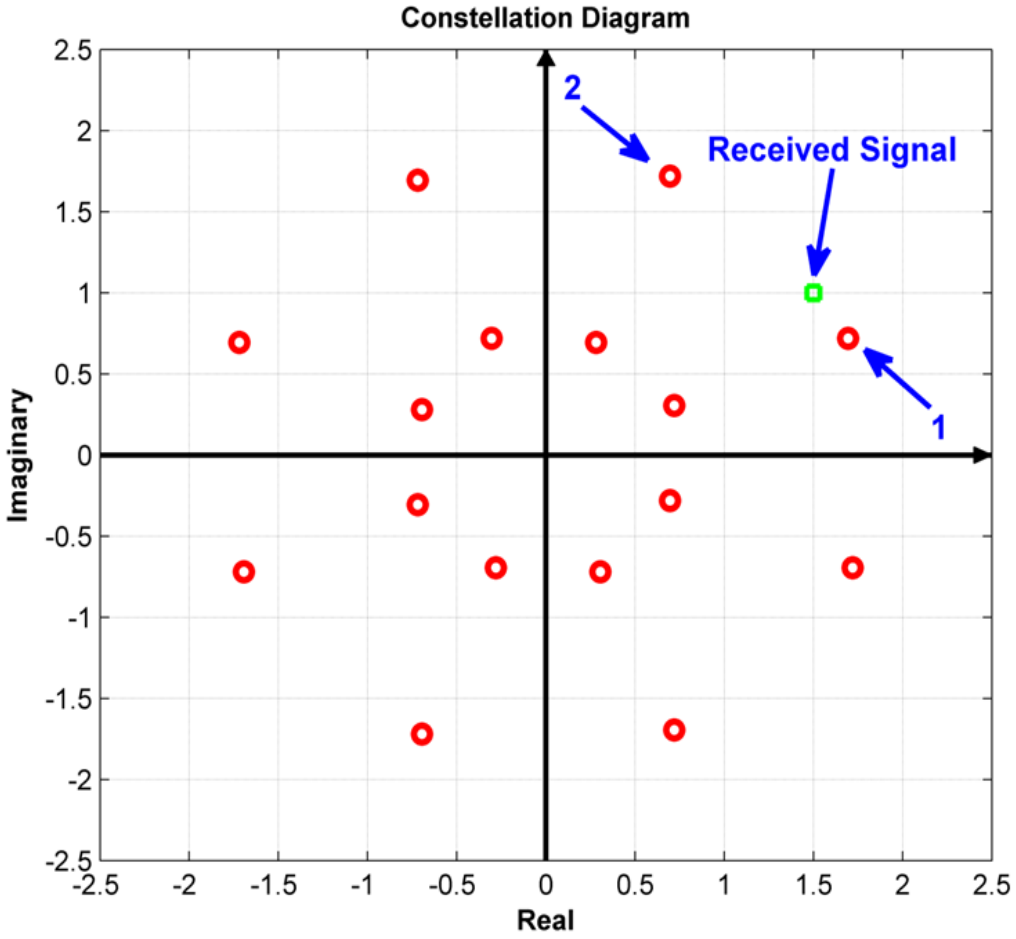

Fig. 4.3 Illustration of decoding algorithm on the signal constellation received in the boresight direction.

4.3 Error Rate Calculation

The simulation results shown in this section are calculated by MATLAB functions.

4.3.1 Symbol Error Rate

Based on the preferred reference constellation recognition scheme and decoding algorithm, the symbol error rate (SER) of the DAM system is calculated as a function of transmission angles. The DAM transmitter used in this example is configured on a 2-element array with 2-bit phase control, λ/2 element spacing, and 45° offset phase between arms. The SER is calculated statistically. The process includes the following steps:

- Step 1: Generate the reference constellation (Fig. 4.3) at the intended direction, which is boresight in this example.
- Step 2: A random signal is transmitted to an investigating direction, added by a random AWGN noise generated by a MATLAB function.
- Step 3: Decoding Algorithm is applied. The belonging of the received signal point is determined by calculating the minimum distance from it to all the reference constellation points. Record the successes and errors.
- Step 4: Repeat step 2&3 10^6 times to obtain a statistical result.
- Step 5: Repeat step 4 with the change of transmitting angle from -90° to 90°.
- Step 6: Repeat Step 5 with the change of SNR levels (SNR refers to E_s/N_0).

A simulated result is shown in Fig. 4.4. In general, in the boresight direction, the transmitted signal is demodulated with the lowest error rate. At angles away from boresight however, the error rate increases rapidly to level of an approximately 50% at about 10°, and to almost 100% at 20°-30° varies at SNRs. The error rate plot demonstrates the security feature of DAM scheme.

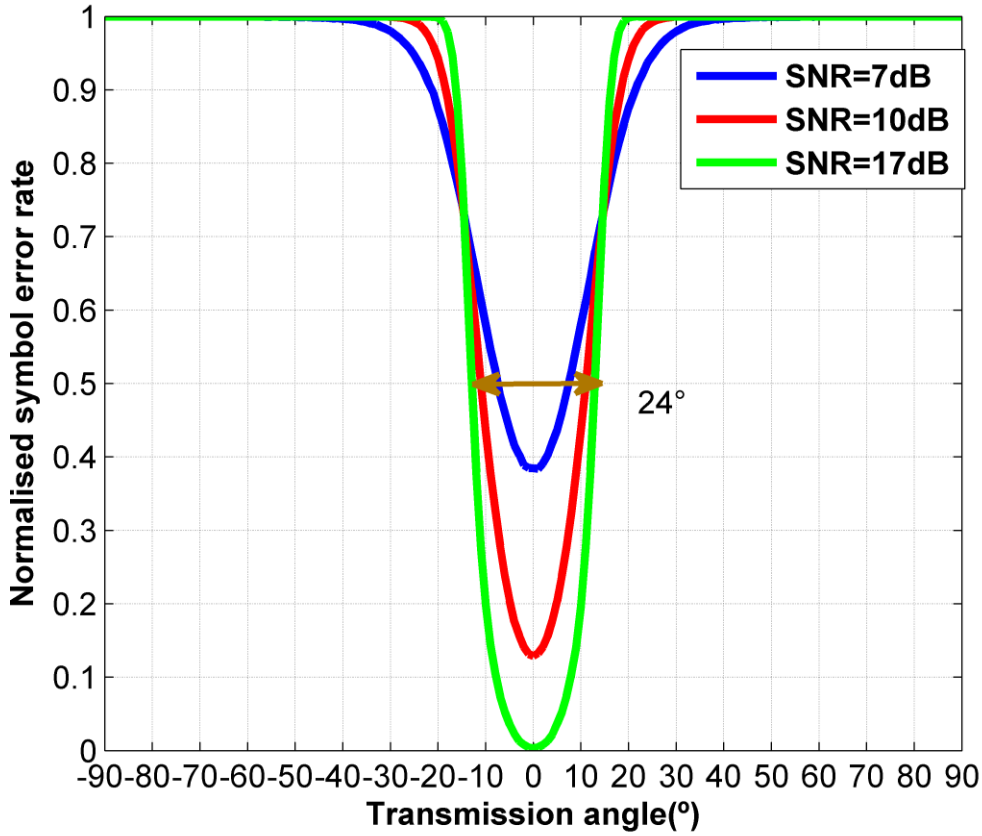

Fig. 4.4 Symbol error rate calculated as a function of transmission angles subject to various levels of SNRs.

4.3.2 Error Rate Beamwidth

Traditionally, only the error rate in the intended direction is of interest. Thus the error rate is usually in logarithmic scale. However, the focus of this research is in the eavesdropping directions. We aim to reduce the possibility that eavesdropper can demodulate information with low error rate. Therefore, the symbol error rate plotted in Fig. 4.4 is in linear scale. The term "Error Rate Beamwidth" (ERB) is used in this thesis to describe the security level provided by the DAM transmitter. Referring back to Fig. 4.4, at SNR = 17dB (here SNR = E_s/N_0), the angular width of the SER curve (green one) is about 24° at 50% (pointed out by the double arrow). This example demonstrates the concept of ERB. The threshold is 50% in the example, but it can be any percentage from

0 – 100%. Therefore, the ERB is defined as the angular difference (in degree) where the error rate is at a pre-defined percentage. Basically the smaller the ERB is, the securer the system is. The purpose why we introduce the concept of ERB is that it can reflect the level of security provided by different DAM system configurations. As mentioned in section 3.2.4, the offset phase $\varphi_D$can be used to adjust the distribution of constellation. The system error rate is sensitive to the change of constellation distribution, because minimum distance decoding is applied. Thus to measure how the constellation distribution influence the error rate performance, the ERB is calculated as a function of offset phase φ_D, and the simulated results are shown in Fig. 4.5.

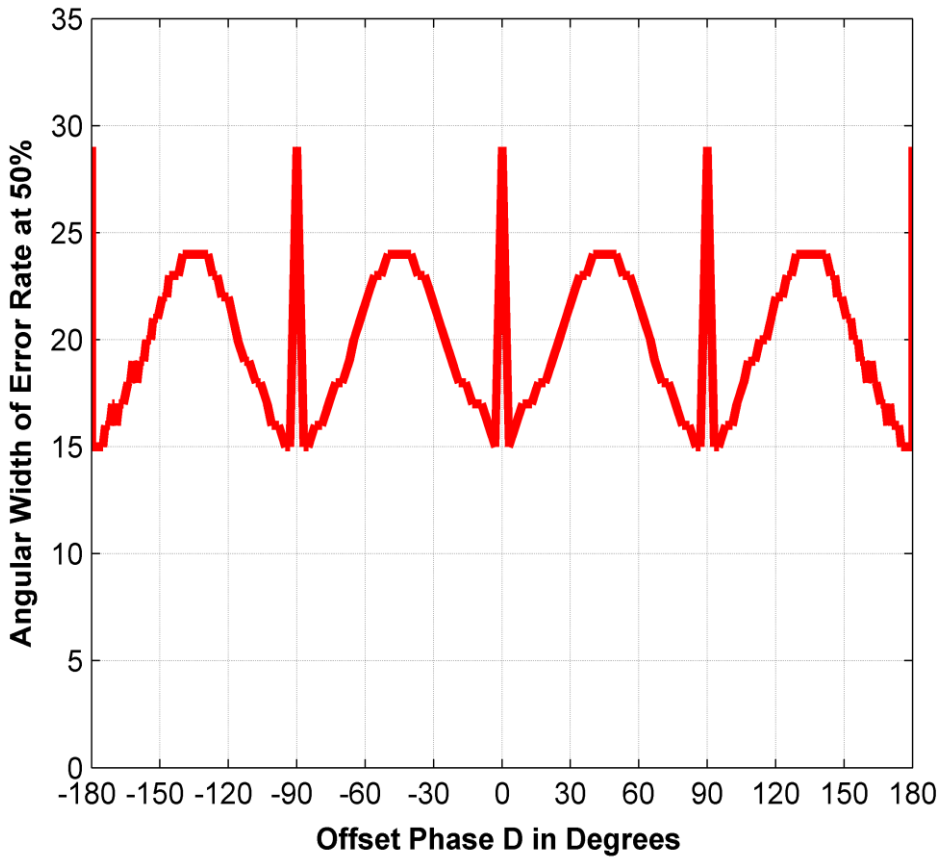

Fig. 4.5 The ERB obtained under the SNR of 17dB

The first most noticeable point shown in Fig. 4.5 is that the maximum value of ERB peaks at about 28° when the corresponding set of offset phase is {-90°, 0°, 90° and 180°}. The ERB curve shown in Fig. 4.5 is of triangular-wave type, except the discontinuity occurring at above offset phases. In other words, at $\varphi_D = \frac{n\pi}{2}, n = -1, 0, 1, 2$, the eavesdropper located outside the angular range from -14° to 14°, would have a demodulation error rate more than 50%. The reason causing this discontinuity is the reduction of distinct constellation data points. Recalling equation (3.3), substituting θ=0° and $\varphi_D = \frac{n\pi}{2}, n = -1, 0, 1, 2$:

$$AF(0,t) = e^{j\varphi_A(\mathrm{t})} + e^{j\left(\varphi_B(\mathrm{t}) + \frac{n\pi}{2} - \pi \sin 0\right)}$$

$$= e^{j\varphi_A(\mathrm{t})} + e^{j\left(\varphi_B(\mathrm{t}) + \frac{n\pi}{2}\right)} \quad n = -1, 0, 1, 2 \tag{4.1}$$

Then substituting $\varphi_A(\mathrm{t}), \varphi_B(\mathrm{t})$ according to Table 3.1 into (4.1), there will be only 9 signals including 0 (the origin). That means the number of distinct constellation points generated in the boresight direction reduces from 16 to 9 when the offset phase $\varphi_D$is set to above values. The constellation containing only 9 data points in the presence of AWGN is illustrated in Fig. 4.6. Comparing it to Fig. 4.2, apparently the distribution of red circles is looser. Under the same SNR, the overlapped area of blue dots is significantly reduced. Therefore, the error rate should have reduced as well. The corresponding SER is shown by Fig. 4.7, where the error rate in the boresight direction is much lower than that in Fig. 4.4. Also the ERB at 50% is 28°, which matched the simulated results in Fig. 4.5. The SER curve shown by Fig. 4.8 is a logarithmic version of that shown by Fig. 4.7, with 3dB off in SNR (3dB was taken off to make the green curve converge). A conclusion can be drawn by comparing Fig. 4.8 to Fig. 4.4 that, even

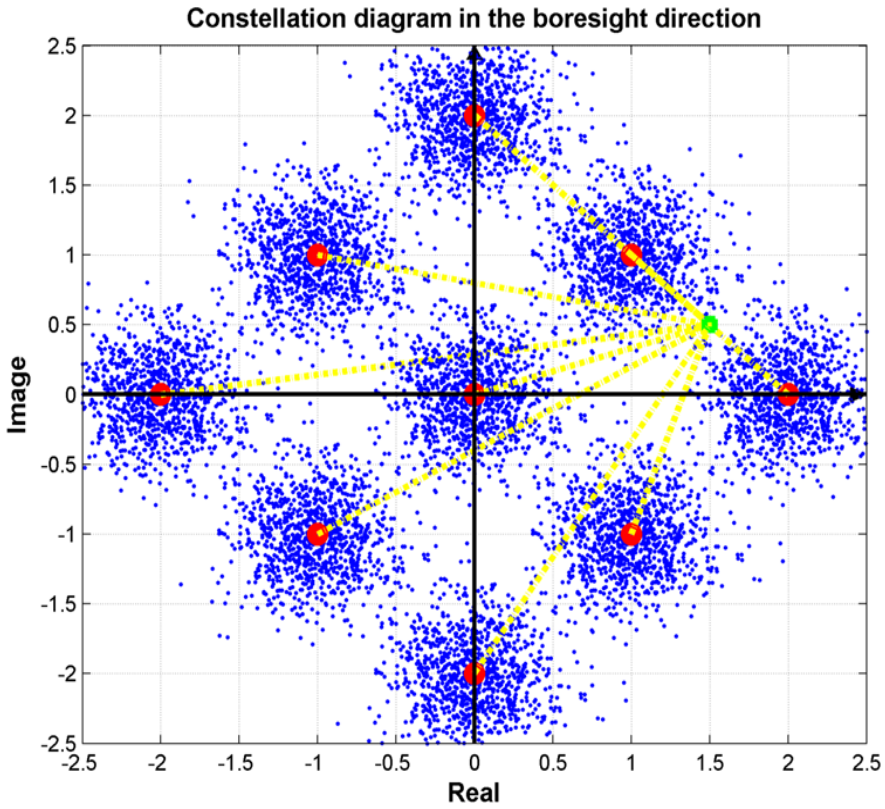

Fig. 4.6 Boresight signal constellation with only 9 points in the presence of AWGN.

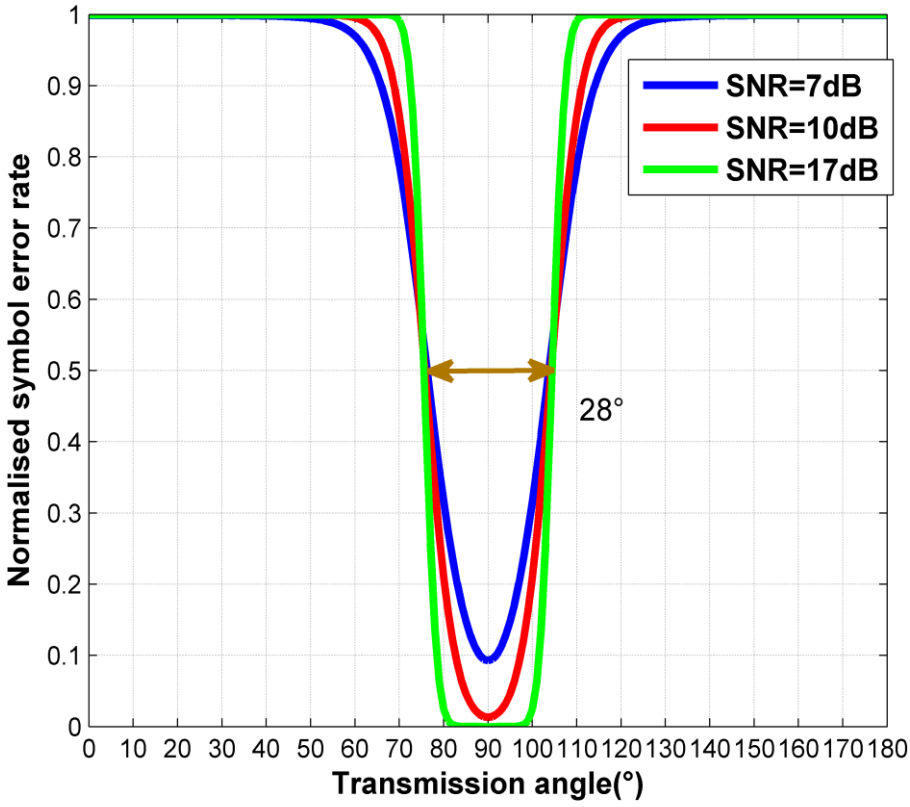

Fig. 4.7 Symbol error rate calculated based on the constellation shown in Fig. 4.6.

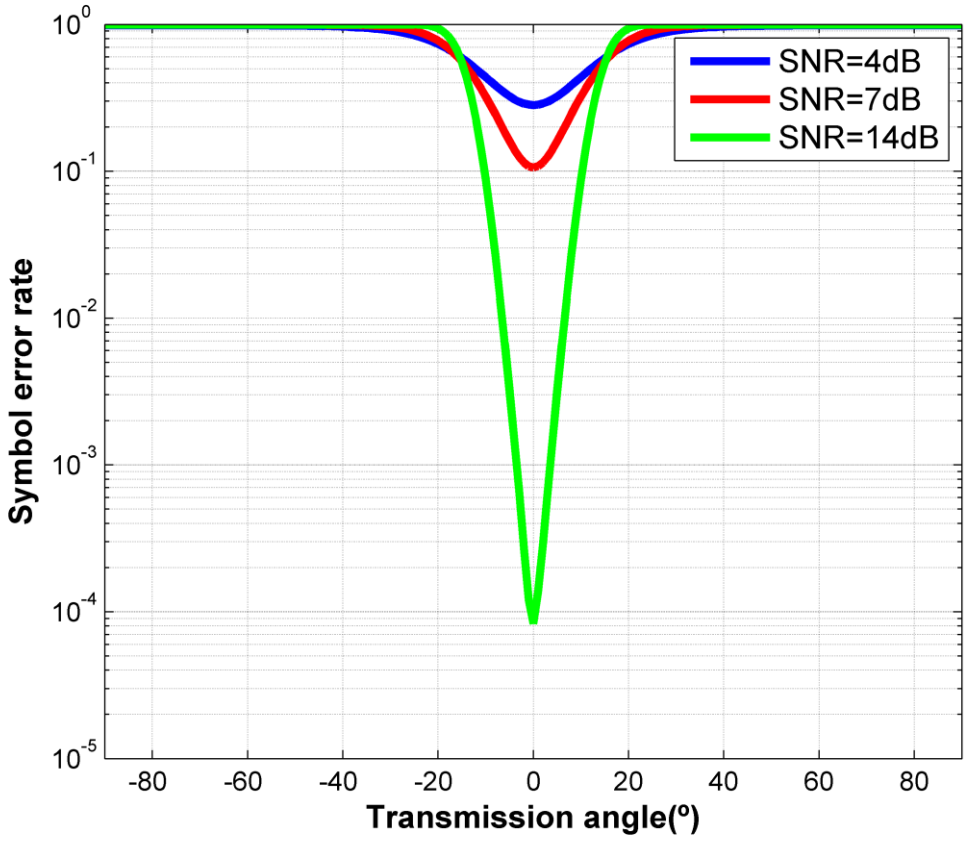

Fig. 4.8 The SER in logarithmic scale of that illustrated by Fig. 4.7 with 3dB off.

suffering 3dB power attenuation, the SER of this 9 points QAM (Fig. 4.6) at the broadside direction is still much better than that of 16 points QAM (Fig. 4.3).

The second point to notice from Fig. 4.5 is that the minimum value of ERB is about 15°. This is obtained when the offset phase $\varphi_D$is bigger or smaller than $\frac{n\pi}{2}$ for 1-2°. At these special φ_D, constellation points are just about to overlap. An example constellation is shown in Fig. 4.9. In Fig. 4.9, when the offset phase between array elements is set to -2°, the Euclidean distances between symbol pairs like "2 & 5" are very small. The corresponding SER curves under different SNRs are shown in Fig. 4.10. We can observe a significant increment of error rate in the broadside direction. Additionally, the curves are no longer symmetric to the broadside direction. That is because when observation

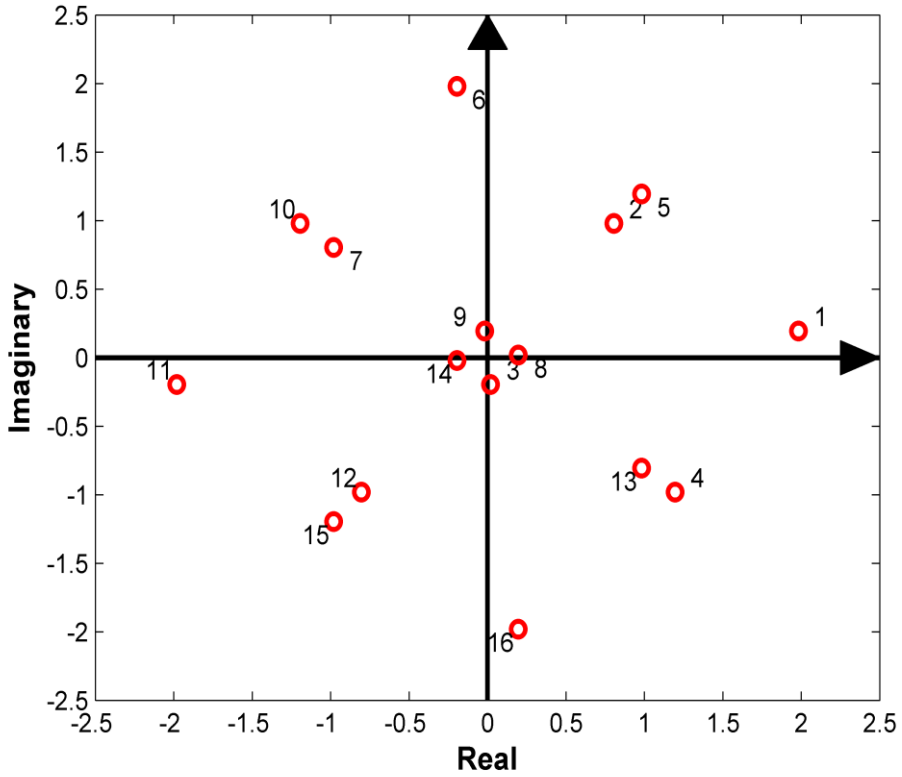

Fig. 4.9 Constellation received in the boresight when offset phase is set to -2°.

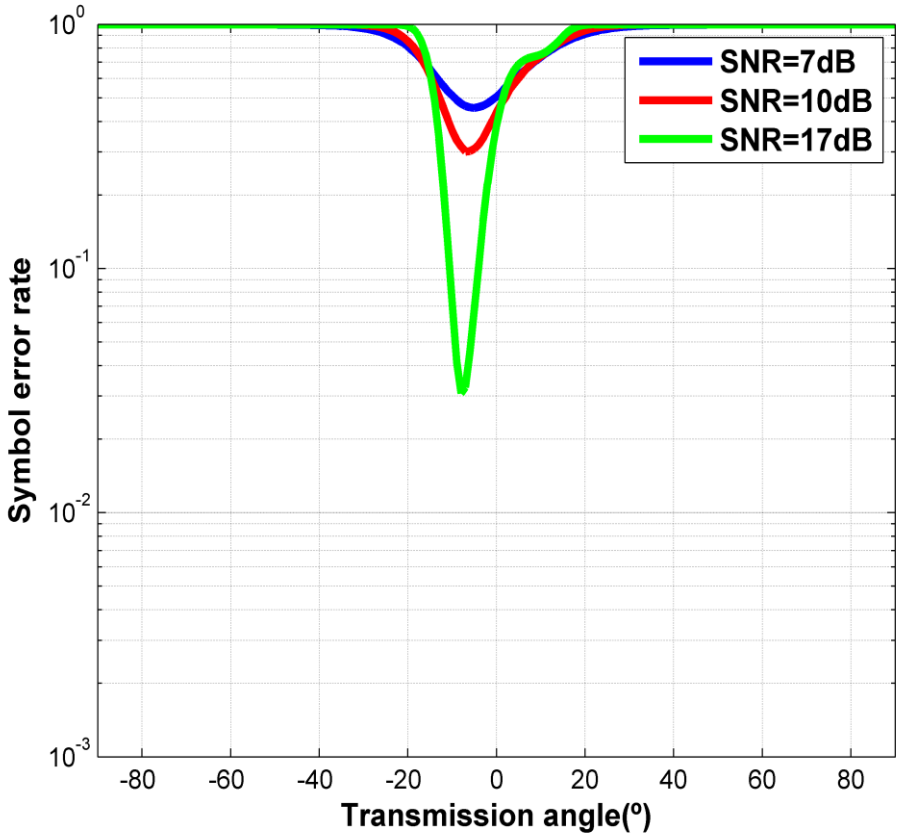

Fig. 4.10 Symbol error rate calculated based on the constellation shown in Fig. 4.9.

angle moves towards -10°, the constellation points pairs like "2 & 5" tend to separate from each other. Therefore the average Euclidean distance will increase to have a relatively low error rate performance.

The last point to mention is that the second highest peak value in Fig. 4.5 is about 24°, which can be obtained when φ_D is set to around $\pm 135°, \pm 45°$. Recalling Fig. 4.4, the ERB is 24° at $\varphi_D = 45°$. They are matched too.

The simulated ERB shown in Fig. 4.5 illustrates the relationship between the distribution of the constellation and error tolerance. The basic trend is that the larger average distance between all the constellation points, a wider ERB can be obtained.

4.3.3 The initial work to Control Error Rate Beamwidth

The motivation to control the ERB is that a narrower ERB means smaller angular range for potential eavesdropper to demodulate information with low error rate. That makes the system safer. In section 4.3.2, we demonstrated that the ERB is sensitive to constellation distribution. But the constellation distribution is not that free to control. Another factor, which affects the error rate, is the power level. SNR is proportional to the power level, and error rate is inversely proportional to the SNR. Traditionally, the power beamwidth can be reduced either by increasing the number of array elements, or increasing the distance between them. As the increase of element number also raises the system cost, we attempt to control the ERB through increasing the distance between array elements. The error rate shown in Fig. 4.11 is calculated according to a DAM transmitter configured on

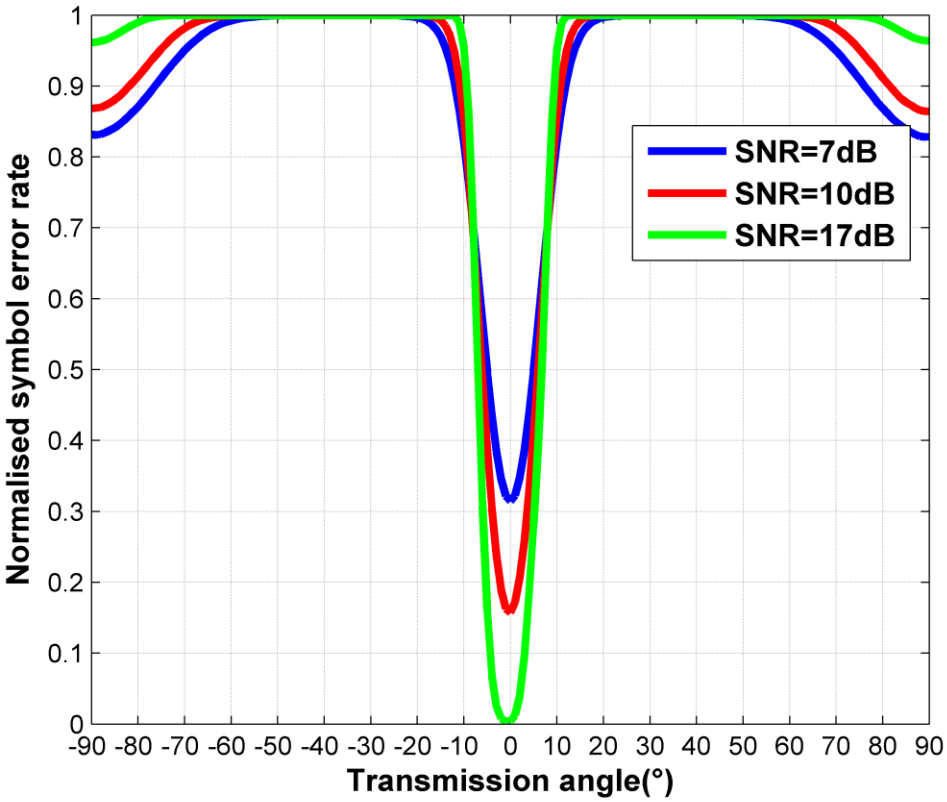

Fig. 4.11 Symbol error rate calculated when the distance between array elements is increased to 0.85λ and offset phase is set to 31°.

a 2-element array with element spacing of 0.85λ. In Fig. 4.11, the ERB is much narrower than that in Fig. 4.4. Error rate increases rapidly to level of an approximately 50% at about 5°-7°, and to almost 100% at 11°-18° varies at SNRs. The overall performance of ERB as a function of offset phase is shown in Fig. 4.12. A significant reduce of ERB is illustrated. Results shown in Fig. 4.11 & Fig. 4.12 demonstrate a fact that: the error rate beamwidth in DAM scheme can be adjusted through changing the radiation power beamwidth. A further discussion of the error rate beamwidth control is given in the next section.

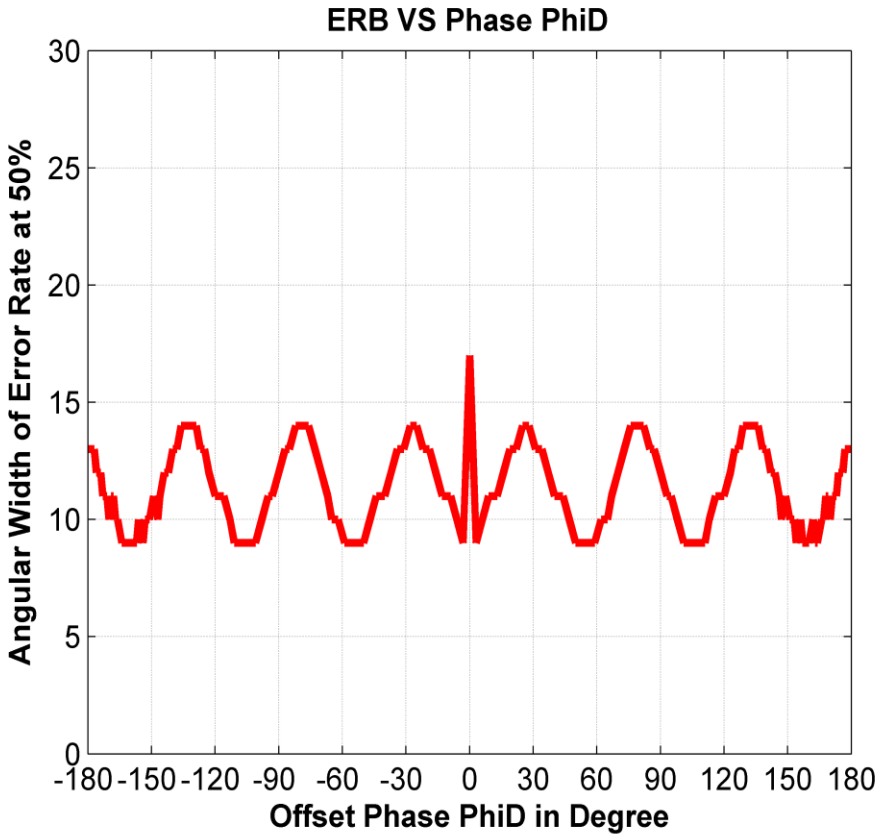

Fig. 4.12 The ERB obtained when the element spacing is increased to 0.85λ.

4.4 Superiority of DAM System in Error Rate Performance

4.4.1 Security Challenge

When considering the use of a DAM scheme as a method for providing a secure means of wireless data transmission, the most important attribute of the technique is the angular dependence of the directly imposed modulation scheme with transmission direction. In basic terms, a DAM system transmits a signal with a known form of modulation to an

intended recipient in a desired direction. The transmitted signal can then be successfully demodulated by a receiver with knowledge of the modulation scheme. As the transmit angle moves away from the intended direction, the form of the modulation imposed on the transmitted signal changes. Thus although the signal may be detectable, accurate demodulation becomes increasingly difficult. Such a process can be demonstrated by the error rate performance. However, there are limitations on the effectiveness of the approach. Two particular scenarios in which conventional DAM transmitter may be vulnerable to successful demodulation by an eavesdropper are: i) if an eavesdropper is located at angles close to the intended transmission direction; ii) if the eavesdropper is located away from boresight, but close to the transmitter so that the received SNR is much higher than that at the location of the intended recipient.

4.4.2 System Description

For illustrative purposes, consider a system based on a two element array of isotropic radiators in which each element is controlled by a 2-bit phase shifter. Next assume that the antenna is configured to transmit information using symmetrical 8-ary Phase Shift Keying (8-PSK) to an intended recipient located broadside to the array. The concept of a parallel transmitter system similar to Fig. 4.1 is considered: first, conventional baseband data modulation is assumed to be applied to the carrier signal prior to being fed to the array; second, baseband data is imparted onto the carrier by directly controlling the phase shift components of each array element. The constellation representing the 8-PSK used in both examples is shown in Fig. 4.13. For the DAM array system, each constellation point is generated by a pre-defined pairs of element phase shifts as described in Table 4.1.

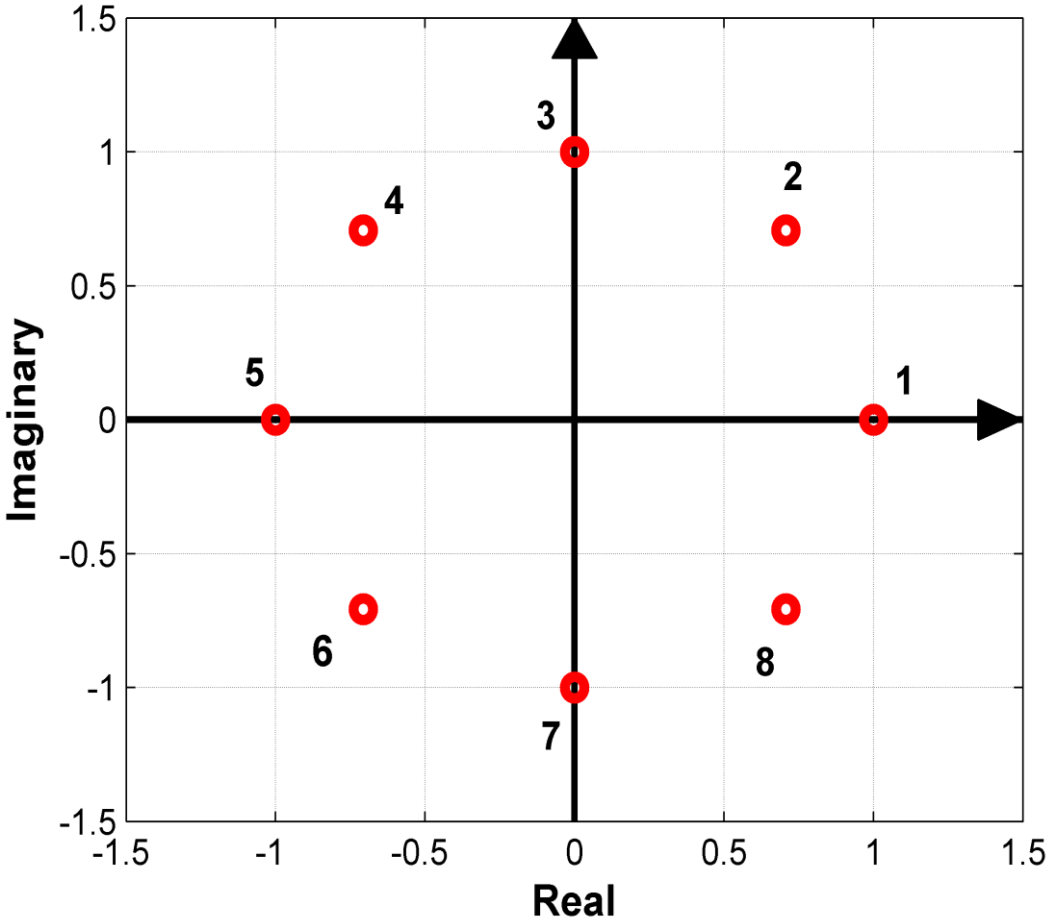

Fig. 4.13 The 8-PSK signal constellation transmitted in the direction of the intended recipient for both a conventional and a DAM array

Table 4.1 Element phase shift of the array

Constellation point	Phase shift of element 1	Phase shift of element 2
1	22.5°	-22.5°
2	22.5°	67.5°
3	112.5°	67.5°
4	112.5°	157.5°
5	-157.5°	157.5°
6	-157.5°	-112.5°
7	-67.5°	-112.5°
8	-67.5°	-22.5°

4.4.3 System Error Rate and Analysis

Next, a simple communication system is modelled, in which the element spacing of the transmit DAM array is initially set at a half wavelength. The system error rate performance is calculated as a function of receive angle in the far-field of the array. For the simulations reported here, data corresponding to each of the 8-ary PSK states are transmitted with the addition of Additive White Gaussian Noise (AWGN). The simulated received signals for both the conventional baseband modulation system and the DAM system are then demodulated according to the minimum distance decoding algorithm. In order to generate a representative system performance the symbol error rate (SER) data are calculated from 10^6 individual simulations for each detection angle and at a given signal (symbol) to noise ratio (E_s/N_0). In order to make a valid comparison between conventional base-band modulation and the DAM system both schemes adhere to the 8-PSK modulation illustrated by the constellation diagram shown in Fig. 4.13.

The symbol error rates of conventional baseband modulation and the DAM systems are calculated as a function of transmission angle in the half-plane from -90° to 90° and are shown in Fig. 4.14. There are two points to be noted for the SER plotted in Fig. 4.14. Firstly, the given signal (symbol) to noise ratio E_s/N_0 is 15dB due to the un-coded 8-PSK symbols shown in Fig. 4.13. Secondly the Y-axis has a linear scale because this research focuses on investigating the error rate performance at sidelobe angles rather than at broadside (the numerical value of the probability of symbol error for the 8-PSK modulation at broadside is approximately $2\text{x}10^{-3}$ at the given E_s/N_0 of 15dB).

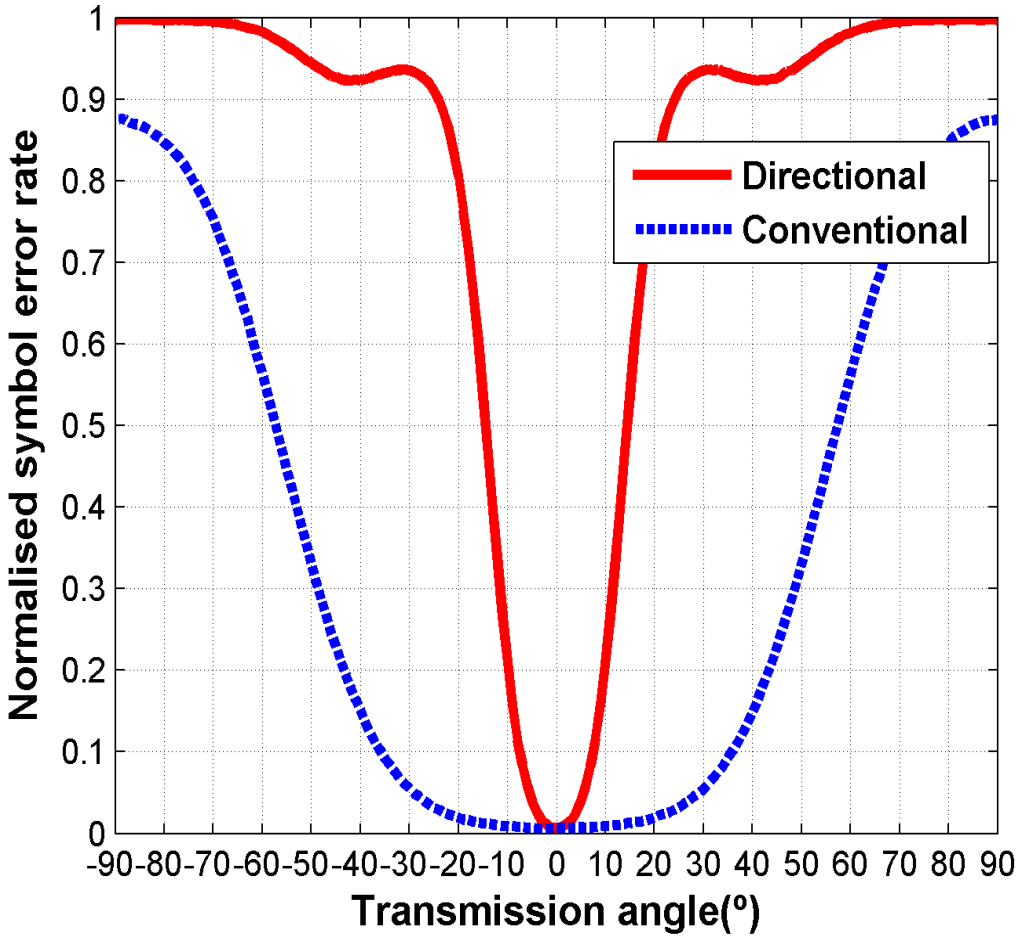

Fig. 4.14 Simulated error rates obtained for DAM (red solid line) and conventional modulation (blue dashed line) schemes for a two element array with 0.5λ spacing and isotropic radiators.

Then a benchmark is provided by Fig. 4.15, which can be referenced to Fig. 4.3-5, page 193 of "Digital Communications" written by Proakis [73]. Fig. 4.15 shows a simulated SER of both QPSK and 8-PSK in logarithmic scale with the change of SNR (E_b/N_0). In last paragraph, we mentioned that the probability of symbol error for the 8-PSK at broadside is approximately $2\text{x}10^{-3}$ at the given E_S/N_0 of 15dB. The relationship between E_S/N_0 and E_b/N_0 in this case is:

$$E_S/N_0 = E_b/N_0 + 10 * \log_{10}(\log_2 8) \quad (4.2)$$

where 8 is the number of symbols of the 8-PSK. Therefore, the E_S/N_0 of 15dB is equivalent to E_b/N_0 of 10.23dB. According to Fig. 4.15, the probability of SER is $2x10^{-3}$ when E_b/N_0 is around 10.23 dB, which matches the result mentioned in last paragraph.

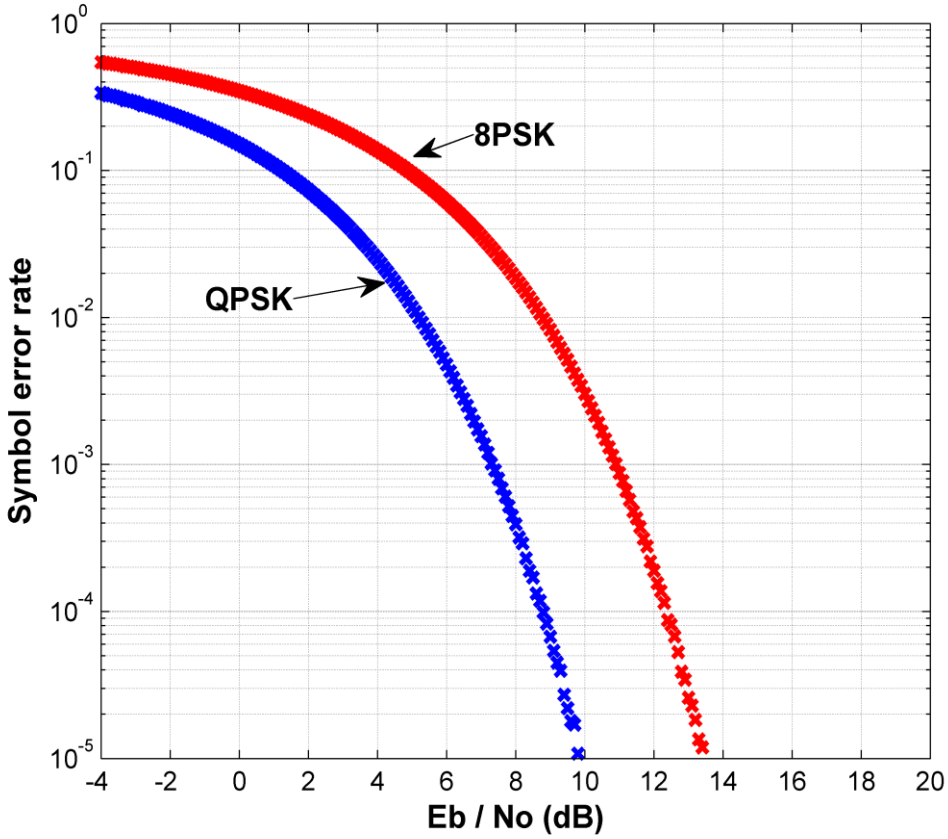

Fig. 4.15 The simulated SER of QPSK and 8-PSK in logarithmic scale varies with SNR (E_b/N_0).

Additional comments are given on the difference in the SER performance of the two systems: i) At angles away from boresight, the SER of the directly modulated system is higher than that produced by conventional baseband modulation; ii) At some transmission angles the SER is higher than 7/8(*Note that a SER of 7/8 corresponds that of conventional 8-PSK when the received power tends, to zero, i.e. a random guess*). This is because the error rate performance of the two different modulation systems are due to different processes: For conventional modulation, and in the absence of multi-path, the

error rate is purely a function of the relative amplitude of the array transmit pattern with respect to the noise level, as the signal constellation pattern is independent of angle (ignoring the trivial aspect of pattern rotation). For the DAM system however, the situation is more complex as the angular error rate performance is a function of both the radiated signal power level and the angular dependence of the signal constellation pattern. The difference in two processes is illustrated with the aid of Fig. 4.16 and Fig. 4.17. The radiation patterns corresponding to the different constellation points of the DAM transmission are shown in Fig. 4.16, along with a comparable power pattern of a conventional transmitter. From Table 4.1, the phase sets that map to the points "1,3,5,7" are different from those that map to the points "2,4,6,8". This process results in two

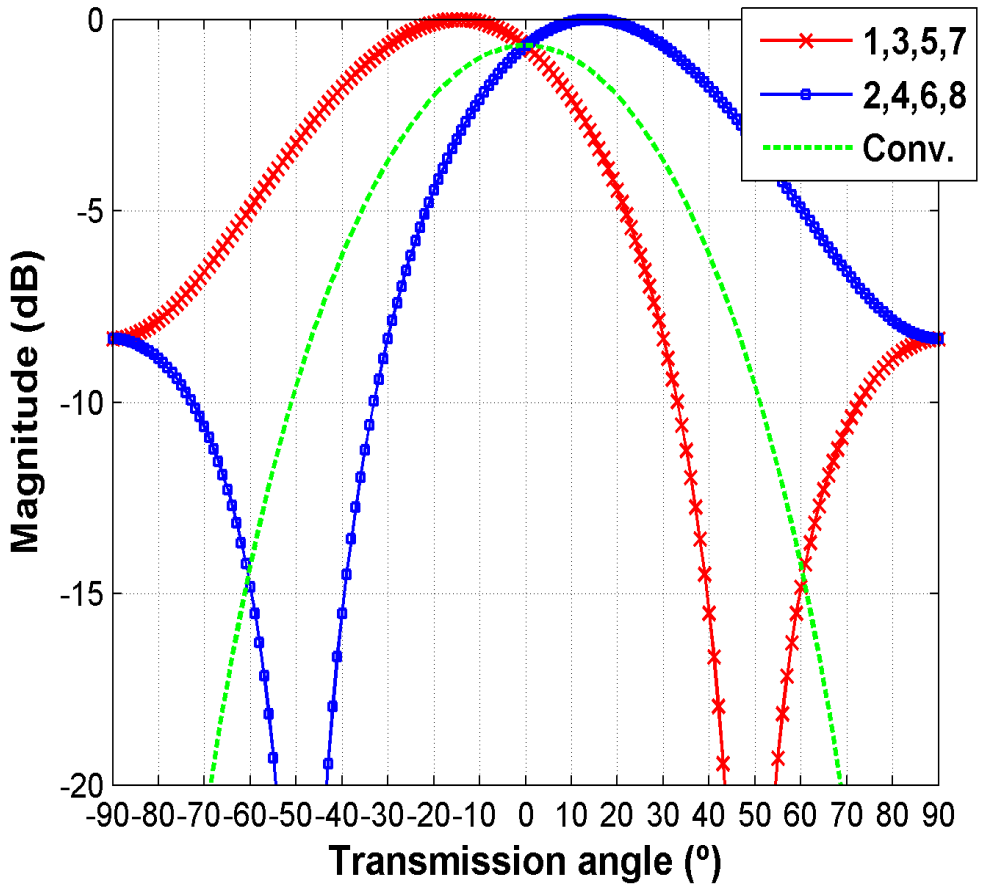

Fig. 4.16 Radiation patterns of DAM transmitter when sending constellation points "1, 3, 5, 7" (red crossed) and "2, 4, 6, 8" (blue squared), and relative magnitude of the radiation pattern sent by a conventional transmitter (green dashed) to achieve the same power level at broadside

different radiation patterns (the red squares & blue crosses as shown in Fig. 4.16). An important point to note here is that the DAM system does not radiate maximum power to the broadside recipient. Hence to make a valid comparison with the SER performance of a conventionally modulated system (i.e. the constellation patterns sent to broadside are exactly the same), power of conventional transmitter (green dashed line) is reduced to ensure that it matches the power radiated by DAM system in the boresight direction. It is clear that the SER performance of the conventionally modulated system (Fig. 4.14) is basically a direct response to its transmit power pattern (Fig. 4.16), but that the SER of DAM system shows no obvious response to its transmit power pattern. To further explain this, Fig. 4.17 illustrates the received noiseless constellation patterns at an angle of 75° compared to the ideal 8-PSK pattern. The transmission angle of 75° is chosen for illustration because according to Fig. 4.14, the SER of DAM system approaches 100% while that of conventional modulated system is still below the theoretical upper bound of 7/8. Referring to Fig. 4.17(a), the noiseless constellation pattern received from the traditional baseband modulated system maintains the shape of 8-PSK, but with a significantly reduced power level (also shown in Fig. 4.16) and the theoretical SER has an upper bound of 7/8 when the signal power is approaches zero. However in the DAM system (Fig. 4.17(b)), the power level of constellation at 75° is more than 10dB greater than that of the corresponding traditional 8-PSK constellation, but the new mapping of DAM constellation is significantly distorted from that of the original 8-PSK. Hence, for an undesired recipient at 75°, who has no knowledge of the new mapping relationship, but uses the traditional 8-PSK constellation as a reference for demodulation, the SER will be significantly increased and could exceed the 7/8 bound.

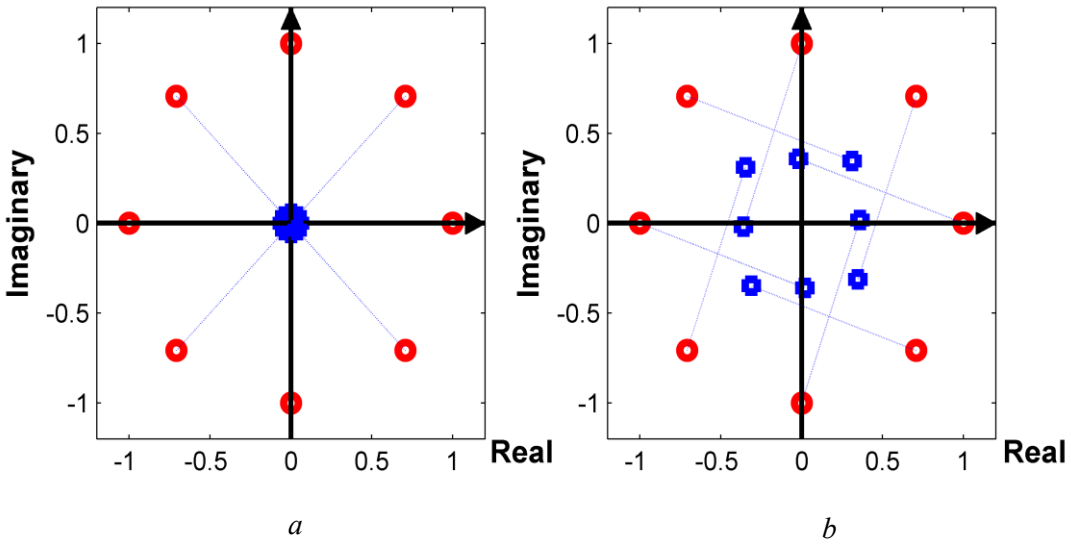

Fig. 4.17 Constellation diagrams showing a comparison between ideal 8-PSK (red circles) and received noiseless constellation pattern (blue squares) at 75° in a) conventionally modulated system; b) directional modulated system.

4.4.4 A Potential Eavesdropper Located at an Angle Close to the Intended Transmission Direction

This first example is presented to illustrate how the angular dependence of the DAM system constellation can be exploited to minimise interception by an eavesdropper located close to the intended recipient. From Fig. 4.14, it is clear that the DAM system exhibits a much smaller modulation error rate beamwidth than that of the conventionally modulated system. The dramatic difference in the modulation ERB of the two systems is a direct consequence of the angular dependence of the signal constellation generated by the DAM approach as discussed in the previous section. To further reduce the modulation ERB of the antenna array system the author takes the intuitive approach of increasing the spacing between the array elements, as this reduces the conventional power beam width of the main lobe of radiation. Unfortunately, this approach results not only in traditional,

power-pattern, grating lobes but also in "modulation" grating lobes - angles at which the signal constellation repeats its boresight distribution. As an example, Fig. 4.18 shows the corresponding system error rates for a two-element array with two wavelength element spacing. In this example, the boresight ERB has been reduced from 102º and 29º to 22º and 7.5º for the conventional and the DAM systems respectively, but with the penalty of generating grating lobe error rate regions at which the error rate approaches that at the intended boresight direction.

To reduce, or even eliminate the error rate grating lobe regions shown in Fig. 4.18 the

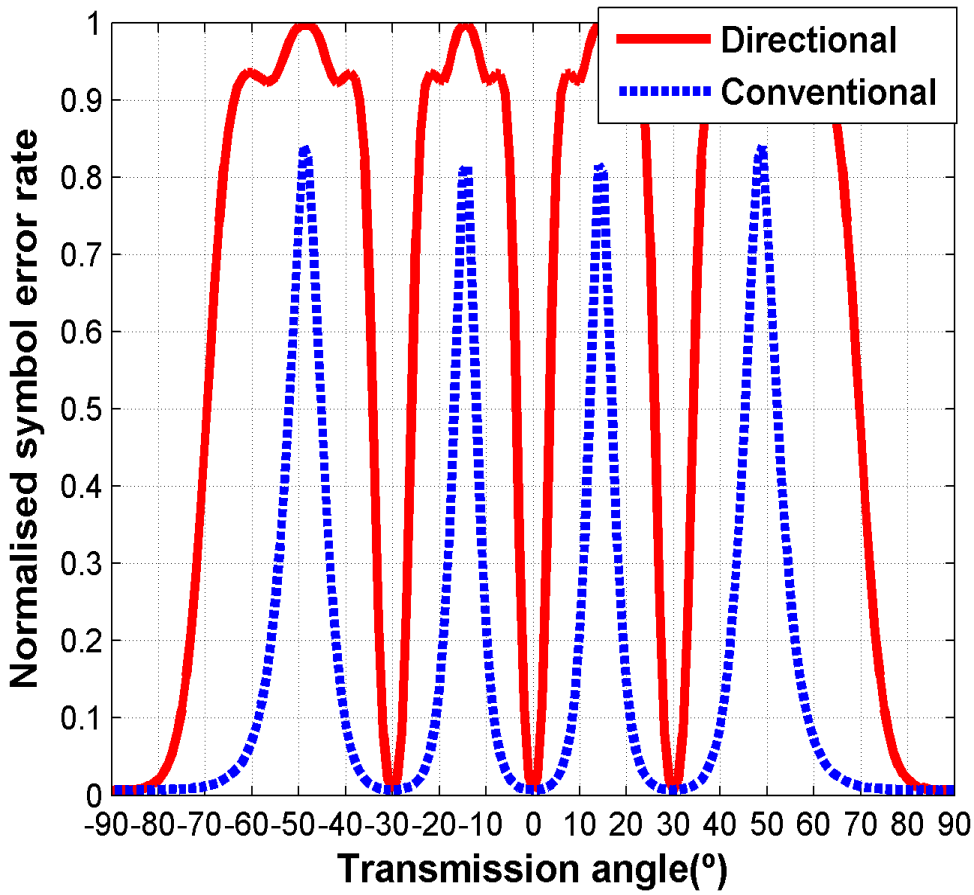

Fig. 4.18 Simulated error rates obtained for DAM (red solid line) and conventional modulation (blue dashed line) schemes for a two element array with 2λ spacing and isotropic radiators.

assumed isotropic radiators may be replaced with more directional array elements. If elements are used which have a directive main beam response and low sidelobes (or even nulls) in the angular directions corresponding to the grating lobe directions, then by using the principle of pattern multiplication, the directional error rate of the system can be enhanced without introducing error lobe regions. To illustrate this scenario, re-consider the above example of a two element array with two wavelengths spacing but with the isotropic elements replaced by waveguide horns with 2λ wide apertures [64]. The results for these examples are shown in Fig. 4.19 where it is observed that the grating lobe error

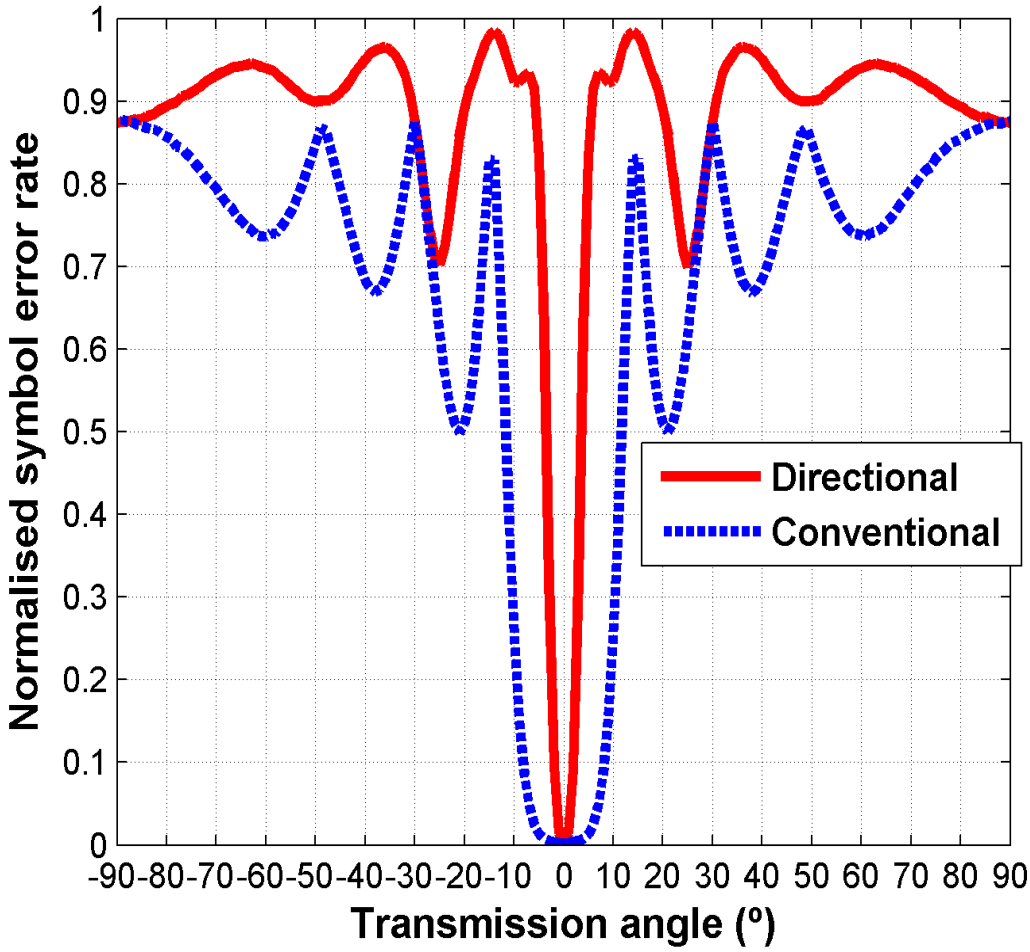

Fig. 4.19 Simulated error rates obtained for DAM (red solid line) and conventional modulation (blue dashed line) schemes for a two element array with 2λ spacing and directive elements

rate angles associated with both the conventional and the DAM modulation schemes have been suppressed. Also, the error rate performance of the DAM scheme compared to the conventional baseband modulation scheme shows improved error rate characteristics at angles away from boresight and exhibits a significantly narrower detection bandwidth at boresight (7º compared to 20º). Obviously the error rate beamwidth can be further reduced by increasing the element spacing and using correspondingly larger aperture antennas as the array elements. As an example, Fig. 4.20 shows the error rate performance of an array with 6λ element spacing and 6λ wide aperture elements for both conventional and DAM transmission systems. From Fig. 4.20, it is observed that the ERB have been reduced to 7° and 2.6° for the conventional and DAM schemes respectively. The main conclusion to draw from the results shown in Fig. 4.14, Fig. 4.18, Fig. 4.19 and Fig. 4.20, is that the DAM array system has a narrower angular detection region than that of the conventionally modulated system, so the possibility of successful demodulation from potential eavesdroppers located at angles very close to the intended transmission direction is significantly reduced. Another conclusion that can be draw from Fig. 4.14, Fig. 4.19 and Fig. 4.20 is that the DAM array system has a higher error rate performance than conventional system at almost all transmission angles away from broadside.

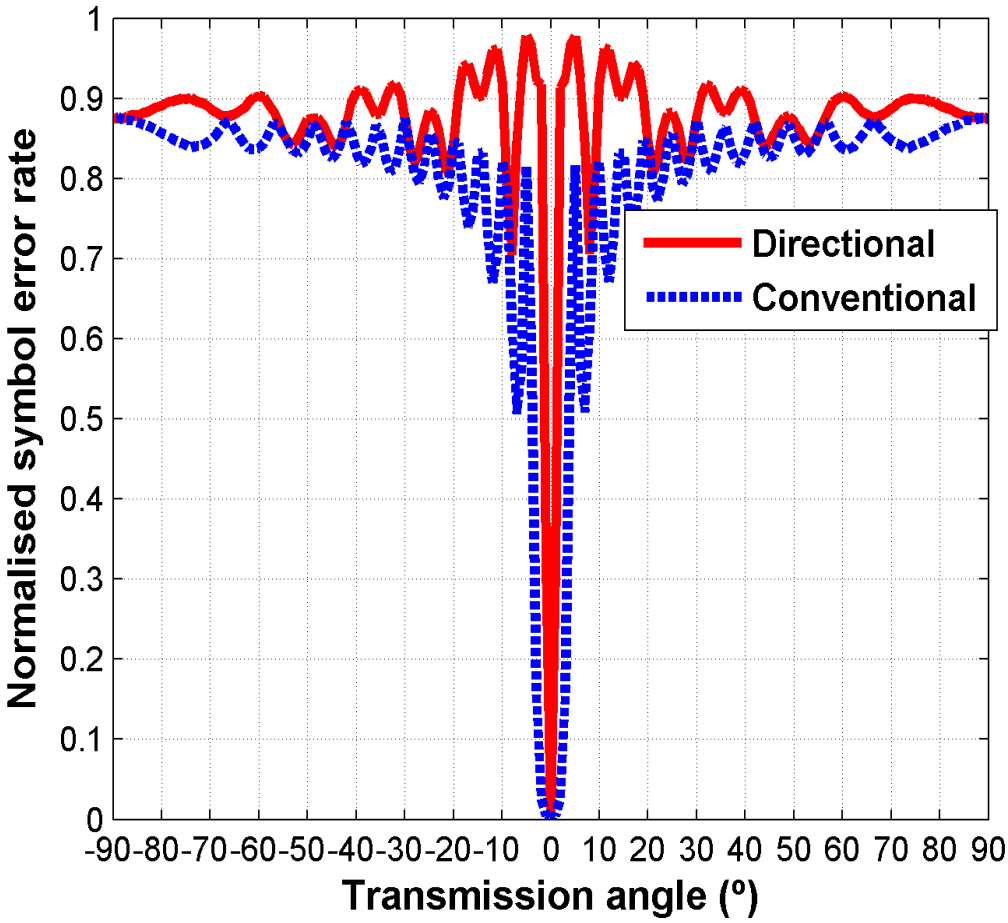

Fig. 4.20 Simulated error rates obtained for DAM (red solid line) and conventional modulation (blue dashed line) schemes for a two element array with 6λ spacing and directive elements

4.4.5 A Potential Eavesdropper Located Close to the Transmitter

This second example is presented to illustrate how the DAM system constellation can minimise the possibility of interception by an eavesdropper located closer to the transmitter than the intended recipient. In this situation the signal power received by eavesdropper may be several dB higher than that received by desired recipient. To investigate this scenario, the author first examines and compares the effect of the system E_s/N_0 on the error rate performance of the two modulation schemes. To illustrate this

difference, the previous example of a two element array with 2λ spacing is used for illustration again. Consider first the case of transmitting 8-PSK using conventional modulation for boresight E_s/N_0 levels of 15dB and 20dB respectively. The simulated error rate versus transmission angle for this example is shown in Fig. 4.21. The main points to note from Fig. 4.21 are that the error rate performance around the grating lobe angles is dramatically reduced – for example at about ±20°, the error rate drops from approximately 50% to 25%. This indicates that a potential eavesdropper located away from boresight, but at a grating lobe direction and closer to the transmitter than the intended recipient (so that the received power level is higher) could potentially

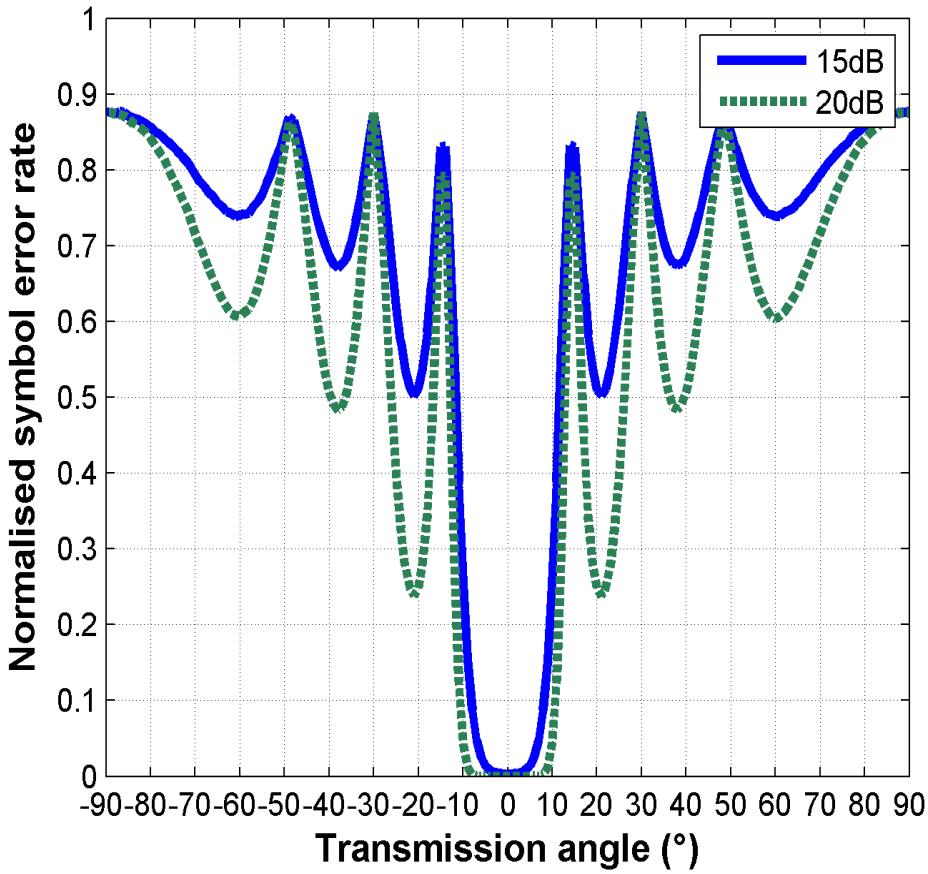

Fig. 4.21 Simulated error rates obtained for conventional modulation using a two-element array with an element spacing of 2λ for E_s/N_0 =15dB (solid line) and E_s/N_0=20dB (dashed line)

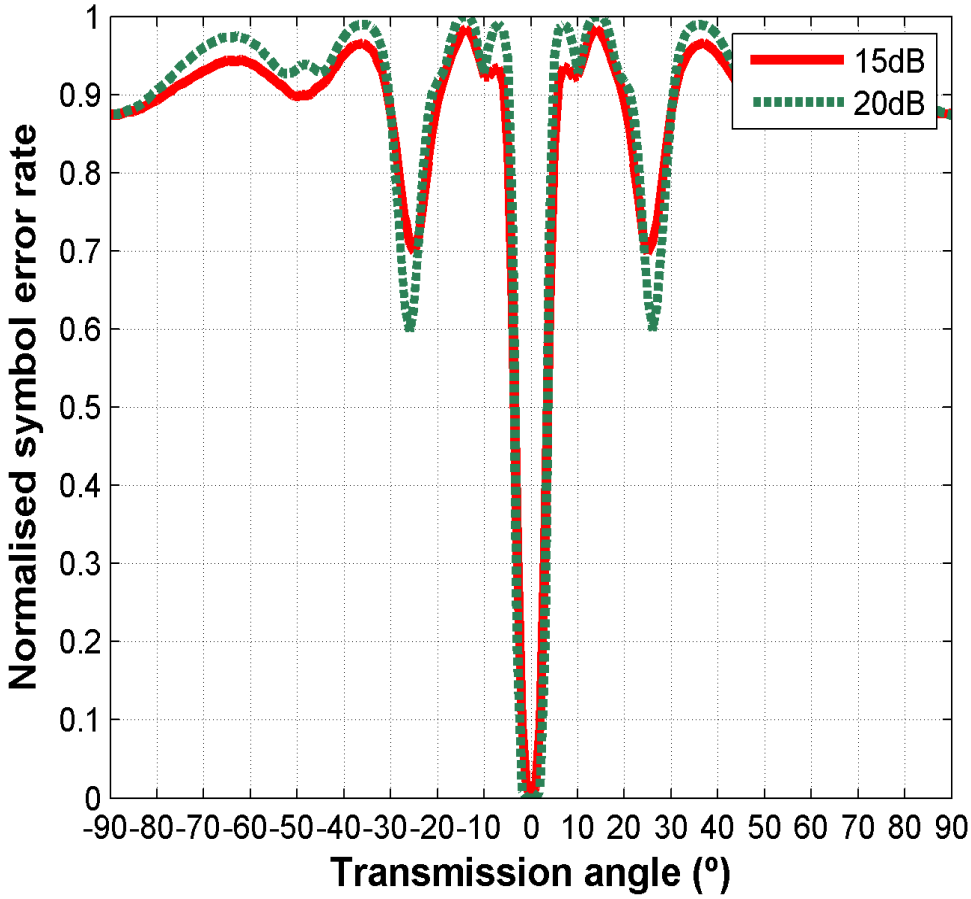

Fig. 4.22 Simulated error rates obtained for DAM using a two-element array with an element spacing of 2λ for E_s/N_0=15dB (solid line) and E_s/N_0=20dB (dashed line)

demodulate the transmission. Next consider a similar example but with the system configured to transmit DAM. The results of this simulation are given in Fig. 4.22. And it is observed that not only does the DAM scheme result in a much narrower ERB at boresight, but it also provides much higher error rates at the grating lobe directions compared to conventional modulation scheme. It is also noted that the fluctuations of error rate in DAM system are much smaller than that observed in the conventional modulation system. This property provides enhanced security against eavesdroppers located close to the transmit antenna.

4.5. Summary

In this chapter, the additional security provided by a DAM scheme was discussed. A new assumption about reference constellation recognition was introduced first as this recognition scheme can utilise the properties of DAM in providing secure communications much better than conventional methods. Next minimum distance decoding was selected as the decoding algorithm and simulated symbol error rate of an example DAM transmitter was calculated and analysed. In the end, a conventional method of reducing the range of interception with low error rate was demonstrated on DAM transmitter.

Chapter 5

Simultaneous, Multi-channel, Spatially Directive Data Transmission Using Direct Antenna Modulation

As indicated in Chapter I, conventional multiplexing methods can share a single channel in the time domain or the frequency domain. In this chapter, a space multiplexing scheme using direct antenna modulation (DAM) based on an array with 2-bit phase control is presented. By switching each element phase properly, the line-of-sight (LOS) communication channels generated by the scheme can be independent from each other at various directions. This method considers space as an additional domain for multiplexing when desired receivers are spatially separated.

5.1 Original Contribution

Compared to the work reported in [18], the author proposed a method which has two main differences:

First, instead of using continuous phase shifters [18] [19], the DAM transmitter proposed in this research utilises discrete 2-bit phase control which makes the hardware implementation relatively cheap, simple and more practical. The required 2-bit quadrature phase control can be achieved using diode phase shifters [29], hybrids or mixers as described in [24], or microelectromechanical systems (MEMS) phase shifters [74]. However, as a trade-off, the system has limited phase shift states, which constrains the number and locations of the recipients who are able to receive independent information. Thus the system based on 2-bit phase control is more suited to scenarios where the number and locations of desired receivers are pre-known by the transmitter and do not change in real time. Nevertheless, this limitation can be addressed by using higher order digital phase shifters if necessary.

Second, the use of 2-bit phase control also simplifies the element phase state calculations and alleviates the need to use other optimisation techniques to calculate the element phase shifts [18] [16] [21]. Instead, as the phase states are constrained, a simple predictive algorithm is combined with analytic results to calculate the required phase states for a given operational requirement. The most exciting aspect of this method is that it uses an exhaustive search to find the entire independent constellation. With this feature, a system designer is allowed to choose the most suitable transmission plan dependent on a balance between requirements and system cost.

5.2 Theoretical Background

5.2.1 System Description

Initially, and for clarity, let us consider the generation of DAM using a conventional approach based on an array with independent element phase control. Recalling the array factor of an N-element linear phased array with uniform amplitude again:

$$AF(\theta) = \sum_{n=1}^{N} e^{-j\left[(n-1)\frac{2\pi}{\lambda}dsin\theta+\beta\right]}$$

$$n = 1,2,\cdots N \tag{5.1}$$

where λ is the wavelength in free space, d refers to the distance between elements, θ is the transmission angle (0° is normal to the array), and β is a progressive phase. In the concept of a DAM system, it is more convenient to replace β with a time dependent phase shift φ(t). Therefore the array factor of DAM array system can be expressed as:

$$AF(\theta,t) = \sum_{n=1}^{N} e^{j\varphi_n(t)} \times e^{-j\left[(n-1)\frac{2\pi}{\lambda}dsin\theta\right]}$$

$$n = 1,2,\cdots N \tag{5.2}$$

Assuming that the elements radiate isotropically and with unit amplitude, the far-field signals generated by such an N-element DAM array can be simply represented by the array factor expressed by (5.2). As indicated in Section 5.1, only 2-bit phase control is used in the DAM array system. Thus the phase shift, i.e. the value of $\varphi_n(t)$ in (5.2), can be chosen from [0°, 90°, 180°, 270°].

For a general DAM system based on an N-element linear array with 2-bit phase control, the schematic structure is shown by Fig. 5.1, and two important properties can be identified:

1) Theoretically, up to 4^N different phase combinations can result in 4^N discrete signals points on a constellation diagram. However, at some special angles, the number of distinct constellation points reduces to $(N+1)^2$. These transmission angles are termed as angles-of-convergence (AoC) in this work.
2) The common phase interval of [0°, 90°, 180°, 270°] is 90°, i.e. $\pi/2$. Due to the periodicity, adding or subtracting a phase shift that is an integer multiple of $\pi/2$ does not result in a new phase.

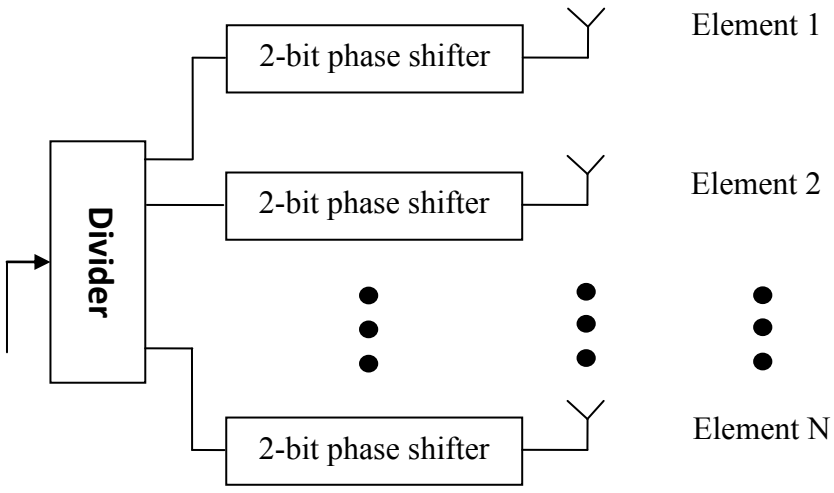

Fig. 5.1 Schematic structure of the DAM transmitter consisted of an N-element array with 2-bit phase control.

According to the properties listed above, 4^N groups of phase combinations result in only $(N+1)^2$ distinct constellation points when the following condition is met:

$$\frac{2\pi}{\lambda} d \sin\theta = \frac{\pi}{2} K$$

$$K = \cdots -2, -1, 0, 1, 2 \cdots \tag{5.3}$$

As a result, the reduced signal constellation pattern received at the AoC can be expressed as:

$$AF_r(K,t) = \sum_{n=1}^{N} e^{j\left[\varphi_n(t) - (n-1)\frac{K\pi}{2}\right]}$$

$$n = 1,2, \cdots N; K = \cdots -2, -1, 0, 1, 2 \cdots \tag{5.4}$$

And the AoC can be calculated from (5.3) as:

$$\theta = 57.3 sin^{-1}\left(\frac{K\lambda}{4d}\right) \qquad deg$$

$$K = \cdots -2, -1, 0, 1, 2 \cdots \tag{5.5}$$

To illustrate the properties 1) and 2), a specific example is given based on a 4-element DAM array transmitter with element spacing of half wavelength. According to property 1), at the AoC, the signal constellation pattern will reduce from 256 to 25 points. Also according to (5.5), the AoC are determined by the integer value of K, and can take specified values of [-90°, -30°, 0°, 30°, 90°] for K = -2, -1, 0, 1, 2. A simulated constellation diagram is shown in Fig. 5.2, which shows the constellation patterns received at angles of 0° (broadside), 4° and 30° respectively. Firstly at 4° (not an AoC), 256 distinct signals (blue dots) can be observed. Secondly at angles of 0° and 30° (AoC),

only 25 discrete signals can be distinguished (if the signal located at origin is also calculated). At the AoC, some system phase combinations result in identical signals. Thus when the observation angle is moved from a non-AoC to AoC, the number of distinct points is reduced, which is predicted by property 1). Thirdly, the constellations received at 0° (red circles) and 30° (green crosses) coincide. However, it should be stressed that although these constellations occupy the same locations, they are totally independent in terms of baseband data mapping.

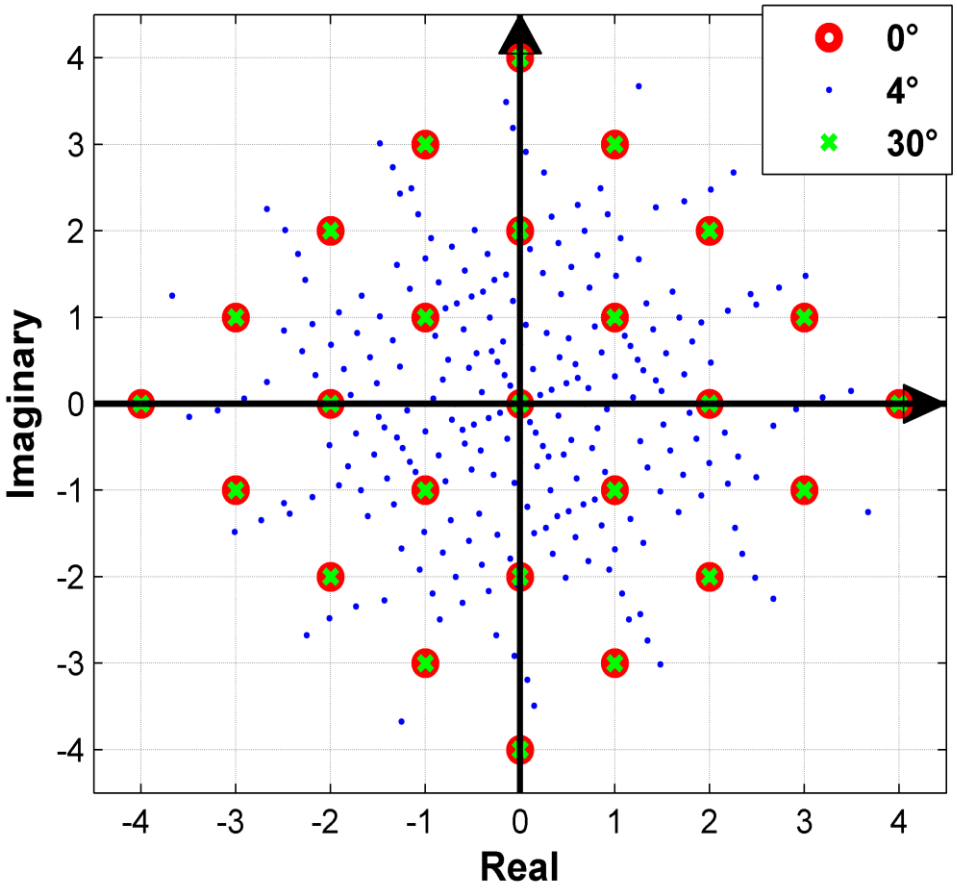

Fig. 5.2 Constellation pattern of signals received in 0°, 4° and 30° respectively when the DAM transmitter is consisted of a 4-element array with element spacing of λ/2.

5.2.2 Theoretical Analysis

The work reported in [21] used convex optimization to converge the constellation points as much as possible. Now in the transmitter system described by Fig. 5.1, the angles where the overlapping happens are deterministic, i.e. AoC. To explain how space multiplexing can be achieved, we firstly consider communication between a transmitter and a desired receiver located at an AoC, θ_A. In this case, up to 4^N different element phase configurations will result in $(N+1)^2$ discrete signals on constellation diagram (including the origin). As a result, there must be some integer number (S for example) of constellation points, each of which can be generated by more than one (R for example) element phase configuration. Such a scenario can be illustrated by Fig. 5.3(a), in which a matrix $\overline{A}$ with S columns and R rows contains all the relevant phase configurations for the array system. Thus to generate any constellation point for the receiver at θ_A, the transmitter only needs to select an arbitrary phase configuration from the corresponding column.

Next, another independent desired receiver is located at a different AoC, θ_B. There will be a similar matrix $\overline{B}$ as shown in Fig. 5.3(b), which consists of I rows and J columns. Again, to modulate any constellation point for the receiver at θ_B, the transmitter can select an arbitrary element from the corresponding column.

Now, assume that the entire set of system phase combinations consist of a complete set X. Matrix $\overline{A}$ and Matrix $\overline{B}$ can be seen as two subsets of X. When these two subsets overlap, then the system phase combinations contained within the shadow area as depicted in Fig. 5.3(c) can be used to generate constellation points for both two receivers located at θ_A and θ_B simultaneously. The required phase combinations can also be described by a matrix C with P (P$\leqslant$J) rows and Q (Q$\leqslant$S) columns as shown in Fig.

5.3(d), whose columns are subsets of matrix A and rows are subsets of matrix B. From matrix C, it is clear that the information imposed on the constellation points sent to angle θ_A can be completely independent of those sent to angle θ_B.

CP at θ_A: CP_1 CP_2 ⋯ CP_S

$$\overline{A} = \begin{bmatrix} A_{11} & A_{12} & \cdots & A_{1S} \\ A_{21} & \ddots & & \\ \vdots & & A_{rs} & \vdots \\ A_{R1} & & \cdots & A_{RS} \end{bmatrix}$$

-CP is short for constellation point

- A_{rs} represents an arbitrary combination of phase shift of each array element for a N-element array.

Fig. 5.3(a)

CP at θ_B: CP_1 CP_2 ⋯ CP_J

$$\overline{B} = \begin{bmatrix} B_{11} & B_{12} & \cdots & B_{1J} \\ B_{21} & \ddots & & \\ \vdots & & B_{ij} & \vdots \\ B_{I1} & & \cdots & B_{IJ} \end{bmatrix}$$

Fig. 5.3 (b)

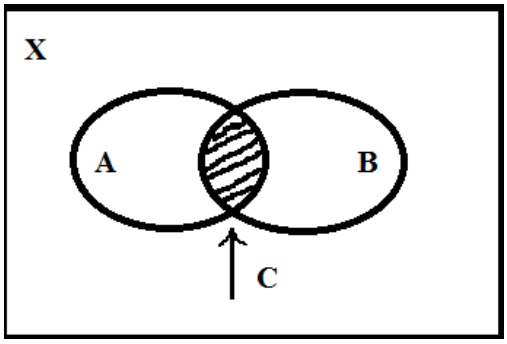

Fig. 5.3 (c)

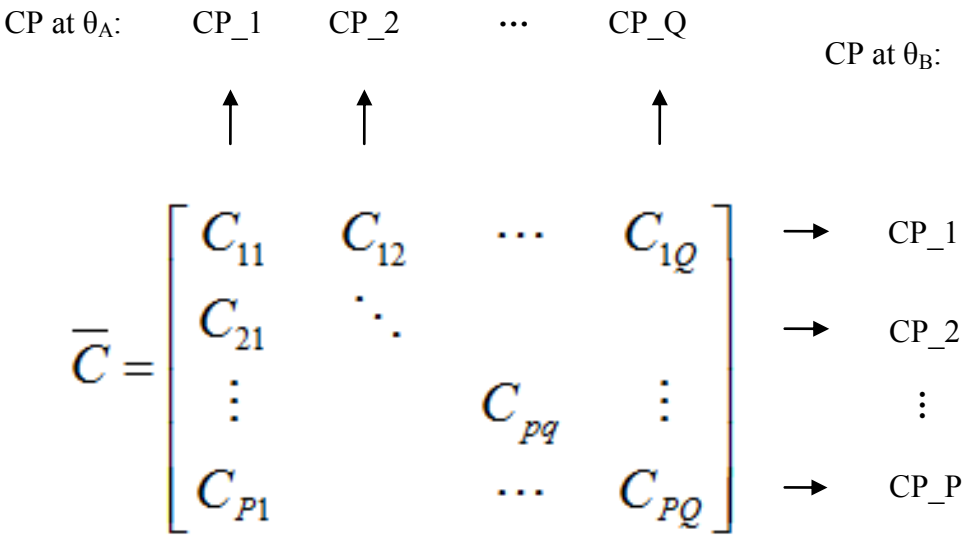

Fig. 5.3 (d)

Fig. 5.3 Matrix of element phase configurations which can support independent communication (a) to θ_A only; (b) to θ_B only; (c) to both angles in the "set" format and (d) to both angles simultaneously in matrix format.

The Venn diagram representation shown in Fig. 5.3 provides a convenient way to interpret the proposed method for achieving space multiplexing. It should be noted, however, that the analysis based on Fig. 5.3 is only valid at AoC given by equation (5.5).

5.3 Space Multiplexing

Based on the theoretical analysis (Section 5.2.2), a general algorithmic method can be introduced, which can be used to provide solutions of system phases for achieving independent and simultaneous communication to multiple recipients at different directions.

5.3.1 Introduction to the Algorithmic Method

The algorithmic method is first demonstrated by assuming a transmit array with N-elements and inter-element spacing d. The phase of each element can be switched by a 2-bit digital phase shifter. The AoC set can be calculated by equation (5.5), which also gives the maximum number of possible receivers R. Users can pre-define the signal patterns they expect to utilize as M-ary or M-QAM. A detailed description to the algorithmic method is given below along with a flow chart shown in Fig. 5.4.

- *Step 1. System Initial State:*

  Select one angle from AoC set as the first required transmission direction. The full constellation diagram at this selected AoC is then generated according to pre-defined system parameters N and d. The user is then allowed to select any M-ary/M-QAM sub constellation as their signal pattern. In this step, the computational complexity can be reduced because only partial phase sets which correspond to the selected signal pattern (M-ary/M-QAM) will be included in subsequent computations (an example to illustrate this process will be given later).

- *Step 2. Next desired AoC:*

  Select the next AoC as the required transmission direction to transmit independent information.

- *Step 3. Exhaustive computation*

  An exhaustive computation is conducted to find all the potential signal points which can be generated for the receiver at AoC chosen in step 2. Here potential means all the returned constellation points can be sent independently and simultaneously while still maintaining the M-ary/M-QAM sent to receiver at the initial AoC selected in Step 1.

- *Step 4. Decision*

  If at least M valid constellation points are found in step 3, the user can choose a signal pattern (M-ary/M-QAM) for AoC_receiver selected in step 2. If additional AoC are required, steps 2-4 are repeated as necessary.

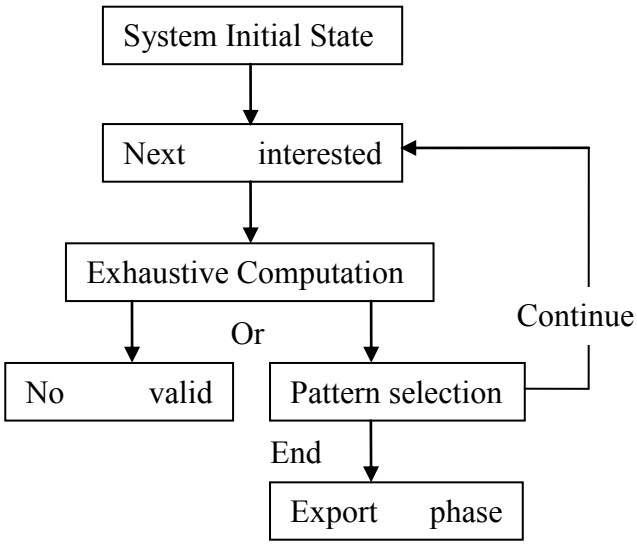

Fig. 5.4 The flow chart of the algorithm used to determine constellation points.

Next, a specific example is given to illustrate the algorithm. The transmit antenna in this example consists of an array of 4 elements, with half a wavelength spacing. Using equation (5.5), the AoC set includes {±90°, ±30°, 0°}. Two receivers "Rx_A" and "Rx_B" are positioned at 0° (broadside) and 30° respectively and both signal transmissions are chosen to be 4-ary constellations.

Step1: assume the users select 0° as their first transmission angle. The total possible constellation points that can be generated by the transmit array is displayed in Fig. 5.5. The users can now choose any 4-ary signal patterns for transmission. The numbers in Fig. 5.5 indicate potential "resource" each constellation point possesses. Here, the term "resource" refers to the number of different system phase combinations which generate the same signal point. In this example, assume the users choose the four inner most signal points "ABCD" as their symbol pattern for broadside recipient Rx_A. Each symbol has 24 resources. Therefore, among the entire 256 (4^4) system phase sets, only 96 (24x4) of them will be included in subsequent computation, thus reducing computational complexity. The system initial state is generated, and the system phase sets “owned” by the selected symbol patterns "ABCD" consists of a matrix with 4 column and 24 rows, which can be related to the matrix described in either Fig. 5.3(a) or (b).

Step 2: The second AoC associated with Rx_B is 30°.

Step 3: All the independent constellation points generated by the 4-element transmit array for Rx_B at 30° are computed and are displayed in Fig. 5.6. These 12 constellation points are described as “independent” because they are selected according to the rule that: each can be generated by at least 4 different system phase combinations, and simultaneously these 4 phase combinations can be used to generate symbols “ABCD” at broadside.

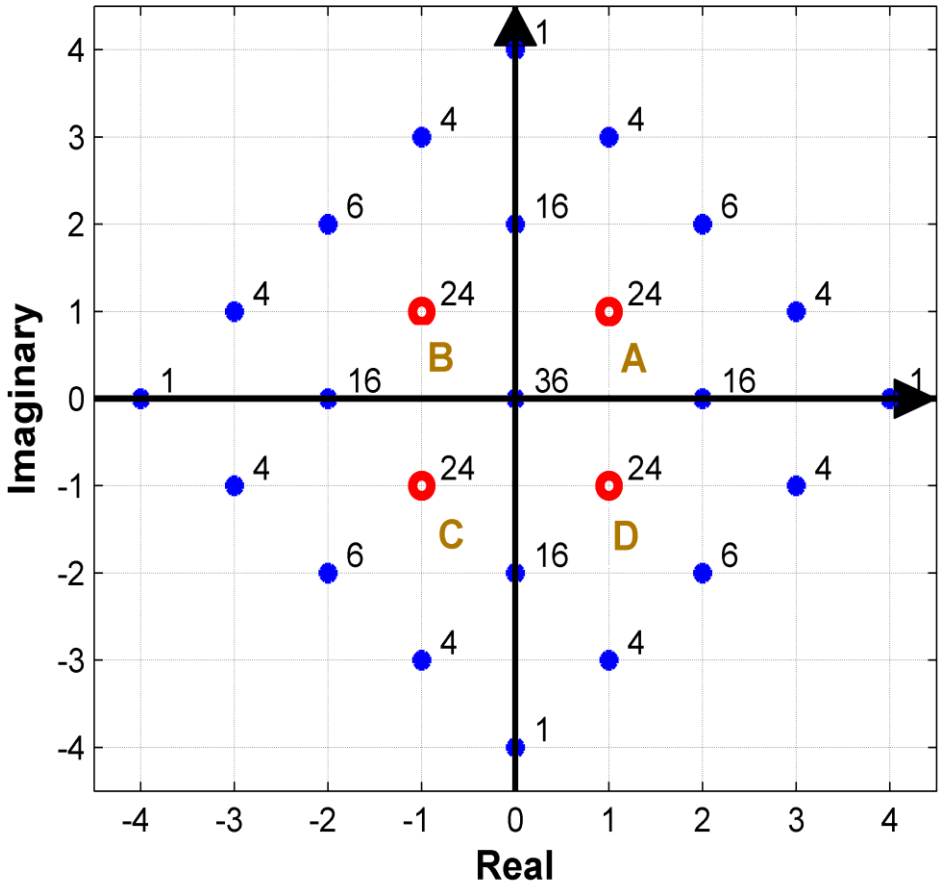

Fig. 5.5 Constellation patterns of signals received at 0° when the DAM transmitter consists of a 4-element array with element spacing of λ/2.

Step 4: As 12 possible constellation points are found in step 3, the users are free to select a 4-ary pattern for Rx_B. In this example, assume they choose points "1234" as the symbol pattern for recipient Rx_B. The derived 16 phase combinations provide a solution for space multiplexing toward 0° and 30° with symbol patterns "ABCD" and "1234" respectively. As described in Fig. 5.3(d), they form a matrix with 4 columns and 4 rows as listed in Table 5.1.

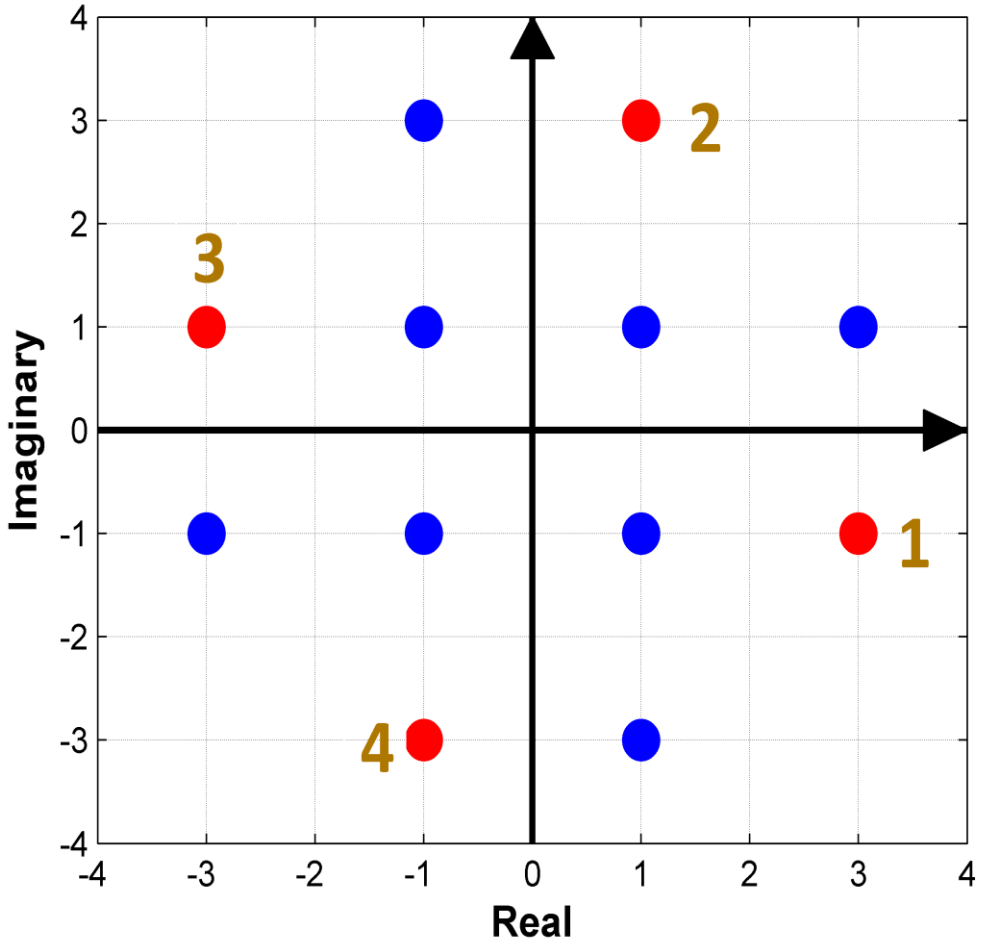

Fig. 5.6 Constellation patterns of signals received at 30° when the DAM transmitter is consist of a 4-element array with element spacing of λ/2.

Table 5.1 System phase combinations

Phase Comb	A	B	C	D
1	0,90,90,270	0,90,180,180	270,90,180,270	0,0,180,270
2	90,90,270,0	90,180,180,0	90,180,270,270	0,180,270,0
3	90,270,90,0	180,180,0,90	180,270,270,90	180,270,0,0
4	270,0,90,90	180,0,90,180	270,270,90,180	270,0,0,180

From Table 5.1, the transmitter can always find a suitable set of system phase combination to simultaneously send independent symbols to Rx_A and Rx_B. For illustrative purpose, two arbitrary symbol sequences are modelled for the receivers as shown in Fig. 5.7. Assume the information to be sent to broadside receiver is the symbol sequence "ABCD DBAA". At the same time, the transmitter needs to send "2133 4114" to the receiver at 30º. Thus the concurrent sequence for the transmitter is "A2 B1 C3 D3 D4 B1 A1 A4". All the relevant system phase combinations can be easily found from Table 5.1.

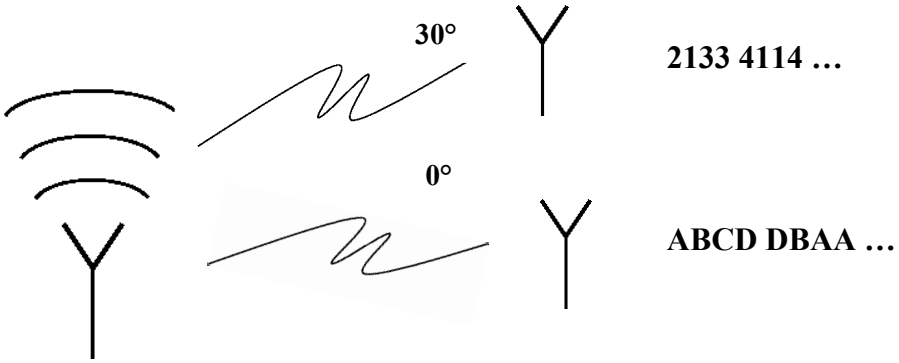

	A2	B1	C3	D3	D4	B1	A1	A4 …
Element1	**90**	**0**	**180**	**180**	**270**	**0**	**0**	**270**
Element2	**90**	**90**	**270**	**270**	**0**	**90**	**90**	**0**
Element3	**270**	**180**	**270**	**0**	**0**	**180**	**90**	**90**
Element4	**0**	**180**	**90**	**0**	**180**	**180**	**270**	**90**

Fig. 5.7 A possible transmission scheme for a DAM transmitter to send independent symbol streams to receivers at 0° and 30° simultaneously.

5.3.2 Other Transmission Schemes

Three further examples are presented. For the first scenario, we assume independent QPSK transmissions to receivers located at ± 45º. In this case ± 45º must be included in the AoC. According to equation (5.5), suitable element spacing is 0.354λ. The minimum number of array elements in this example is 4. As shown in Fig. 5.8(a), the two selected constellation patterns have the same distribution, but the QPSK sent to -45° (red circle) is independent from that sent to 45° (blue diamond). This example shows that the AoC can be adjusted by changing the element spacing of the array.

Next, for the second scenario, the modulation patterns required by receivers located at 0º and 30º are QPSK and 16-QAM respectively. Here, the element spacing is 0.5λ so that the angles 0º and 30º are included in AoC. However, a 4-element array is not sufficient to generate a QPSK and a 16-QAM simultaneously. Such a conclusion can be draw from simulation as the prediction algorithm provides no solution using 4-element array. Consequently, the minimum number of array elements is increased to 6 (the reason why an array with odd elements is not considered is explained in Section 5.4), and the resulting constellation patterns for receivers at 0° and 30° are shown in Fig. 5.8(b).

Finally, we assume that 16-QAM is required by both receivers located at 0º and 30º. As the transmission angles are the same as in the previous example, the element spacing is still 0.5λ. Again, according to simulation, a 6-element array cannot generate two independent 16-QAMs at the required angles. The minimum number of array elements is found to be 8 and the corresponding constellation diagrams are shown in Fig. 5.8(c). The patterns of red circles (0°) and blue squares (30°) are selected as independent 16-QAMs for the two receivers (the green crosses could also be selected for independent transmission, but they cannot form the required 16-QAM).

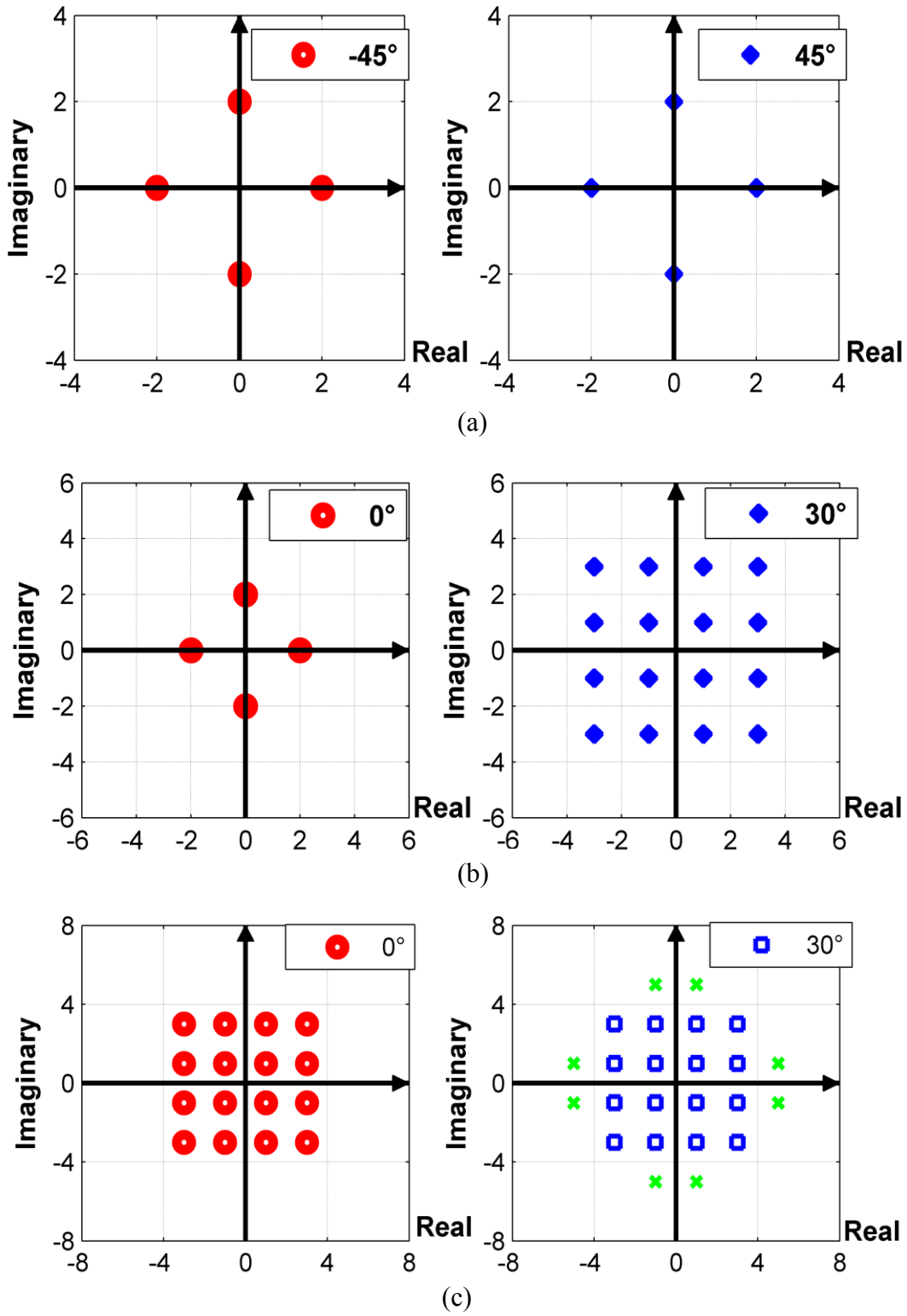

Fig. 5.8 Constellation patterns used for providing independent communications towards two spatially divided recipients based on: (a) 4-element DAM array system with 0.354λ element spacing; (b) 6-element DAM array system with 0.5λ element spacing; (c) 8-element DAM array system with 0.5λ element spacing.

5.3.3 Space Multiplexing toward Three Recipients

All the previous examples of space multiplexing via using DAM have been illustrated for the case of two independent receivers only. However, as indicated by Fig. 5.4, the proposed algorithm can provide solutions for multiple users. To illustrate this, a DAM transmitter based on an 8-element array is used for demonstration, which can simultaneously send independent QPSK to three recipients located at AoC of 0º and ±30º respectively.

Step 1: Assume that broadside is the first desired transmission angle. With this 8-element array, there are up to 65536 (4^8) system phase combinations. But they only result in 81

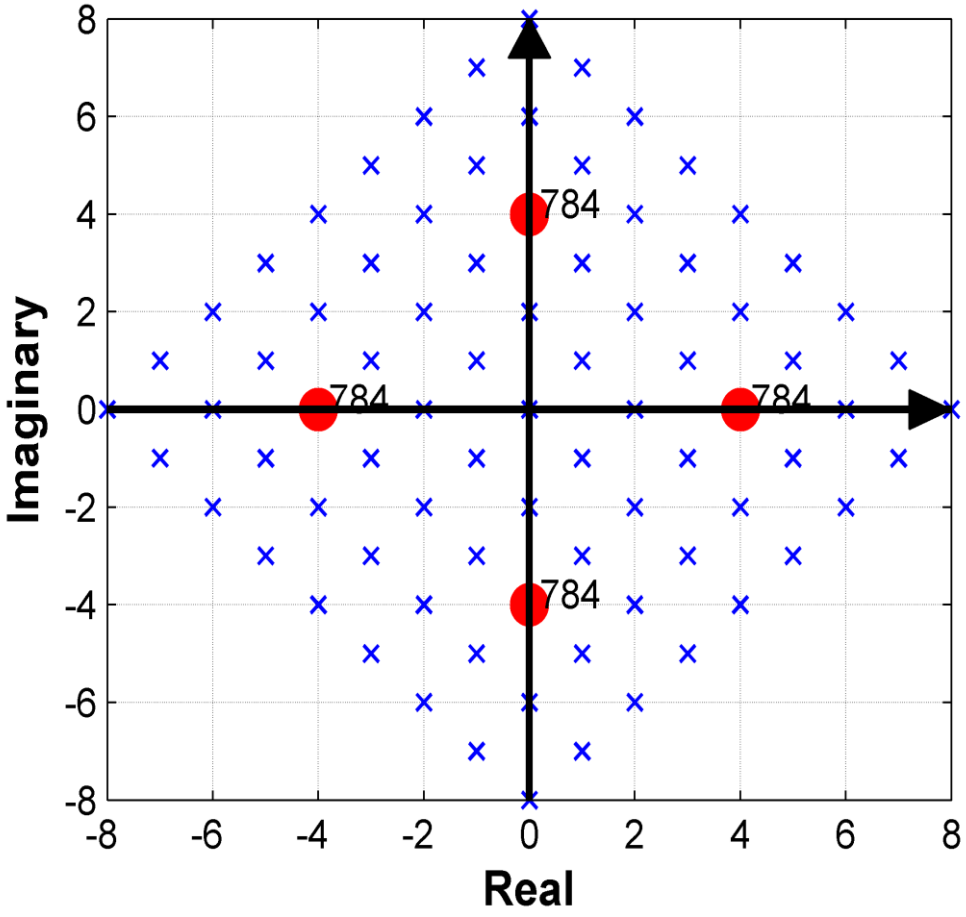

Fig. 5.9 Constellation patterns of signals received at 0° when the DAM transmitter is consisted of an 8-element array with element spacing of λ/2.

($(8+1)^2$) discrete constellation points. The corresponding constellation is shown in Fig. 5.9, where the 4 red circle points are selected by users to form the required QPSK transmission at broadside. Each of these four points can be generated by 784 different system phase sets. Hence, only 3136 (784x4) phase sets is generated by the system initial state to be considered in subsequent computations.

Step 2: The users select -30° as the next transmission angle.

Step 3: An exhaustive computation is conducted against the 3136 phase sets exported in step 1 and all the possible independent constellation points for the recipient at -30° are calculated and displayed in Fig. 5.10.

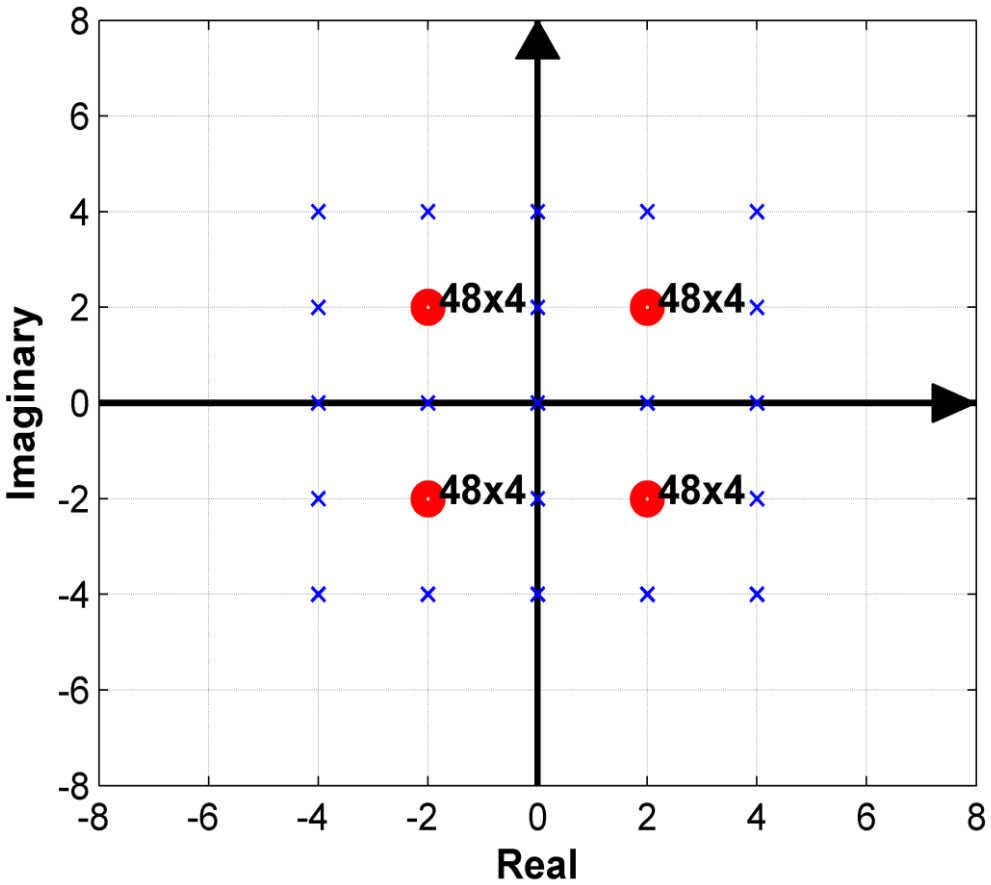

Fig. 5.10 Constellation patterns of signals received at -30° when the DAM transmitter is consisted of a 8-element array with element spacing of λ/2.

Step 4: From the 25 points found in step 3, the users select 4 (red circles) of them to form the QPSK pattern for receiver at -30° as shown in Fig. 5.10. Each of these 4 points can be generated by 192 (48x4) different system phase combinations. However, these 192 phase combinations are in 4 different groups, and each group contains 48 combinations. These 4 groups map to 4 selected constellation points in step 1 (the red circles in Fig. 5.9). As there is one more transmission angle to accommodate, the algorithm repeats from step 2.

Step 2 (repeated): 30° is chosen as the next required transmission angle.

Step 3 (repeated): Exhaustive computation is conducted against the 768 phase sets exported from step 4. All the independent constellation points generated for recipient at 30° are shown in Fig. 5.11.

Step 4 (repeated): as there are only 4 points found in step 3 (repeated), users have no other choice but choose all of them to form a standard QPSK for receiver at 30°. As shown in Fig. 5.11, each constellation point can be generated by 128 (8x16) different system phase combinations. These 128 phase combinations are in 16 groups, so each group has 8 elements. The 16 groups are map to 16 different pairs of constellation points from two independent QPSK patterns (Fig. 5.9 & Fig. 5.10) transmitted to 0° and -30°. Because there are no more transmit angle to be considered, the algorithm terminates after exporting all the 512 system phase sets found in this step.

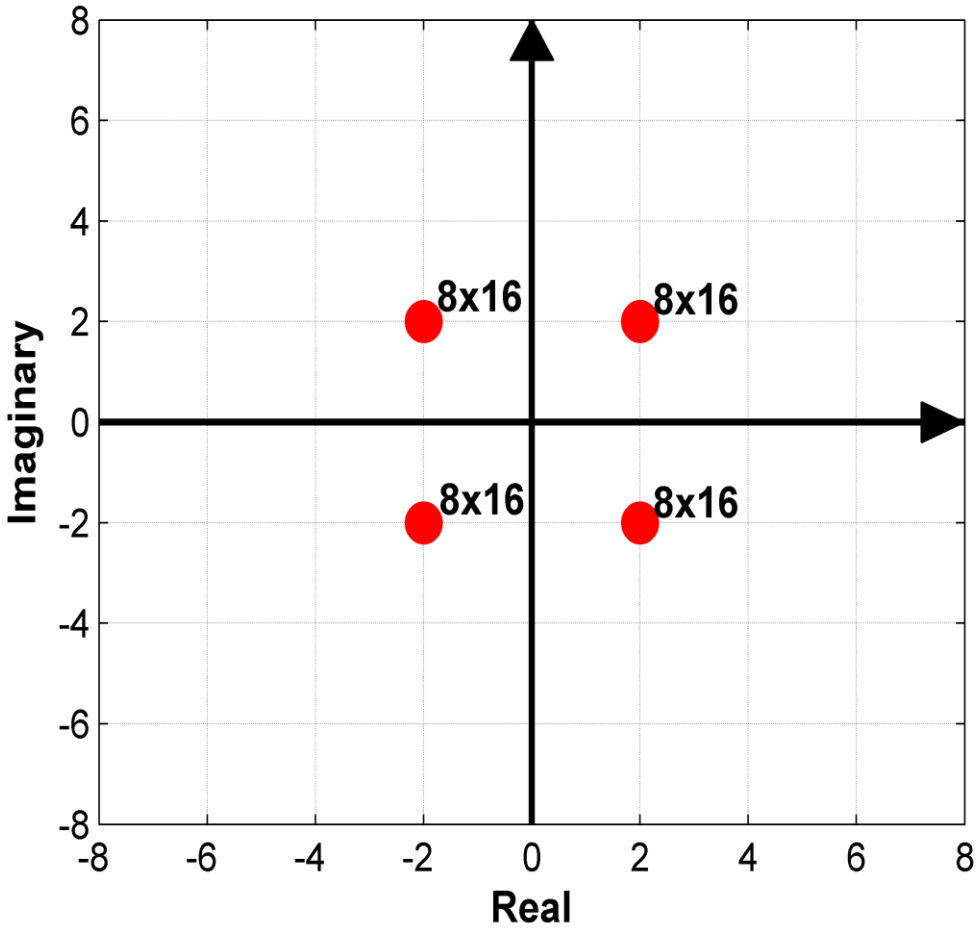

Fig. 5.11 Constellation patterns of signals received at 30° when the DAM transmitter is consisted of a 8-element array with element spacing of λ/2.

The computations for this example were calculated by implementing the algorithm in MATLAB and the whole process took less than 15 seconds. The resulting communication scenario is described by Fig. 5.12. To modulate three independent QPSK patterns, the minimum number of required system phase sets is 64 and these phase sets consist of a 3-dimentional matrix (4x4x4), where three dimensions refer to three transmission angles respectively. 512 system phase sets are found in step 4(repeated) means there will not be only one solution of the required 3-dimentional phase sets matrix.

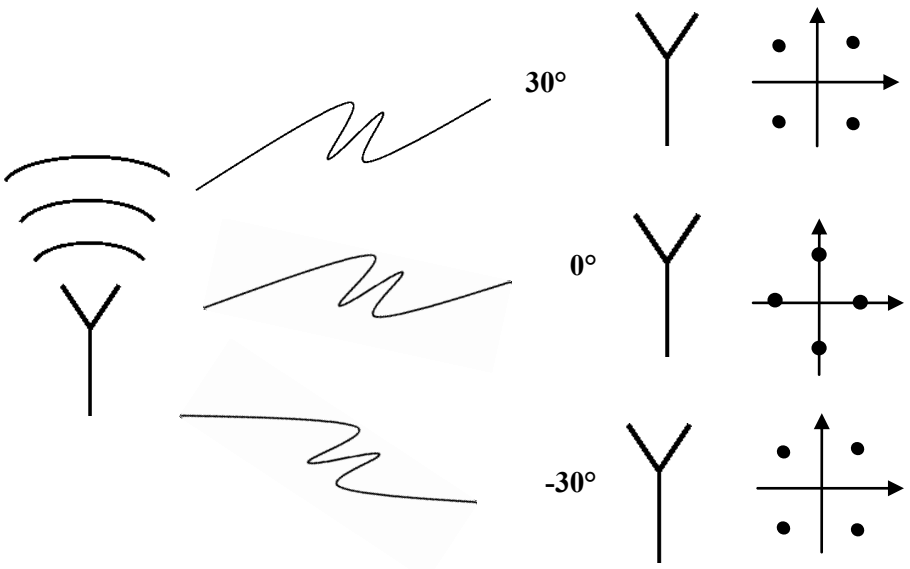

Fig. 5.12 Illustration of transmitting independent QPSK patterns to 0º and ±30º simultaneously.

5.4 Arrays with an Odd Number of Elements

Arrays with an odd number of elements are not discussed in section 5.3, because the independent signal patterns generated by them at AoC are symmetrical to one of the coordinate axes only. One particular pattern example is BPSK. It is symmetrical to either x-axis or y-axis, which is not a standard pattern. Users may be more interested in standard M-ary/M-QAM patterns, thus they may prefer arrays with an even number of elements. In this section, we will demonstrate the algorithmic method proposed in this chapter can be applied to the arrays with an odd number of elements as well.

The example DAM transmitter is configured on a 3-element array, and the distance between elements is still $\lambda/2$. There are up to 64 (4^3) system phase combinations. They only result in 16 ($(3+1)^2$) distinct data points on the constellation diagram received at one

of the AoC. The constellation received at broadside is shown by Fig. 5.13. The inner most four constellation points "ABCD" are marked by different colours. If they form a standard QPSK, there is no independent signal pattern found at other AoC. But if they are split into two BPSK patterns as shown in Fig. 5.13, two 6 point QAM can be found at 30° respectively. The Fig. 5.14(a) illustrates the scenario that the broadside recipient chooses symbol points "AC" to form the BPSK. Then the independent pattern available for receiver at 30° is a 6 point QAM, which is symmetrical to x-axis. In contrast, if broadside recipient chooses "BD", then the receiver at 30° can have a different 6 point QAM, which is symmetrical to y-axis.

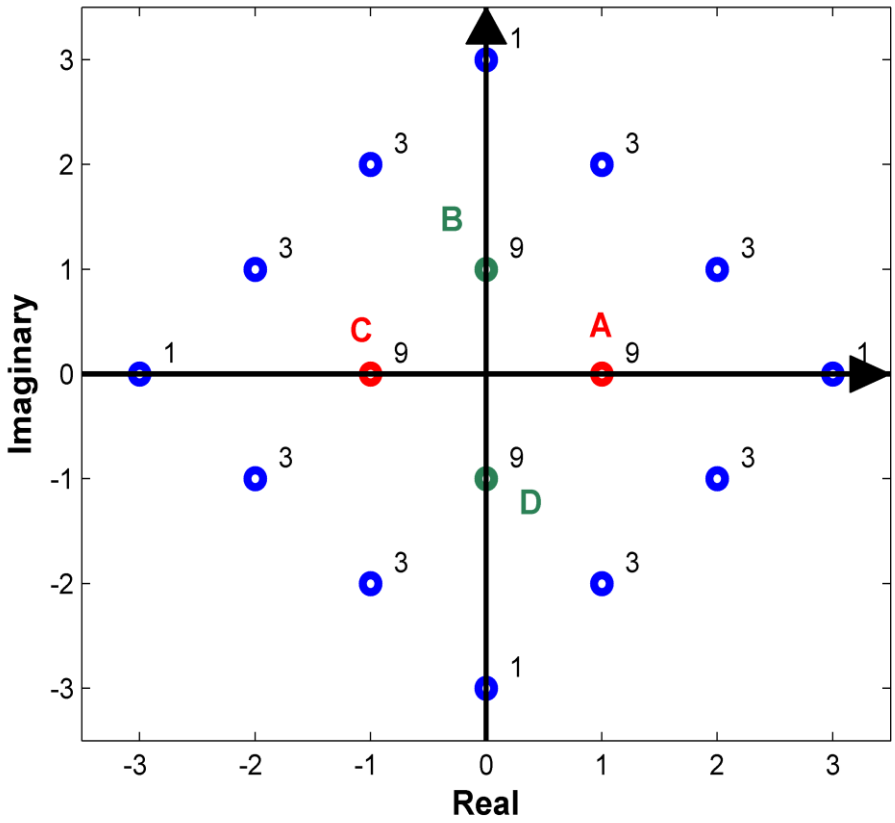

Fig. 5.13 Constellation pattern of the signals received at 0° when the DAM transmitter consists of a 3-element array with element spacing of λ/2.

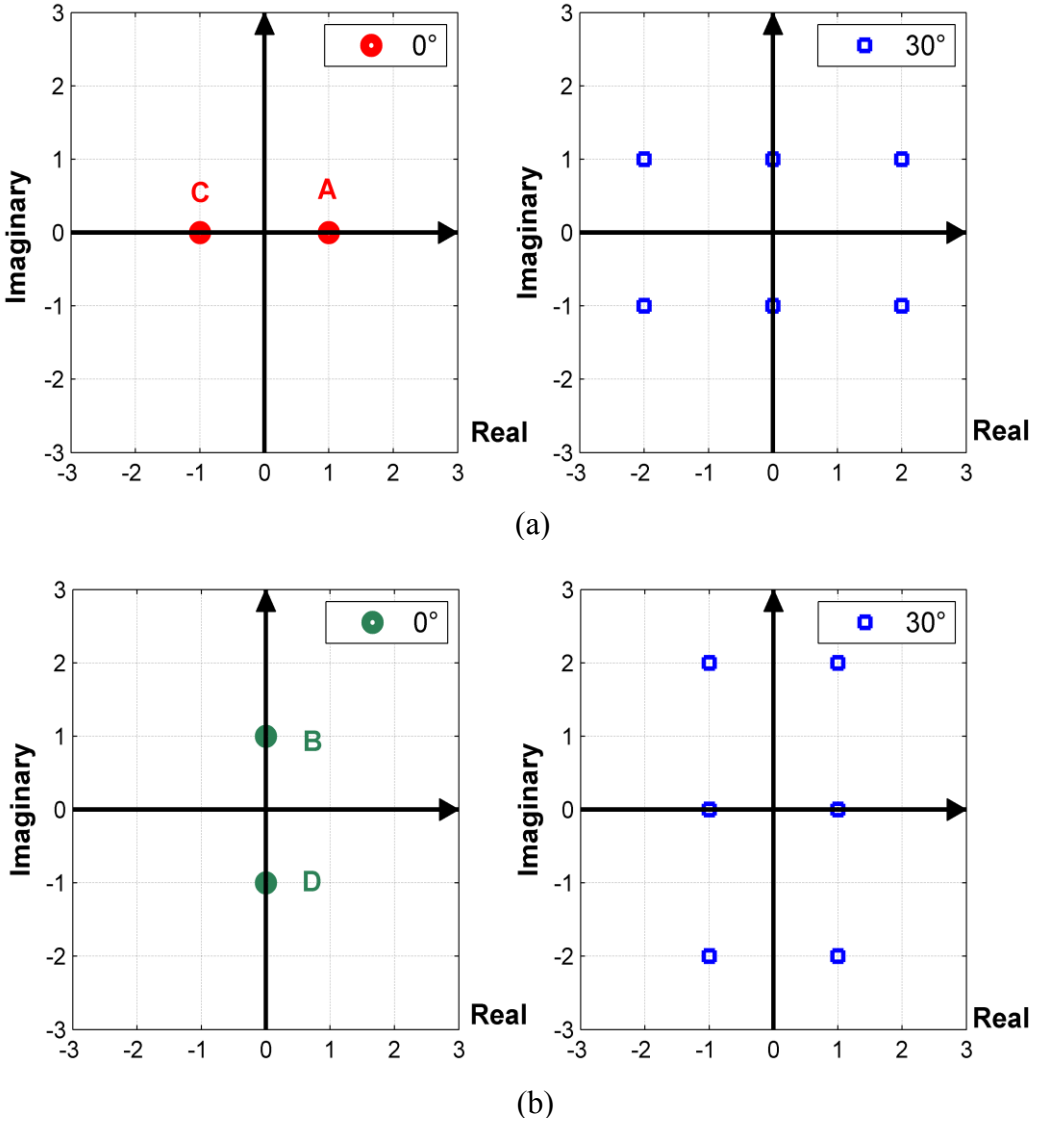

Fig. 5.14 Constellation patterns used for providing independent communications towards two spatially separated recipients generated by a 3-element DAM array system with 0.5λ element spacing. Two different BPSKs are chosen at broadside: (a) ±1; (b) ±j.

5.5 Computational Complexity

The software computation mainly consists of three parts: system initial state generation, signals calculation and independence check. To describe the computational complexity, we denote N as the number of array elements, and M as the cardinality of the constellation selected by users. For the N-element array with 2-bit phase shifters, the overall number of phase combinations is 4^N. This could be a very large number with increasing of N. But in fact, the initial state is only required to be calculated once and the phase combinations can be recorded for every different values of N for future use. As the cardinality of the pattern selected by user is M, the number of phase combinations (resources) R can be described as:

$$R = \sum_{i=1}^{M} r_i \tag{5.6}$$

where r_i is the number of the resource associated with each constellation point. The signals transmitted to the second AoC are calculated according to these R phase combinations. In the simulation, these R resources are still recorded in M groups. An independence check is conducted group by group. And for every group, there are $(N+1)^2$ -1 possible point locations on the constellation diagram to check (the origin is excluded). The overall computational time cost T can be approximated as:

$$T = t_1 \times 4^N + t_2 \times \sum_{i=1}^{M} r_i + t_3 \times M \times [(N+1)^2 - 1] \tag{5.7}$$

where t_1, t_2, t_3 are used to describe the unit time cost in simulation of each computation for phase generation, signal calculation and independence calculation respectively.

It is inevitable that the computational complexity increases exponentially so that the algorithm is difficult to use when the array scale is very large. However, the exhaustive search also has the advantage that it generates all the possible constellation points which are eligible for independent transmission and also provides options for the selection of different pattern combinations for a particular transmission.

5.6 Additional Comments

There are two issues regarding the proposed algorithmic method which require further explanations in this section.

5.6.1 Power Consideration

A fact can be noticed from Fig. 5.5 is that the more resources a constellation point has, the less power it can transmit. For this particular broadside example, there is a tradeoff between resource and power. But from a system level, this becomes a power balance between multiple users. The constellation points shown in Fig. 5.6 are all independent to the symbol pattern “ABCD” in Fig. 5.5. That is because the broadside user sacrifices his power efficiency to provide more freedom for the user at 30°. As a contrary example, assume the broadside user selects the symbols “1+3j, -3+j, -1-3j, 3-j” in Fig. 5.5 for better power performance. Then the user at 30° will only have symbols “±1±j” to use. Therefore compared to conventional transmitting system, power performance of DAM array system is not always optimized for one desired recipient, but balanced between multiple users.

5.6.2 Non-Ideal Scenarios

All the examples considered in this paper are based on arrays with ideal isotropic elements with uniform amplitude. In a real system this will not be the case, but the algorithmic method can still be used providing that the radiating properties of the array elements are taken into consideration. This could be achieved by either measurements of the array embedded element patterns or by full-wave simulation using appropriate modelling software. The main consequence of an array with non-isotropic element patterns is that the constellations at angles away from boresight will have reduced power levels which could result in an increase in error rate. A second consequence which could occur with an array of non-identical elements is that the overlapping of signals at AoC is not ideal, and in this case an additional optimization procedure similar to that used in [18] may be required. These and other 'real-world' factors add to the complexity of the approach but do not affect the basic concept or validity of the method. The main concern is that the error rate may increase at certain transmission directions, but this will depend on the exact details of the array construction.

5.7 Summary

A directly modulated array antenna has been configured to provide simultaneous, but independent data transmission to multiple recipients at different spatial locations. The system is based on low-level and low cost, 2-bit, switched phase control of the array elements. An algorithmic procedure has been developed to calculate array parameters (primarily, the number of array elements and element spacing) according to the system

requirements in terms of the number of independent users and the modulation level. Several, specific examples have been presented to illustrate the capabilities of the approach including the simultaneous transmission of high order QAM modulation schemes to different users. Although the use of 2-bit phase control provides advantages that include reduced system cost and simplified control algorithms, the number of independent users that can be accommodated is limited. However, the method reported here is general and can be extended to higher order discrete phase control, in which case the number of independent users that can be accommodated can be significantly increased.

Chapter 6

Extended Applications of Using Direct Antenna Modulation to Provide Communication Security

The communication security provided by conventional DAM scheme has been discussed in Chapter 4. Here "conventional" means the system purely relies on the *direction dependent* property. Such a system provides a general protection, but is not flexible enough to tackle some special security threats. In some scenarios the locations of eavesdroppers may have been pre-detected, so that the transmitter may want to maximise the information uncertainty at these eavesdropping angles. When multiple reflecting paths exist, they can possibly be used to provide extra communication security. Combined with property of *signal convergence* introduced in Chapter 5, two extended DAM transmission schemes are discussed in this chapter.

6.1 Information Security Enhanced by DAM with Multi-Level of Constellations

The property of signal convergence has been detailed introduced in Chapter 5. Due to this property, the DAM system can generate constellations with different orders. In the scenarios that potential eavesdroppers are pre-known, the DAM transmitter can be configured to force low-level constellation at eavesdropping directions, while keeping high-level constellation at intended transmitting angle. Assume the high-level constellation consists of N data symbols, and the low-level constellation contains M data symbols. When the number M is much smaller than N, the information uncertainty caused by multi-level of constellations makes accurate demodulation by eavesdroppers theoretically impossible.

6.1.1 System Description

Recalling the example structure of a DAM transmitter (Fig. 3.2 in Section 3.2.1) as shown in Fig. 6.1, consider a two element array of isotropic elements separated by a distance d. Let each element have independent 2-bit discrete phase control with phase values defined by φ_A and φ_B respectively. Additionally let one channel of the array have an additional phase shift component defined by φ_D. Under these conditions the far-field signal radiated by the array at an angle θ may be described as:

$$S(\theta, t) = e^{j\varphi_A(t)} + e^{j\left(\varphi_B(t) - \frac{2\pi}{\lambda} d \sin\theta + \varphi_D(t)\right)} \tag{6.1}$$

where λ is the radiating wavelength of the array and $\varphi_A(t), \varphi_B(t)$and $\varphi_D(t)$ indicate a defined set of phase shift combinations at time t. The radiated signal $S(\theta, t)$ can be

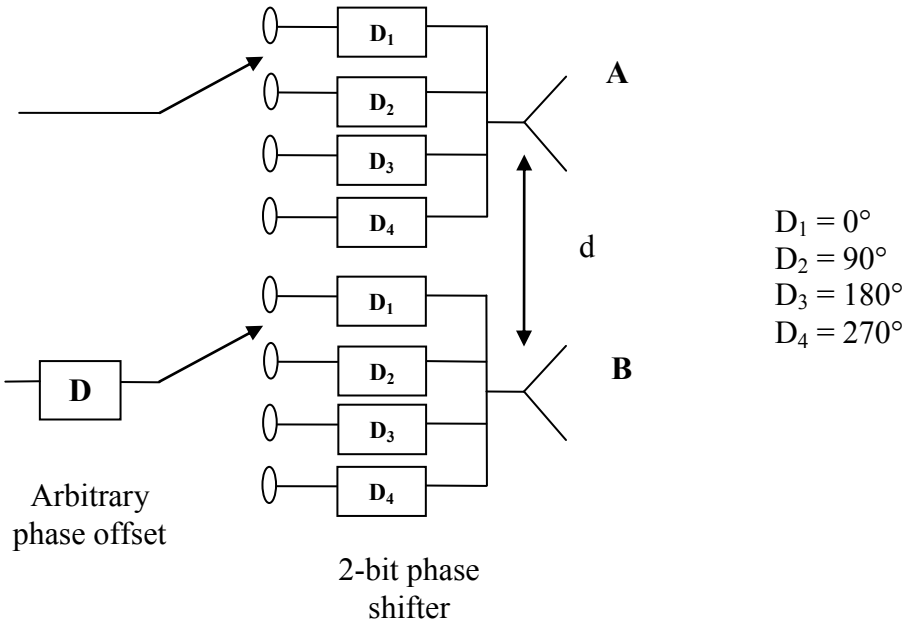

Fig. 6.1 Schematic illustration of a two-element phased array configured for direction dependent modulation.

resolved into real and imaginary components to provide a discrete point on a constellation diagram at time t. By substituting all the possible sets of phase combinations that can be generated by the system into (6.1), the far-field constellation diagram at a given angle θ, will contain up to 16 unique data points. As explained in section 5.2, the property of signal convergence results in a reduction of constellation orders from 16 to 8 at AoC (angles of convergence). Now we introduce an offset phase shift φ_D. The condition of signal convergence for the 2-element DAM transmitter is shown below:

$$-\frac{2\pi}{\lambda} d \sin\theta + \varphi_D = \frac{\pi}{2} K$$

$$K = \cdots -2, -1, 0, 1, 2 \cdots \tag{6.2}$$

Therefore, the special angle θ at which only 8 unique data points can be distinguished is jointly determined by offset phase φ_D and the integer number K:

$$\theta = -57.3sin^{-1}\left(\frac{\pi K\lambda - 2\lambda\varphi_D}{4\pi d}\right) \qquad deg$$

$$K = \cdots -2, -1,0,1,2\cdots \tag{6.3}$$

Assume the eavesdropping angle is pre-detected. The offset phase can be used to force the low-level constellation to the eavesdropping angle. The required offset phase φ_D can be calculated according to:

$$\varphi_D = \frac{\pi}{2}K + \frac{2\pi}{\lambda}d\sin\theta \qquad deg$$

$$K = \cdots -2, -1,0,1,2\cdots \tag{6.4}$$

6.1.2 Scenario of One Pre-Known Eavesdropper

There are two different orders of constellations existing in the same transmitting system. When applying this property in secure communication, it is intuitive that the constellation with the higher order is sent to the desired recipient, while the one with the lower order can be purposely transmitted to a pre-known eavesdropper.

To illustrate the property of a DAM system transmitting a reduced number of constellation points, consider a specific example in which the two elements of the array are separated by half a wavelength. Assume we wish to transmit a signal to an intended recipient in the boesight direction using a 16 point QAM modulation scheme, but that an unwanted eavesdropper is monitoring the transmission at an angle of 15° away from boersight. The very nature of DAM will ensure that as the observation point moves away from borsight, the distribution of the original 16 points in the constellation diagram will change and that this will result in an increased demodulation error rate. However to

provide additional security the offset phase between two arms of array can be set to 47º. This phase offset is calculated by substituting d = λ/2, K=0 and θ=15º into (6.4). The simulated constellations for this specific case are shown in Fig. 6.2 where the constellation in the boresight direction contains 16 distinct points, but has only 8 points in the specified direction of the eavesdropper at 15°. The key point demonstrated by this example (Fig. 6.2) is that the offset phase shift φ_D can be used to force the constellation to contain only 8 unique points at a prescribed angle. As the constellation intercepted by eavesdropper has only 8 effective data points, it is virtually impossible to demodulate the correct information conveyed by the desired constellation with 16 point QAM pattern.

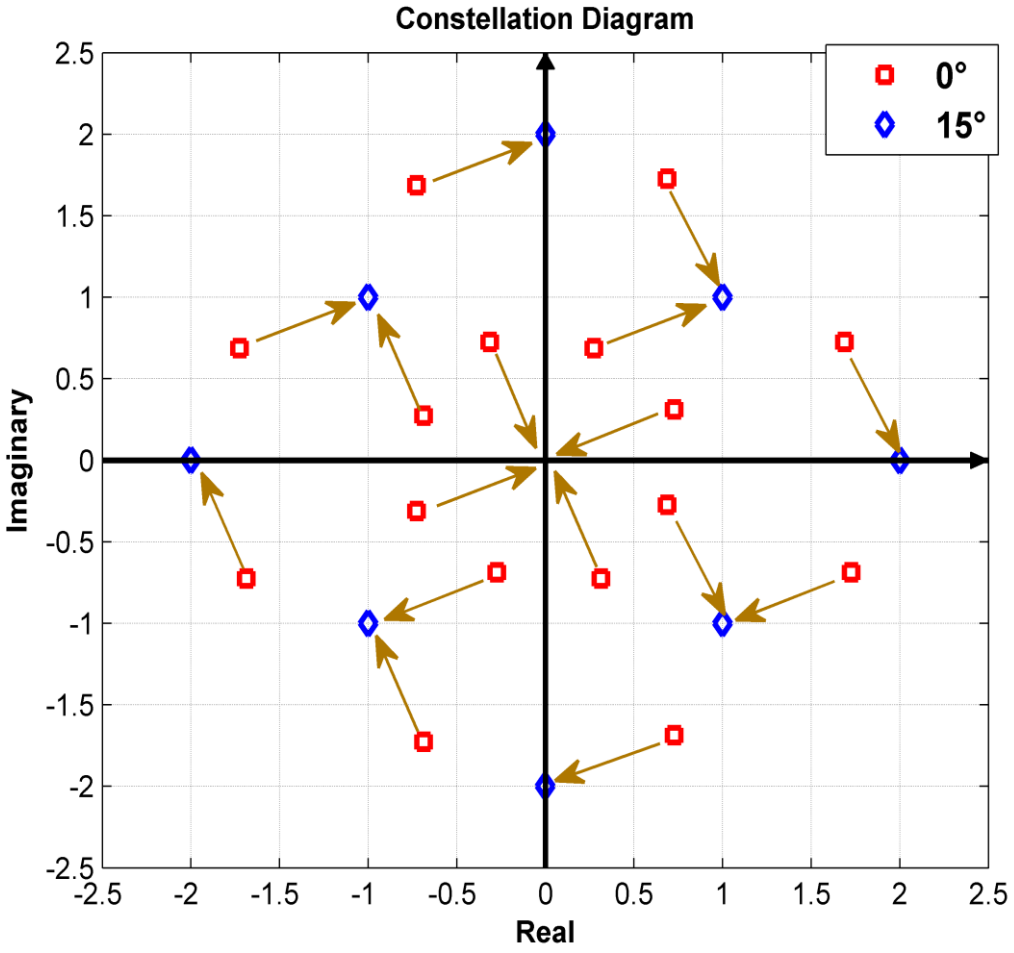

Fig. 6.2 The system is configured to transmit a unique 16 point constellation (squares) to 0° while simultaneously transmitting only 8 points to 15° when φ_D=46.6°.

In this example system, the distance between array elements is half a wavelength. In this case, the set of transmitting angles having a reduced-level of constellation points has a dependent relationship. By substituting φ_D=47º and d = 0.5λ into (6.3), the set of AoC is {49º, 15º, -14º, -48º} when K = -1, 0, 1, 2 respectively. When the system is configured to have 8 point QAM pattern in 15º, the whole set of angles receiving 8-QAM patterns has been determined.

6.1.3 Scenario of Two Pre-Known Eavesdroppers

The example system illustrated in section 6.1.2 can only secure the transmission against one arbitrary eavesdropping angle. In this section, a possible system configuration of DAM transmitter is proposed to have low-level constellations in *two* independent eavesdropping angles.

Referring back to equation (6.3), besides the integer number K, there are two parameters that can be used to determine the AoC: the spacing between the array elements, d, and the phase shift φ_D. Although it may be difficult to change the element spacing in real-time, it does provide an extra degree of freedom with which to control the form of the signal radiated by the array. The key point to introduce element spacing d as a parameter is to let two angles having low-level constellations be independent from each other.

In the case considered here, the system is required to transmit information in the boresight direction using 16 point QAM, but that in addition we wish to prevent accurate demodulation of the signal at two receive angles located at -10° and 20° respectively. To simultaneously meet the condition (6.2), the element spacing d is considered as a variable:

$$\begin{cases} -\frac{2\pi}{\lambda} d \sin 20 + \varphi_D = \frac{\pi}{2} \times 0 \\ -\frac{2\pi}{\lambda} d \sin(-10) + \varphi_D = \frac{\pi}{2} \times 1 \end{cases} \tag{6.5}$$

The combination $\varphi_D = 60°$ and $d = 0.48\lambda$ can be derived from (6.5) when K=0 at θ=20º and K=1 at θ= -10º. The constellation diagrams corresponding to this solution are shown in Fig. 6.3 where it is observed that the desired 16 point constellation is transmitted at boresight but that only 8 distinct constellation points are transmitted at the prescribed eavesdropper angles of -10° and 20°. As demonstrated by this example, if the distance between array elements can be considered as a system parameter, a DAM transmitter can force sending low-level constellations at up to *two* independent, arbitrary transmitting angles to prevent accurate demodulation by eavesdroppers.

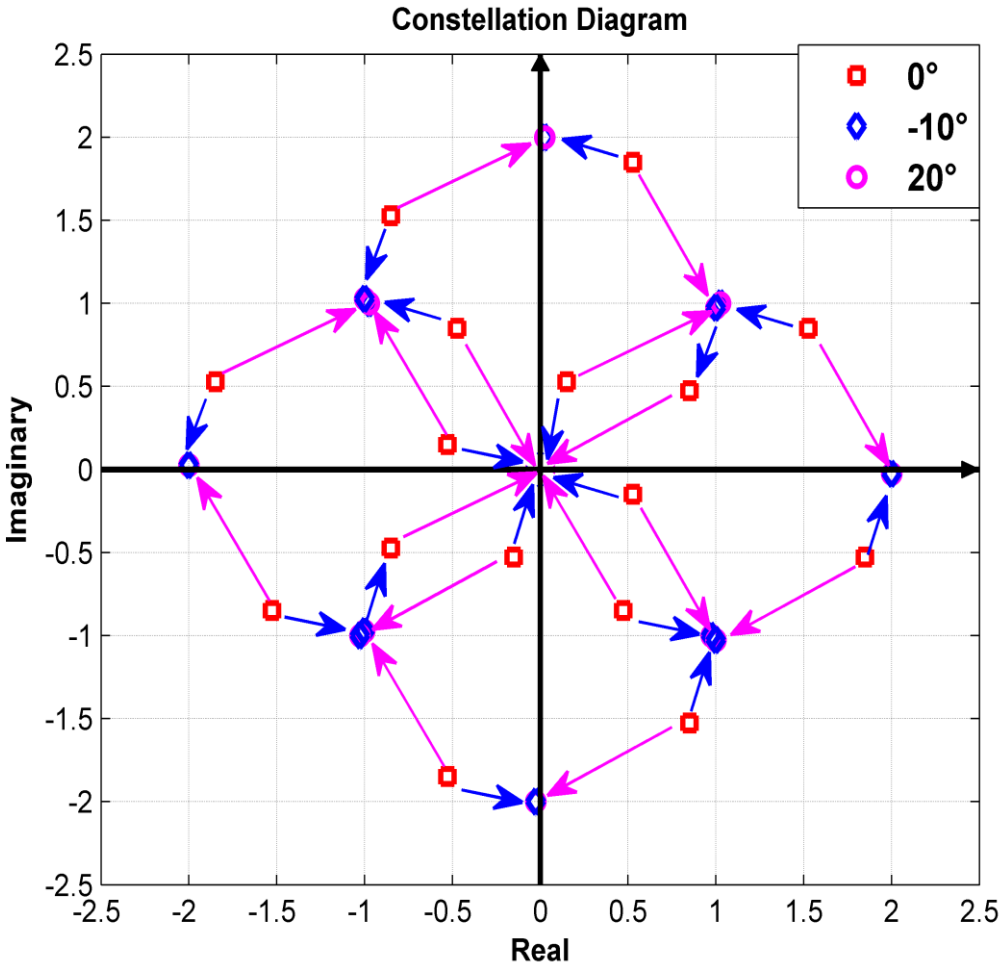

Fig. 6.3 The system is configured to transmit a unique 16 point constellation (squares) to 0° while simultaneously transmitting 8 points to both -10° and 20° when φ_D=60°, d= 0.48λ.

6.1.4 Conclusion

The direction dependent modulation properties of a two-element array antenna configured for direct data modulation via 2-bit phase control have been presented. By controlling the relative phase offset between the two elements of the array, the system can transmit a signal with a 16 point QAM modulation scheme to an intended recipient in a specified direction and simultaneously transmit the same baseband data as a signal with only 8 constellation points the direction of a known eavesdropper. Although the signal in the direction of the eavesdropper may be detected, the reduced number of points in the signal constellation ensures that it cannot be accurately demodulated by conventional schemes. Furthermore, by controlling the spacing between the array elements in conjunction with the phase offset, the system can transmit a reduced 8 point QAM signal in *two* independent directions simultaneously.

6.2 Secure Communications Based on Directly Modulated Antenna Arrays Combined with Multi-Path

The communication security provided by conventional DAM techniques is due to the property of direction dependence. Normally the moving path of a constellation point is continuous along with the change of transmitting angle. Therefore, the smaller the angular difference, the similar the signal pattern on constellation. Such a DAM transmitter is vulnerable to decoding by an eavesdropper located at angles very close to the intended transmission direction. One solution is to have a narrow power beam by combining large inter-element spacing with directive array elements as described in Chapter 4. In this section, we investigate a case that at the recipient, signals are received jointly from one LOS and one reflecting paths. According to Chapter 5, the signals sent to the desired recipient through different paths can be independent. With proper configuration, the LOS and reflecting signals can be independent from each other. In this case, the constellation pattern received at intended direction can be manipulated to be significantly different from that received at angles very close to the intended transmission direction. The security of data transmission is then improved.

6.2.1 Reference System

Before making a valid comparison, a reference constellation signal pattern is defined first for the purely line of sight (LOS) transmission between a transmitter and the intended recipient. In this example, assume a standard 8-QAM signal pattern is chosen, which is shown in Fig. 6.4. It is shown in [55] that such a modulation scheme can easily be generated in the broadside transmission direction by using a two-element array with 2-bit phase control. The array configuration is illustrated in Fig. 6.5. Fig. 6.6 shows the angular

dependent constellation of signals received at 5° away from broadside (which might be detected by an eavesdropper).

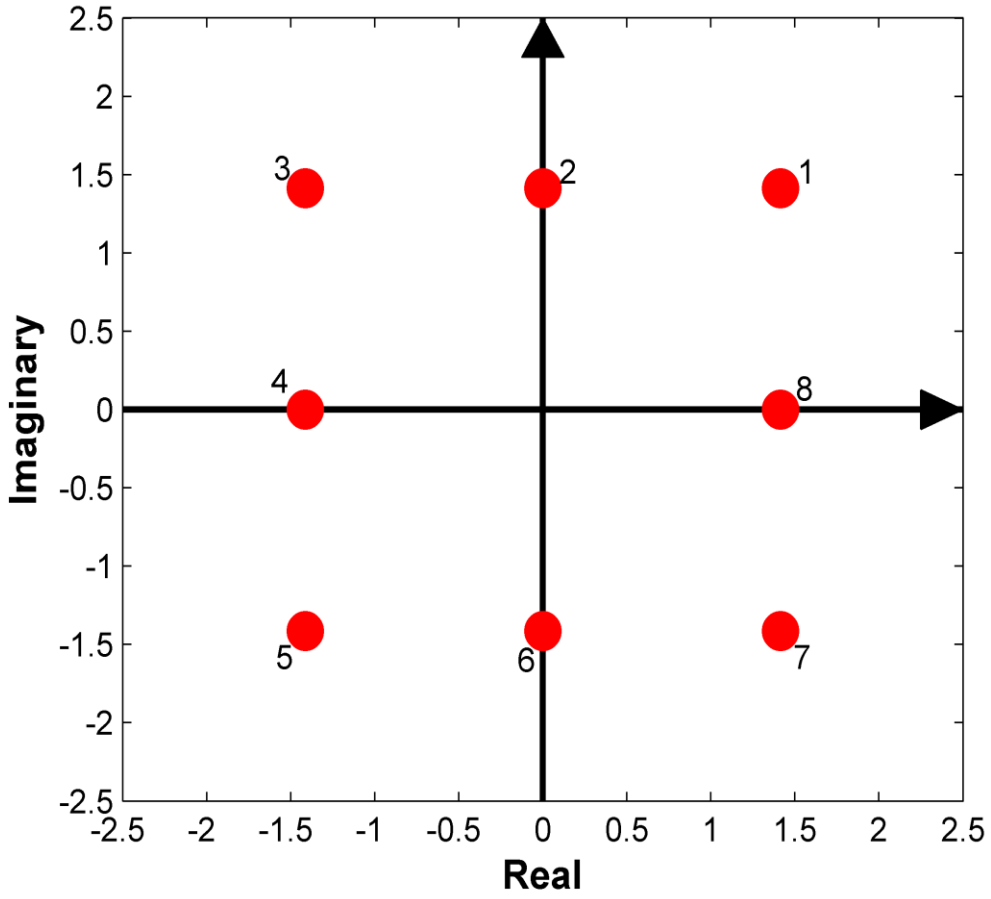

Fig. 6.4 A constellation diagram of reference signal pattern used for the data transmission between transmitter and the intended recipient.

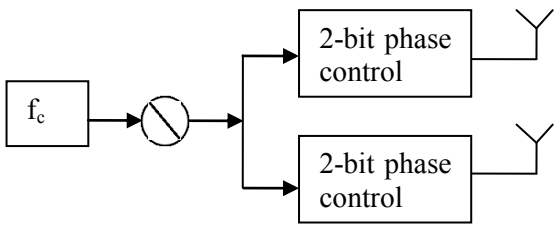

Fig. 6.5 Schematic structure of a 2-bit phase controlled DAM transmitter.

The relevant formulas to calculate constellations illustrated by Fig. 6.4 and Fig. 6.6 are shown below:

$$AF(\theta) = e^{j\varphi_A} + e^{j(\frac{2\pi}{\lambda}dsin\theta+\varphi_B)} \tag{6.6}$$

where θ is the transmitting angle (0° as broadside), d is the distance between array elements, φA and φB are element phase for this 2-element array respectively, whose values are shown in Table 6.1. Fig. 6.4 and Fig. 6.6 show the standard results of the conventional DAM transmitter configured on a 2-element array. Apparently these two constellation patterns are very similar. Thus, in this case, the security provided by such a DAM transmitter system is limited.

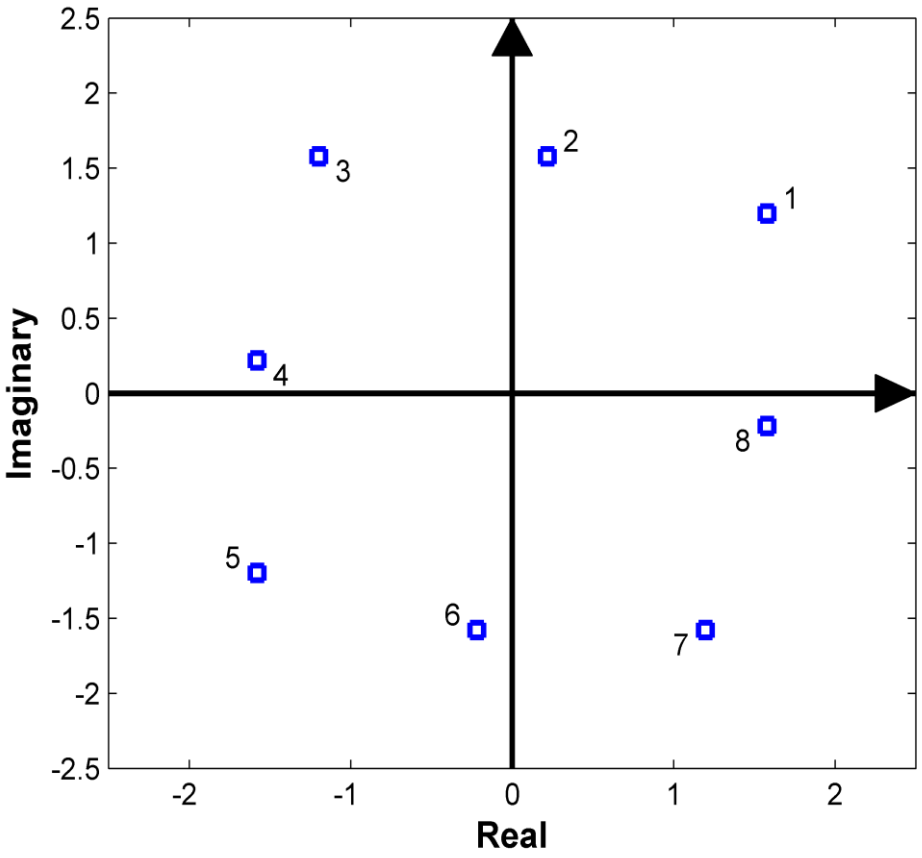

Fig. 6.6 The constellation diagram of signal pattern received at 5° away from broadside when only a LOS path exists.

Table 6.1 System phase pairs

Signal Point	Phase Pairs (°)	
1	45	45
2	45	135
3	135	135
4	135	225
5	225	225
6	225	315
7	315	315
8	315	45

6.2.2 Model of Multi-Path Transmission

In this section we introduce a transmission model having one LOS and one reflecting path. In Fig. 6.7(a), the intended recipient is located at the broadside direction. The signal received by the broadside recipient is a combination of signals transmitted via the LOS path and the reflected path. In this example, the angle between LOS and the reflected path is 30°. As shown in Fig. 6.7(b), the eavesdropper is assumed to be located at 5° away from broadside, and the LOS path is assumed to have the same length as that in Fig. 6.7(a).

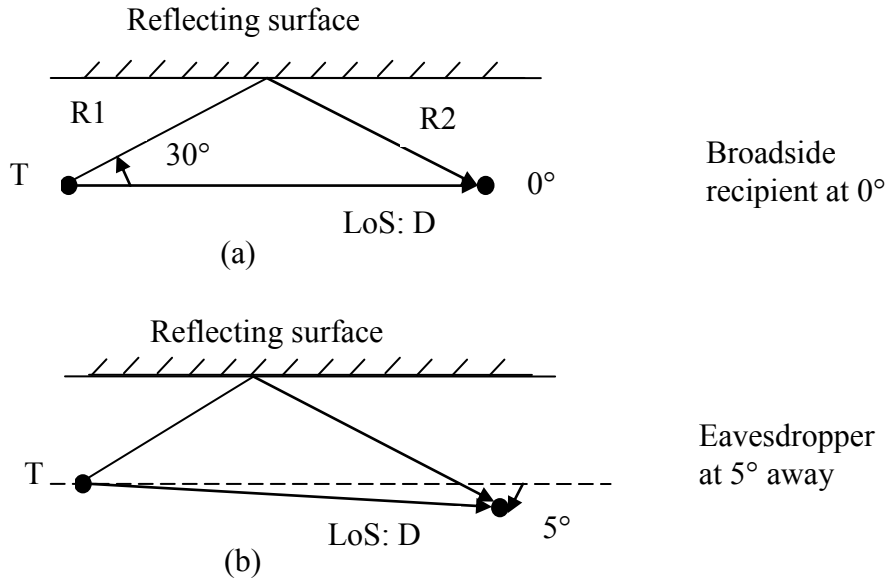

Fig. 6.7 Model of multi-path transmission including one LOS path and one perfect reflect path between: (a) transmitter and broadside recipient; (b) transmitter and eavesdropper at 5° away.

To calculate the far-field signals, the power attenuation and phase rotation caused by the multiple paths needs to be considered. As illustrated in Fig. 6.7, the length of reflected path is denoted as R1 (before reflection) and R2 (after reflection), and the length of LOS path is denoted as D. In this triangle, the length of D is assumed to be always multiple integer of wavelength λ (to ensure no phase rotation caused by the LOS path), while R1 and R2 are changing with the transmitting angle. For convenience, assume the received power at the intended recipient has unit magnitude, and the phase offset is zero (because D is multiple integer of λ). Therefore, the power received through the reflecting path is inversely proportional to the length of the paths. The attenuation ratio ar is calculated as a function of transmitting angle θ below:

$$ar(\theta) = \frac{D}{R1(\theta)+R2(\theta)} \tag{6.7}$$

where $ar(\theta)$is the attenuation ratio of signal amplitude transmitted through reflecting path compared to LoS path. Then the phase shift caused by the reflecting path can be described as:

$$pr(\theta) = \pi + 2\pi * \mathrm{de}[\mathrm{R1}(\theta) + \mathrm{R2}(\theta)] \tag{6.8}$$

The additional π in (6.8) is added because of perfect reflecting surface. Assume that function de(x) can return the remainder of x divided by wavelength λ. In (6.8), the second component returns the phase rotation caused by reflecting path.

To introduce a general formula to calculate the far-field signals received in this transmission model, Fig. 6.7 is re-drawn and shown in Fig. 6.8. The height H is the orthogonal distance from transmitter to reflecting surface. According to Fig. 6.8(a), β is the angle between LOS path and reflecting path when the receiver is located at broadside,

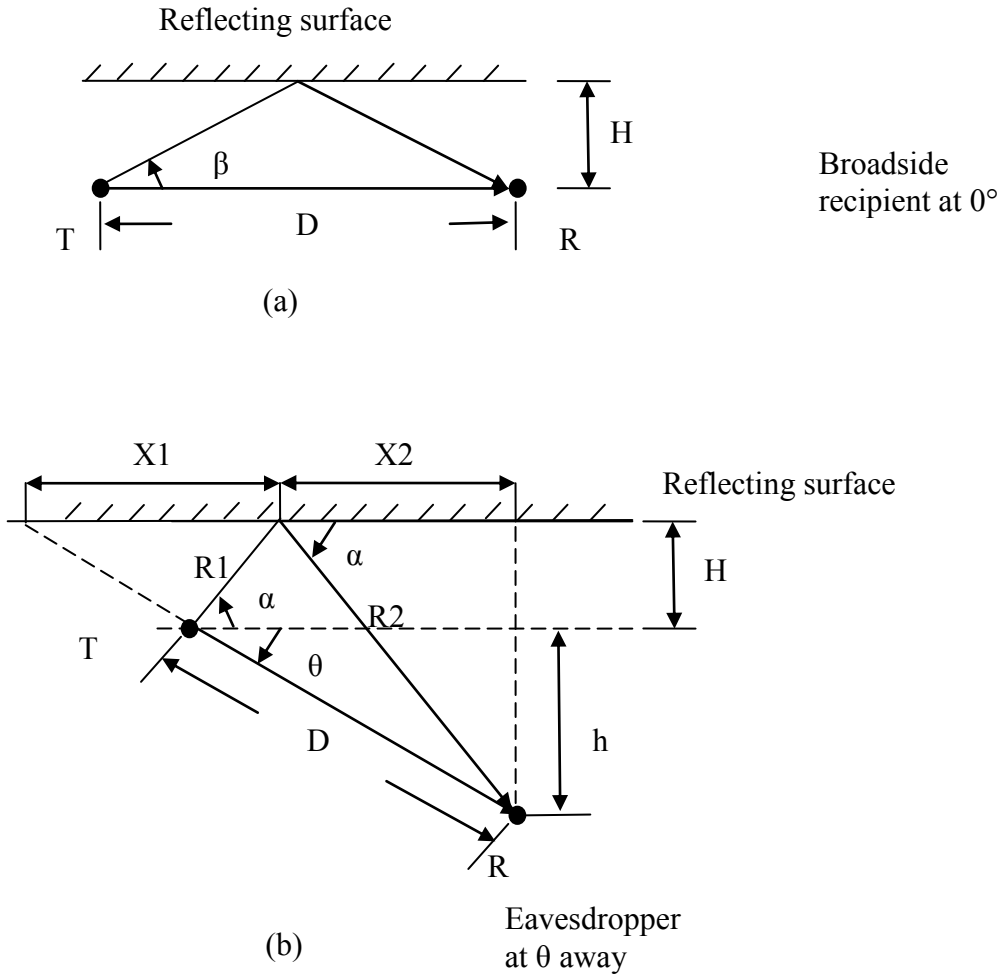

Fig. 6.8 For analysis purpose: model of multi-path transmission including one LOS path and one perfect reflect path between: (a) transmitter and broadside recipient; (b) transmitter and eavesdropper at 5° away.

i.e. when LOS path is parallel to the reflecting surface. The height H is $\frac{D}{2}\tan\beta$. As shown in Fig. 6.8(b), the angle between LOS path and reflecting path is divided into two parts: α and θ. Angle θ indicates the location of eavesdropper away from broadside. Angle α is the angle between the parallel LOS path and the reflecting path at the transmit. In Fig. 6.8, the height 'h' is $D\sin\theta$, and H is still $\frac{D}{2}\tan\beta$. Then according to the triangle (Fig. 6.8(b)) we can have following equations:

$$\begin{cases} X1 + X2 = (H + h) \times \tan\theta \\ X1 = \frac{H}{\tan\theta} + \frac{H}{\tan\alpha} \\ X2 = \frac{H+h}{\tan\alpha} \end{cases} \tag{6.9}$$

Solving the equations gives:

$$\alpha = \tan^{-1}\left(\frac{\tan\beta+\sin\theta}{\cos\theta}\right) \tag{6.10}$$

Referring back to Fig. 6.8, path length R1 and R2 can be described as:

$$\begin{aligned} R1 &= \frac{0.5D\times\tan\beta}{\sin\alpha} \\ R2 &= \frac{0.5D\times\tan\beta+D\times\sin\theta}{\sin\alpha} \end{aligned} \tag{6.11}$$

where angle α can be calculated by (6.10), angle θ is 5° and angle β is 30° in the example model shown in Fig. 6.7. Then the general equation used to calculate the far-field signals received through the reflecting path is:

$$MF(\theta) = e^{jpr(\theta)} * ar(\theta) * (e^{j\varphi_A} + e^{j[\frac{2\pi}{\lambda}d\sin\gamma+\varphi_B]}) \tag{6.12}$$

The attenuation ratio $ar(\theta)$ and phase shift $pr(\theta)$ can be calculated according to (6.7) and (6.8). Angle γ is equal to angle β if the receiver is at broadside, and its value is determined by (6.10) if the receiver is not at broadside. Finally, the received far-field signals can be expressed as (assume the time difference is not considered):

$$S(\theta) = AF(\theta) + MF(\theta) \tag{6.13}$$

For the broadside recipient as shown by Fig. 6.7(a), θ = 0° and γ = β = 30°. Assume the same system phase pairs (Table 6.1) are substituted, the received constellation calculated by (6.13) is shown in Fig. 6.9. For the eavesdropping receiver as shown by Fig. 6.7(b), θ

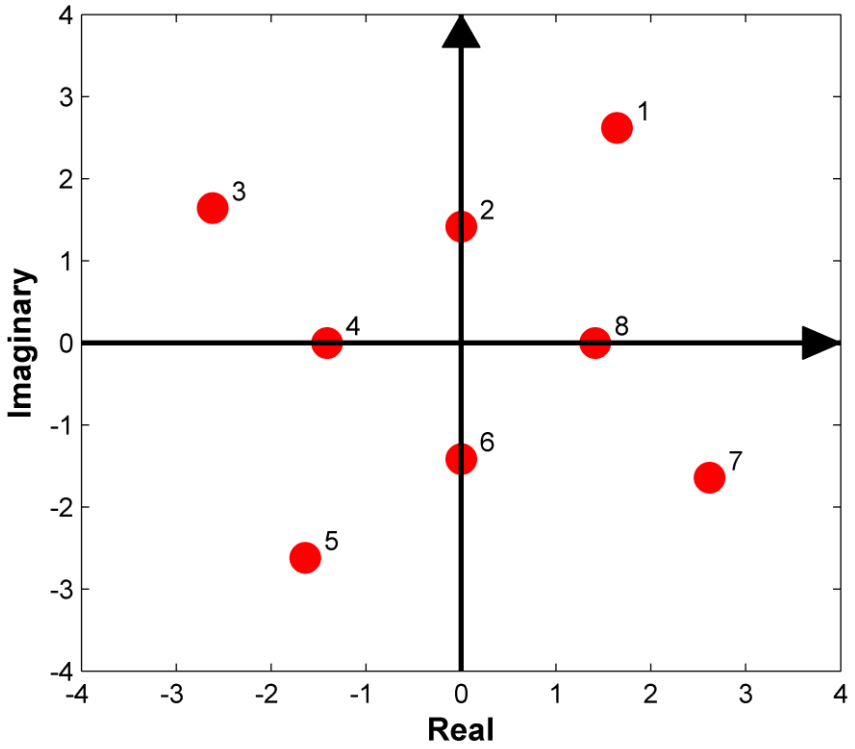

Fig. 6.9 The constellation diagram of signal pattern received at broadside when considering the multi-path reflection.

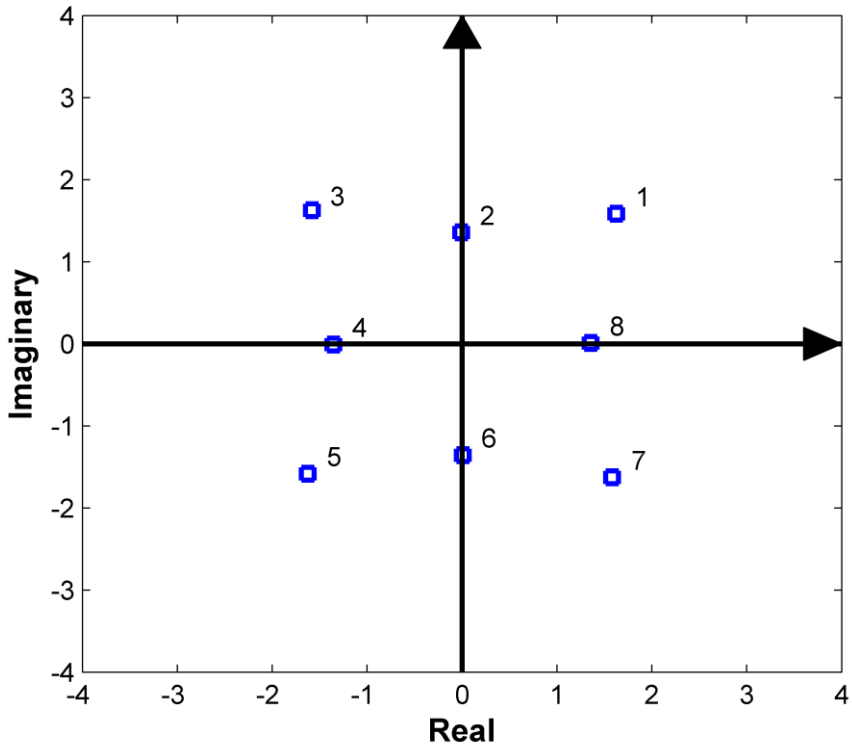

Fig. 6.10 The constellation diagram of signal pattern received at 5° when considering the multi-path reflection.

= 5°, β = 30° and γ = α = 33.7° (according to (6.10)). The received constellation is shown in Fig. 6.10. Comparing Fig. 6.9 & Fig. 6.10 with Fig. 6.4 & Fig. 6.6, the difference between them is much larger in the presence of multi-path transmission than in purely LoS path.

6.2.3 Multi-Directional Transmission Scheme

In last section, we introduced a multi-path transmission model. The constellations received at 0° and 5° are more different than that in conventional case. But the problem is that the broadside constellation (Fig. 6.9) is very different from the reference pattern (8-QAM shown in Fig. 6.4). It is possible to synthesize the required 8-QAM by changing the amplitude or phase at element level of the array, but that could be very time-consuming. The critical difficulty is that signals transmitted to broadside receiver through different paths are dependent so that any changes made to the signals sent through LOS channel will simultaneously affect the ones through other paths. Referring back to Chapter 5, the multi-directional transmission scheme could be a solution because signals transmitted through different paths are independent.

The example DAM array system has the same configuration as the one shown in Fig. 6.5, but the number of array elements is increased to 4. The inter-element spacing is λ/2. By properly configuring the phase states of element antennas, two independent signal patterns can be generated by the DAM transmitter towards the transmission angles of 0° and 30° as illustrated in Fig. 6.11 (detailed configuration have been presented in Chapter 5, section 5.3.1). Therefore, one standard QPSK and one 12 point QAM are modulated in the directions of 0° and 30° simultaneously, and they are independent from each other. According to Fig. 6.7(a), the broadside recipient will ideally detect up to 48 (4x12) signal points, which are the total combinations of signals considering both LOS path and

reflecting path. We simulated all the 48 signals that can be received by broadside recipient with due consideration given to the amplitude attenuation and phase rotations caused by the path differences, and chose 8 of them to form a constellation that is close to the ideal, desired 8-QAM. The resulting constellation is illustrated in Fig. 6.12. It is not perfect, but very close to the ideal (Fig. 6.4). To achieve this 8-QAM pattern, all the 4 signal points sent to broadside (red circles in Fig. 6.11) are chosen and combined with the 4 selected signal points (blue squares in Fig. 6.11) sent to 30°. All the relevant system phase combinations of this 4-element array are listed in Table 6.2. The corresponding signal constellation received at 5° away from broadside is shown in Fig. 6.13. In this example, the constellation received by an eavesdropper at only 5º away is very different from the one obtained by intended recipient at broadside. Also the broadside signal pattern is successfully synthesised to the standard 8-QAM.

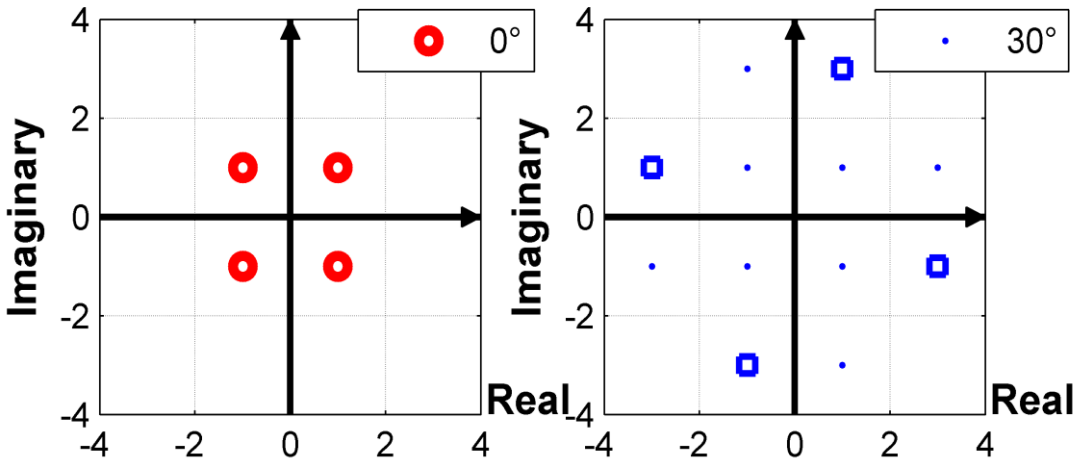

Fig. 6.11 Constellation of independent signal patterns generated by the DAM array towards transmission angles of 0° and 30°.

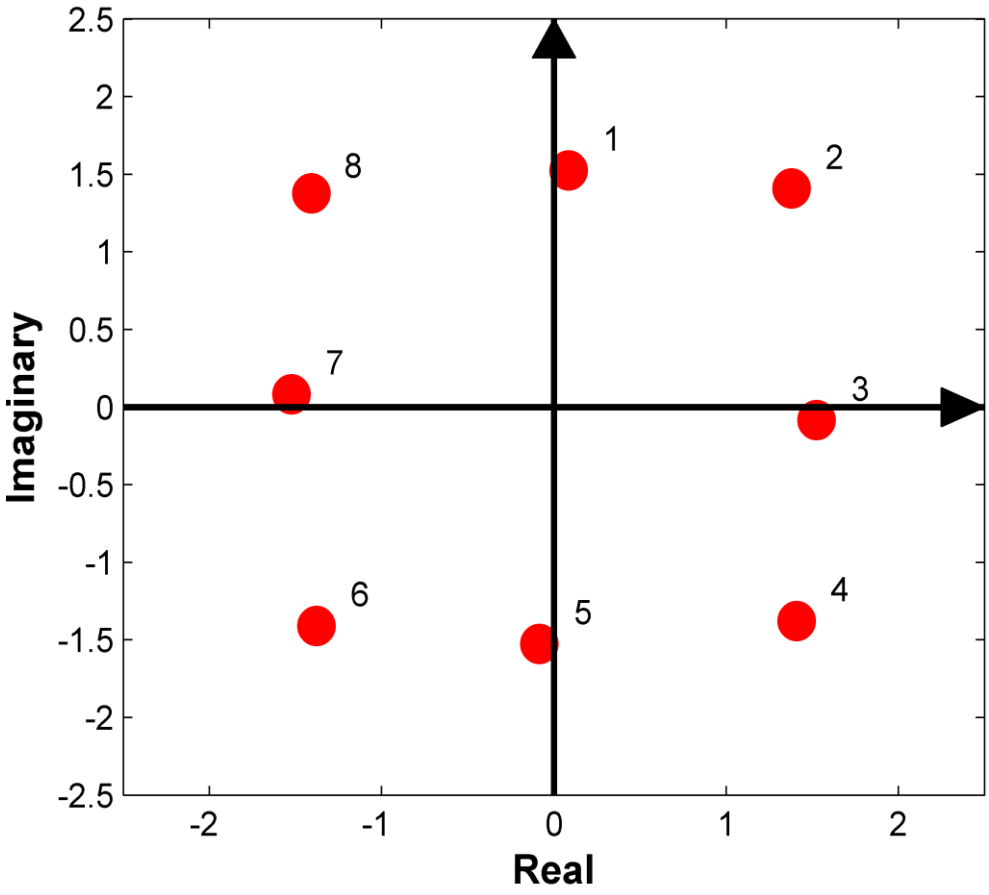

Fig. 6.12 The constellation diagram of the signal pattern received at broadside when considering the multi-path reflection and using a multi-directional transmission scheme

Table 6.2 System Phase Combinations

Signal Point	**Phase Combinations (°)**			
1	90	90	270	0
2	90	270	0	90
3	0	0	180	270
4	0	180	270	0
5	270	270	90	180
6	270	90	180	270
7	180	180	0	90
8	180	0	90	180

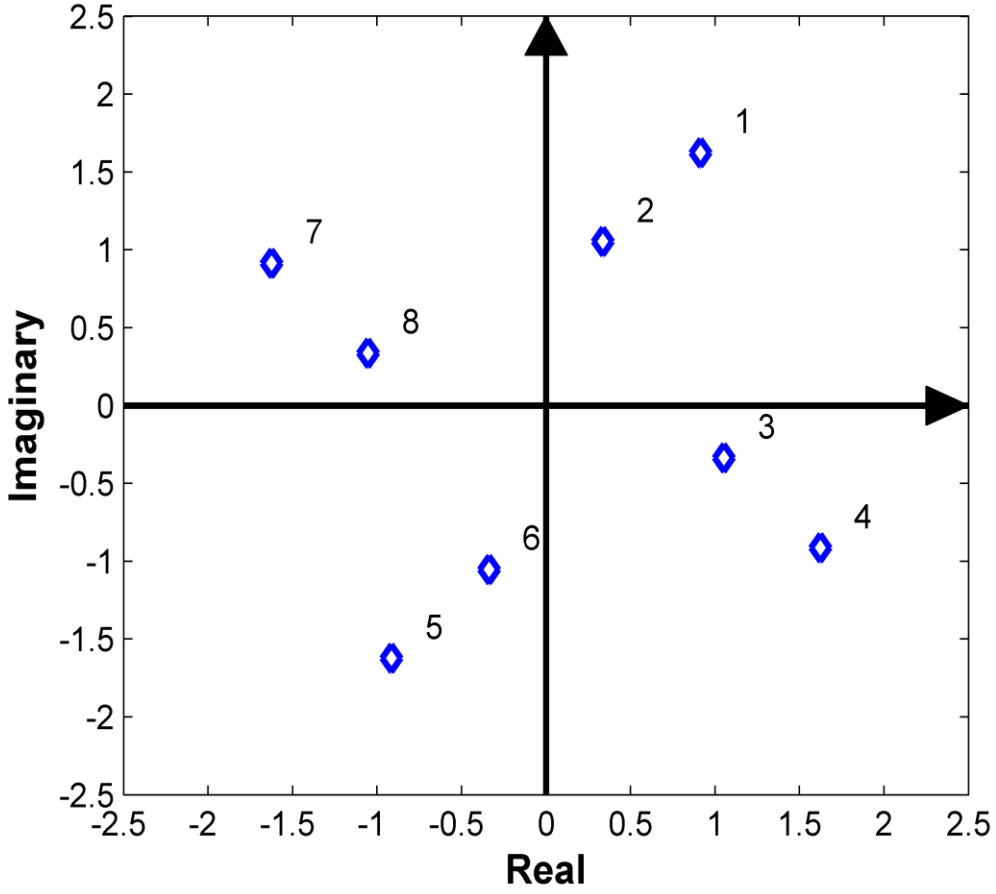

Fig. 6.13 The constellation diagram of signal pattern received at 5° away from broadside when considering the multi-path reflection and using a multi-directional transmission scheme.

Relevant formulas to calculate constellations in Fig. 6.12 and Fig. 6.13 are very similar to equations (6.6) and (6.12). The only difference is the number of array elements increases to 4.

$$S_r(\theta) = \sum_{i=1}^{4} e^{j[\frac{2\pi}{\lambda}d(i-1)sin\theta+\varphi_i]} * (1 + e^{jpr(\theta)} * ar(\theta)) \quad (6.14)$$

where S_r is the sum of signal received through LoS and reflected paths, and φ_i (i=1,2,3,4) is the element phase shown in Table 6.2 for every symbol transmission.

6.2.4 Conclusion

The performance of a directly modulated antenna operating in the presence of multi-path has been examined. The analysis is based on a very simple model of multi-path transmission consisting of one LOS path and one reflecting path. For a conventional DAM array system, the signal constellations received by two recipients at very-close separation angles are different but change gradually. However, by using a DAM system that can provide simultaneous, but independent, multi-directional transmission, the effects of multi-path can be exploited to augment the direction dependent properties of transmission. The result is a system which has enhanced immunity to interception and demodulation by eavesdroppers located close to the intended recipient.

6.3 Additional comments on the technique

In last section, we demonstrated a simple two-ray model including one LOS path and one reflecting path. In that simple model, the broadside recipient can receive a purposely synthesized signal constellation when space multiplexing technique was applied. But in practice, the situation could be completely different. Therefore, additional comments are given below to address the possible difficulty of using space multiplexing technique, in a dynamic multipath environment.

6.3.1 Multipath environment

In the LoS propagation environment, the signal constellation sent by DAM is direction dependent. Now considering a multipath environment, we can roughly say the DAM signal is “path dependent”. In the model shown by Fig. 6.14, the signal constellation varies with the paths between the transmitter and the receiver. We assume that there are N

propagating paths existing between Tx and Rx, and only AWGN is considered. For a traditional baseband modulation transmitter, constellation patterns (for example QPSK) transmitted through N paths may be scaled and rotated (attenuation and propagation delay), but they are still in the same pattern shape (QPSK). However, for a DAM transmitter, besides the attenuation and propagation delay, constellation patterns transmitted through N paths are in N different pattern shapes. The recipient will receive these N different signal patterns, if they all arrive in the given multipath time. The superimposition of them results in a constellation, whose shape is, statistically, always different from the original one. Therefore, the distortion to the constellation pattern caused by a dynamic multipath environment may completely change the relative distribution of symbol points on the constellation, and may damage the mapping between symbols and codebook (symbol points on the constellation may overlap).

Direction dependency is supposed to be a merit when DAM is applied to the LoS secure communications. However, it also makes the DAM hard to use in a practical dynamic multipath environment at this stage. The work presented in section 6.2 was an initial try on utilising the DAM technique under a static multipath environment. At this stage, multipath environment is still a limitation when using DAM practically.

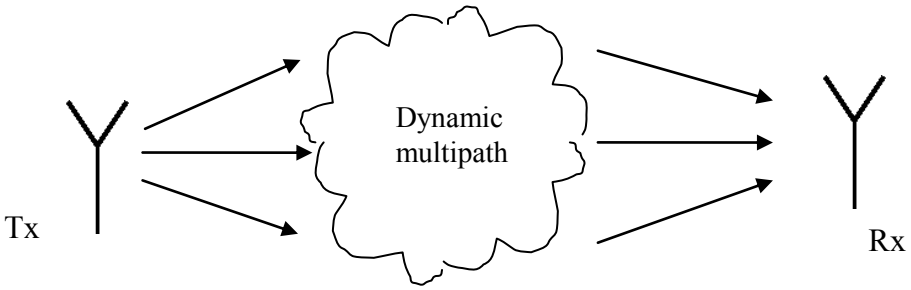

Fig. 6.14 An example communication scenario that one transmitter and one receiver communicate through a dynamic multipath environment.

6.3.2 Comparing to spatial multiplexing

Spatial Multiplexing is a transmission technique which can transmit independent data streams simultaneously over MIMO antenna configuration [61]. The space dimension is multiplexed to provide additional channel capacity [62]. In an N-Tx-M-Rx antenna configuration, the channel transfer functions between them can form an MxN matrix. The independent data streams can be achieved only when the matrix is diagonal [62]. Thus, digital signal processing (DSP) modules are necessary at both Tx and Rx antennas to diagonalise the matrix. Moreover, the propagation conditions between the various Tx-Rx antenna pairs have to be as diverse as possible to ensure that more than one independent data streams are excited. Therefore, spatial multiplexing is advantageous only when the propagation environment is dominated by multipath, in which case the LoS component is very small.

In the contrast, Space Multiplexing technique achieved by DAM is very suitable to use in the LoS propagation environment. As demonstrated in Chapter 5, space multiplexing can be used to transmit independent symbol streams to multiple receivers at different angles. There is no extra DSP module required at receiver side. The transmitter array, on the other hand, needs a strong phase and/or amplitude control unit to implement DAM. As spatial multiplexing is best to use in multipath environment, and space multiplexing requires LoS propagation channels, so these two techniques are complementary.

6.4 Summary

A combined use of the direction dependent property (common property of DAM scheme) with signal convergence property (special property in DAM transmitter with 2-bit phase

control) brings new insight to the application of DAM scheme in providing high quality physical-layer communication security. Compared to the reference one, constellations received at very-close angles away from broadside are significantly different, not only in pattern distribution but also sometimes in constellation orders. This makes demodulation extremely difficult for an eavesdropper even if it may perfectly intercept the signals.

Chapter 7

Conclusions and Future Work

7.1 Summary

This research investigated a novel digital modulation technique called Direct Antenna Modulation (DAM), and demonstrated the concept on phased arrays. DAM had been widely discussed recently and proposed by researchers as a solution for physical-layer encryption. The key attribute of the DAM is direction dependency, which means signals radiated by the transmitter vary with the transmitting angles. This turns into a merit when the technique is applied in the field of secure communications. Many hardware operations for DAM were reported, which utilised near-field mutual coupling or a Fourier Rotman lens etc. Among them, the operation on phased arrays tends to be the most accurate and efficient, but is also expensive. To keep the advantages and reduce the system cost, the phased array system demonstrated in this research uses 2-bit or other low-bit phase control. Such a system showed another important property termed “signal convergence”, which had not been noticed in previous research. With this system property, signal points regularly converge on the constellation diagram, making two different levels of constellation order exist in one system. Chapter 3 introduced a system configuration to implement DAM based on a phased array with 2-bit phase control. Both the basic system

attribute “direction dependent” and the special property “signal convergence” were presented and validated experimentally.

One important application area of DAM is in providing a reliable secure communication link in the physical-layer. Symbol error rate (SER) of the DAM system was calculated statistically as a function of transmitting angle. To adapt the changing constellations of DAM system, minimum distance decoding was employed as the decoding algorithm. Chapter 4 demonstrated different SER performances under various signal-to-noise ratios (SNR), or with the change of constellation distribution. To describe how secure the system is, a concept termed Error Rate Beamwidth (ERB) was used in Chapter 4. The system is considered safer when the ERB is narrower, because in this case the interception range with low error rate is smaller. To achieve a narrower ERB, the DAM system was configured on an array with wider element spacing and directive radiating elements. The increase of distance between array elements results in a smaller power beamwidth at the intended transmitting direction. The ERB is reduced accordingly. The purpose of using directive radiating elements is to nullify or reduce the grating lobes, so that the desired data constellation will not duplicate at un-wanted directions. The method proposed in Chapter 4 provided a general protection against the eavesdropping from angles close to the intended transmitting direction. Also a comprehensive comparison of the SERs between a DAM system and a comparable conventional system was presented. Simulation results showed a superiority of DAM in SER performance.

Another promising application area of DAM is space multiplexing. In a practical transmission scenario, it is possible that several recipients are located at different transmitting directions. The conventional multiplexing methods require these users to share the channel in frequency or time domain. But with space multiplexing, the DAM

transmitter is allowed to simultaneously transmit independent data streams towards these spatially separated recipients. In other words, space is used as an additional domain for multiplexing. When space multiplexing is applied to aforementioned scenario, the advantage is obvious that these spatial separated recipients can receive independent information simultaneously. In this sense, space multiplexing brings extra channel resource (space) and increases the channel capacity. Chapter 5 demonstrated the use of DAM to have space multiplexing in various transmission scenarios. An algorithmic method was proposed based on the special property "signal convergence". Therefore, this method is particularly suitable to be applied in the DAM system controlled by low-bit (2-bit for example) phase shifters. The prediction made by the method is exhaustive. A system designer will have a clear view of all the available options. He can either choose a suitable plan to carry out the space multiplexing, or request a system upgrade to meet the transmission requirements. This becomes a virtue of the method proposed in Chapter 5. Examples of different transmission scenarios were illustrated in Chapter 5, including different requirements on the order of constellations and number/locations of capable recipients.

The conventional DAM system introduced in Chapter 4 provided a general protection against the security threat. However, in some scenarios, the possible locations of eavesdroppers may be pre-detected. Then the DAM system may be optimised to concentrate the protections at these angles. The first transmission scheme discussed in Chapter 6 solely utilised the property "signal convergence". With this property, the system has two different levels of constellation order. A possible plan is that the higher-level constellation is transmitted to the intended recipient, but the constellation with reduced data points (low-level) is purposely sent to those pre-known eavesdropping angles. It will be considerable difficult for an eavesdropper to demodulate the correct

information by using a constellation having only half or less effective data points. In addition, the system can simultaneously defend eavesdropping from two arbitrary directions when the element spacing of the array is also free to adjust. The second scheme demonstrated in Chapter 6 jointly utilised space multiplexing and multi-path propagation channels. With this method, the distribution of constellations at some angles can be synthesised. Usually those synthesised constellations were transmitted to the intended recipients. In the meantime, constellations received at other nearby angles can be very different from the synthesised pattern, resulting in an increased difficulty of accurate demodulation.

7.2 Impact of the work

The contributions of the work to the research of DAM are listed below:

- The use of fixed low-bit phase shifters makes DAM system modelling simple and straightforward. The advantage of this methodology is: 1) it simplifies the computation so that complex optimisation methods are not necessary; and 2) the findings obtained from this basic model can be extended to high-bit level phase control if necessary. “Signal convergence” is a very useful finding due to the benefit of simplified model. This system property provides new solutions for applications of space multiplexing and multi-level constellations.
- A new algorithmic method was proposed for achieving space multiplexing. The reported method "matrix inverse" calculates excitations needed at transmitter

according to requirements from the receivers, including angles and constellation cardinality. While the new method discussed in this work operates in an inverse way. It provides an exhaustive solutions including angles and constellation cardinality for receivers, based on the existing system configuration of the transmit array. Two methods can be complementary in various transmission scenarios.

- The security contributed by DAM in physical-layer comes from the constellation distortion at non-intended directions. The conventional DAM technique ensures that the shape of baseband symbol pattern changes with transmitting angles. Now multi-level constellation discussed in this work provides a predictable reduction in the number of distinguishable signal points at some specific transmit angles. With the transmission scheme proposed in this work, a low-level constellation can be purposely oriented to two independent angles. That makes the accurate decoding even more difficult for eavesdroppers at these angles.

7.3 Future Work

Further investigations can focus on the following five aspects.

First, further effort should be made to find a hardware system with better performance and lower cost. The DAM system configured on an array with continues and lossless phase shifters, is expected to have the best system performance. But the system cost is too expensive. The uses of passive arrays (Caltech), reconfigurable arrays (UIUC), Fourier

Rotman lens (Queen's University) and 2-bit phase shifters (University of Sheffield) have much lower system cost. But they have disadvantages too. The passive arrays rely on the mutual couplings between elements. The system is hard to optimise, and has to choose useful signal points from other redundant ones. Other three methods have limited amp/phase states, which also constrains the system performance of DAM. Therefore, we aim to find a hardware system, which can be extended to provide sufficient amp/phase states without a significant increase of the system complexity.

Second, a proper method can be established to evaluate the security degree provided by DAM. The most commonly used method is calculating the error rate as a function of transmitting angles. Due to the non-standard signal pattern distribution in DAM system, the error rate is calculated statistically, which is suitable for providing a general insight. But when some special transmission schemes are applied, a better evaluation method is expected. For example, multi-level of constellations in DAM can be utilised to purposely mislead pre-known eavesdroppers. The constellation received by an eavesdropper contains only half or less distinguishing data points than the one received by the intended recipient. To evaluate how secure this transmission link is, analysis may be jointly given from both signals reception and information levels.

Third, space multiplexing is a very promising application area of DAM. There were two phase searching methods reported so far. The first method calculated the required phase combinations directly according to the transmission requirements, including order of constellation pattern, number and locations of desired recipients. This method requires an optimisation method (like a genetic algorithm) or some other sorts of matrix operation method (like Moore-Penrose pseudoinverse). The second method calculated the phase combinations strictly based on the hardware systems, including the number of array

elements, the distance between array elements and specifications of phase shifters. As an exhaustive research was carried out, this method provided a system designer a comprehensive prediction, including all the applicable transmitting directions and a complete constellation signal pattern at each prescribed direction for space multiplexing. But both methods involved either linear or exponential computational complexity. Future investigation may focuses on finding a more efficient way for phase searching.

Fourth, encoding and decoding processes are basically nothing special in DAM system. Normally, the choice of forward error correction (FEC) code in DAM is based on the same strategy that used in conventional baseband modulation system. However, it is possible that the "baseband" signal constellation modulated by DAM is in a non-standard form. As shown in Fig. 2, the constellation patterns (a) and (b) are generated by the same DAM transmitter under different phase parameters. The one shown in Fig. 7.1(a) is a standard 8-PSK, so that the Euclidean distances between them are equal. Then Gray coding may be applied to reduce the possibility that 2 or more bits of errors per symbol occur after transmission in AWGN channels under a proper SNR. We then can select any FEC code which has the ability to correct 1 bit error for channel coding. The situation is different for the constellation pattern shown in Fig. 7.1(b). Symbols "1357" and "2468" have different mutual Euclidean distances. Then the choice of FEC code depends on how many bits error will occur for symbols "2468". The strategy of choosing a suitable FEC code for such non-standard constellations will be an interesting topic for future research.

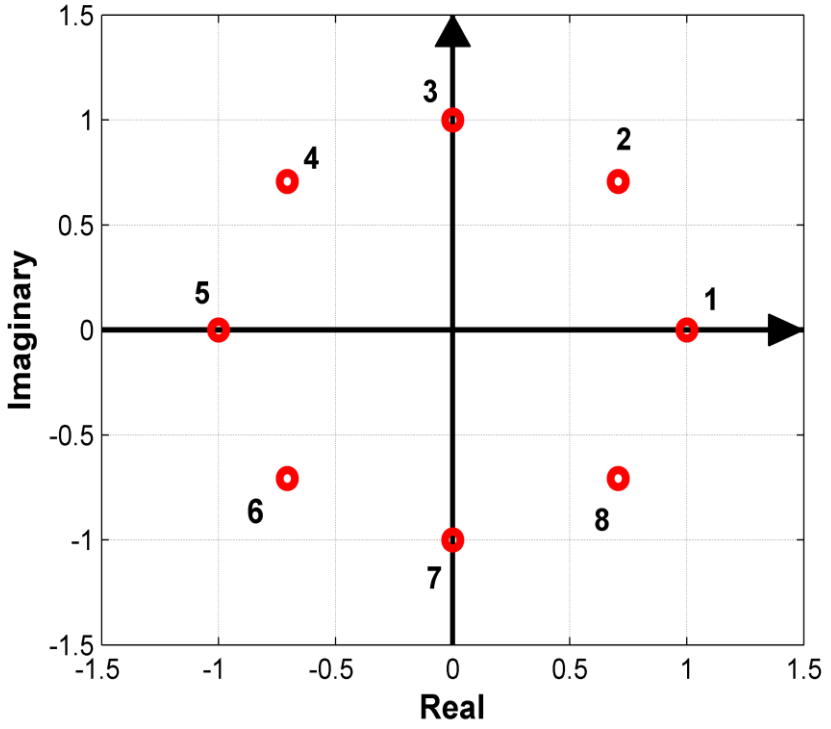

(a)

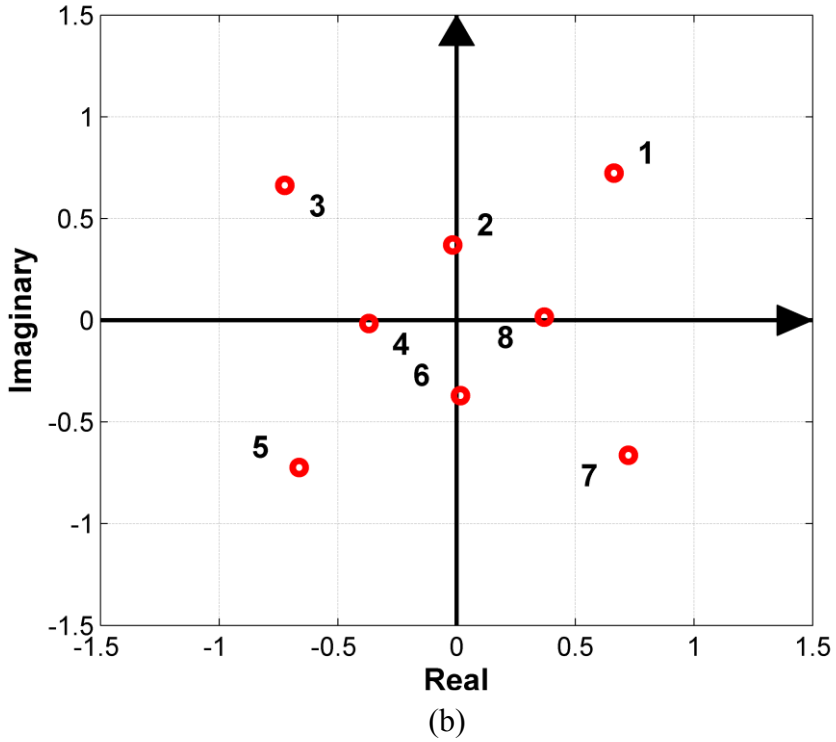

(b)

Fig. 7.1 Selected 8-points QAM modulated by a 2-element DAM array with 2-bit phase shifter when offset phase difference between antennas is set to (a) 45˚, (b) -60˚.

Fifth, a block diagram of a wireless communication system using DAM technique is illustrated in Fig. 7.2. Compared to the conventional system, the system shown in Fig. 7.2 does not have a "baseband modulation unit". Instead, a "phase shifter control unit" is suggested to modulate baseband constellation through directly changing the phase states of the transmitter array. The implementation of such a system is fairly feasible according to the block diagram, but there are a few barriers which make this technique difficult to use in the existing commercial communication system. They are listed below:

- System cost: in DAM transmission system, the cost to generate a given baseband constellation is significantly increased, compared to the conventional method. Ideally, the system needs an N-element antenna array as the transmitter, N continues phase shifters and N linear voltage control components as the control unit.
- Transmission rate: the transmission (symbol) rate is actually the switching rate of the radiation pattern, which can be physically limited by phase shifters, voltage control components and the electronics used for the switching process.
- Multipath fading: a multipath fading environment can cause a distortion to the geometric shape of baseband constellation pattern, in which case the signal pattern may not be recognised at the receiver.

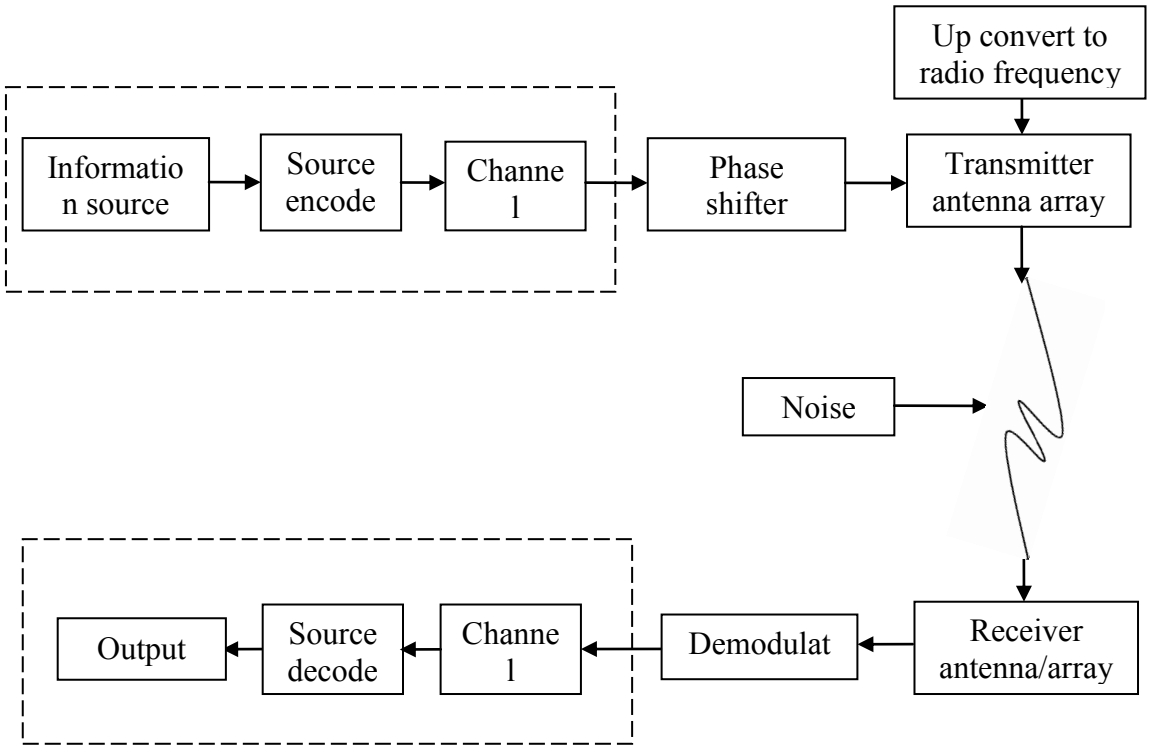

Fig. 7.2 Block diagram of a wireless communication system using DAM technique to modulate baseband signals.

Sixth, the comparison of predicted and simulated BER performance between a DAM and a conventional system were given by [18], when both systems are configured to send a QPSK to the desired receiver. Then, the analysis based on experimental results was given by [19]. Another QPSK analysis between the DAM and the conventional systems was reported in [24]. To make them comparable, the transmit power was adjusted to have exactly the same BER at the desired direction in both systems. A similar conclusion was achieved by above work that the BER curve is narrower in the DAM system than in the conventional one. The difference of BER at a given direction can be seen as the uncertainty caused by modulation techniques. Future analysis can quantify the security provided by such an uncertainty as a measurement to compare the system performance between these two modulation methods.

Seventh, a very interesting security feature provided by the DAM technique is range-dependent protection. Recalling the transmitting scheme reported in section 6.2, which is shown in Fig. 6.8(a). The desired recipient is supposed to receive the signals jointly from the LOS and reflecting paths. According to the triangle drawn in Fig. 6.8(a), only the cross position of the LOS path and reflecting path can receive the desired signal constellation pattern. In other words, the right position of the desired recipient is not only angular-dependent, but also range-dependent. This scheme may help prevent eavesdropping from an un-authorised receiver, who located at exactly the same transmitting angles as desired recipient, but closer or farther from it. Consequently, further investigation can focus on finding modulation schemes having both angular and range dependency.

REFERENCES

[1] A. Mieczakowski, T. Goldhaber and J. Clarkson, "Culture, Communication and Change: Summary of an investigation of the use and impact of modern media and technology in our lives," Engineering Design Centre, University of Cambridge, Cambridge, 2011.

[2] H. E. Shanks and R. W. Bickmore, "Four-dimentional electromagnetic radiators," *Canadian Journal of Physics*, vol. 37, no. 3, pp. 263-275, 1959.

[3] W. Kummer, A. Villeneuve, T. Fong and F. Terrio, "Ultra-low sidelobes from time-modulated arrays," *IEEE Transactions on Antennas and Propagation*, vol. 11, no. 6, pp. 633-639, 1963.

[4] B. Lewis and J. Evins, "A new technique for reducing radar response to signals entering antenna sidelobes," *IEEE Transactions on Antennas and Propagation*, vol. 31, no. 6, pp. 993-996, 1983.

[5] S. Yang, Y. B. Gan and A. Qing, "Sideband suppression in time-modulated linear arrays by the differential evolution algorithm," *IEEE Antennas and Wireless Propagation Letters*, vol. 1, no. 1, pp. 173-175, 2002.

[6] S. Yang, Y. Gan and P. Tan, "Linear antenna arrays with bidirectional phase center motion," *IEEE Transactions of Antennas and Propagation*, vol. 53, pp. 1829-1835, 2005.

[7] S. Yang, Y. B. Gan, A. Qing and P. K. Tan, "Design of a uniform amplitude time modulated linear array with optimized time sequences," *IEEE Transactions on Antennas and Propagation*, vol. 53, no. 7, pp. 2337-2339, 2005.

[8] A. Tennant and B. Chambers, "A Two-Element Time-Modulated Array With Direction-Finding Properties," *IEEE Antennas and Wireless Propagaion Letters*, vol. 6, pp. 64-65, 2007.

[9] V. Fusco and Q. Chen, "Direct-signal modulation using a silicon microstrip patch antenna," *IEEE Transactions on Antennas and Propagation*, vol. 47, no. 6, pp. 1025-1028, 1999.

[10] D. Keller, W. Palmer and W. Joines, "Electromagnetic modeling and simulation of a directly-modulated L-band microstrip patch antenna," in *2007 IEEE Antennas and Propagation Society International Symposium*, Honolulu, HI, 2007.

[11] E. J. Baghdady, "Directional signal modulation by means of switched spaced antennas," *IEEE Transactions on Communications*, vol. 38, no. 4, pp. 399-403, 1990.

[12] C. M. Elam and D. A. Leavy, "Secure communication using array transmitter". United States Patent US 6275679 B1, 14 Aug. 2001.

[13] A. Babakhani, D. Rutledge and A. Hajimiri, "Transmitter Architectures Based on Near-Field Direct Antenna Modulation," *IEEE Journal of Solid-State Circuits*, vol. 43, no. 12, pp. 2674-2692, 2008.

[14] A. Babakhani, D. Rutledge and A. Hajimiri, "Near-field direct antenna modulation," *IEEE Microwave Magazine*, vol. 10, no. 1, pp. 36-46, 2009.

[15] A. Chang, A. Babakhani and A. Hajimiri, "Near-Field Direct Antenna Modulation (NFDAM) transmitter at 2.4GHz," in *IEEE APSURSI '09*, Charleston, 2009.

[16] J. Lavaei, A. Babakhani, A. Hajimiri and J. Doyle, "A study of near-field direct antenna modulation systems using convex optimization," in *2010 American Control Conference (ACC)*, Baltimore, 2010.

[17] J. Lavaei, A. Babakhani, A. Hajimiri and J. Doyle, "Programmable antenna design using convex optimization," in *19th International Symposium on Mathematical Theory of Networks and Systems*, Budapest, 2010.

[18] M. Daly and J. Bernhard, "Directional Modulation Technique for Phased arrays," *IEEE Transactions on Antennas and Propagation*, vol. 57, no. 9, pp. 2633-2640, 2009.

[19] M. Daly, E. Daly and J. Bernhard, "Demonstration of Directional Modulation Using a Phased Array," *IEEE Transactions on Antennas and Propagation*, vol. 58, no. 5, pp. 1545-1550, 2010.

[20] M. Daly and J. Bernhard, "Beamsteering in Pattern Reconfigurable Arrays Using Directional Modulation," *IEEE Transactions on Antennas and Propagation*, vol. 58, no. 7, pp. 2259-2265, 2010.

[21] M. Daly and J. Bernhard, "Directional modulation and coding in arrays," in *2011 IEEE International Symposium on Antennas and Propagation (APSURSI)*, Spokane, WA, 2011.

[22] T. Hong, M.-Z. Song and Y. Liu, "RF directional modulation technique using a switched antenna array for physical layer secure communication applications," Progress *In Electromagnetics Research*, vol. 116, pp. 363-379, 2011.

[23] T. Hong, M.-Z. Song and Y. Liu, "Directional sensitive modulation signal transmitted by monopulse cassegrain antenna for physical layer secure communication," Progress *In Electromagnetics Research*, vol. 17, pp. 167-181, 2011.

[24] T. Hong, M.-Z. Song and Y. Liu, "Dual-Beam Directional Modulation Technique for Physical-Layer Secure Communication," *IEEE Antennas and Wireless Propagation Letters*, vol. 10, pp. 1417-1420, 2011.

[25] O. Malyuskin and V. Fusco, "Spatial Data Encryption Using Phase Conjugating Lenses," *IEEE Transactions on Antennas and Propagation*, vol. 60, no. 6, pp. 2913-2920, 2012.

[26] Y. Zhang, Y. Ding and V. Fusco, "Sidelobe Modulation Scambling Transmitter using Fourier Rotman Lens," *IEEE Transactions on Antennas and Propagation*, 2013.

[27] H. Shi and A. Tennant, "Direction dependent antenna modulation using a two element array," in *European Conference on Antennas and Propagation (EUCAP)*, Rome, Italy, 2011.

[28] H. Shi and A. Tennant, "Characteristics of a two element direction dependent antenna array," in *Loughborough Antennas and Propagation Conference (LAPC)*, Loughborough, UK, 2011.

[29] H. Shi and A. Tennant, "An experimental two element array configured for directional antenna modulation," in *European Conference on Antennas and Propagation (EUCAP)*, Prague, Czech, 2012.

[30] E. A. Jorswieck, A. Wolf and S. Gerbracht, "Secrecy on the physical layer in wireless networks," in *Trends in Telecommunications Technologies*, InTech, 2010, pp. 413-435.

[31] C. E. Shannon, “Communication theory of secrecy systems,” *Bell Sys. Tech. Journ.*, vol. 28, no. 4, pp. 656-715, 1949.

[32] W. Diffie and M. E. Hellman, “New directions in cryptography,” *IEEE Transactions on Information Theory*, vol. 22, no. 6, pp. 644-654, 1976.

[33] R. L. Rivest, A. Shamir and L. Adleman, “A method for obtaining digital signatures and public-key cryptosystems,” *Communications of the ACM*, vol. 21, no. 2, pp. 120-126, 1978.

[34] D. Moore, G.M. Voelker and S. Savage, “Quantitative Network Security Analysis,” *Cooperative Association for Internet Data Analysis (CAIDA)*, NSF-01-160, 2002.

[35] M. Jouini, A. B. Aissa, L. B. A. Rabai and A. Mili, “Towards quantitative measures of information security: A cloud computing case study,” *International Journal of Cyber-Security and Digital Forensics (IJCSDF)*, vol. 1, no. 3, pp. 248-262, 2012.

[36] A. D. Wyner, “The wie-tap channel,” *Bell Sys. Tech. Journ.*, vol. 54, pp. 1355-1387, 1975.

[37] I. Csiszar and J. Korner, “Broadcast channels with confidential messages," *IEEE Trans. Inf. Theory*, vol. 24, no. 3, pp. 339-348, May 1978.

[38] J. Barros and M. R. D. Rodrigues, “Secrecy Capacity of Wireless Channels," in *2006 IEEE Int. Sym. On Inf. Theory*, pp. 356-360, July 2006.

[39] P. K. Gopala, Lifeng Lai and H. E. Gamal, “On the Secrecy Capacity of Fading Channels," *IEEE Trans. Inf. Theory*, vol. 54, no. 10, pp. 4687-4698, Oct. 2008.

[40] Z. Li, R. Yates and W. Trappe, “Secret Communication with a Fading Eavesdropper Channel,” in *IEEE Int. Symp. Inf. Theory*, Nice, 2007.

[41] R. Negi and S. Goel, "Secret communication using artificial noise," in *IEEE Vehicular Tech. Conf.*, 2005.

[42] O. Alrabadi and G. Pedersen, "Directional space-time modulation: A novel approach for secured wireless communication," in *IEEE International Conference on Communications*, Ottawa, ON, 2012.

[43] A. Khisti and G. W. Wornell, "Secure Transmission With Multiple Antennas I: The MISOME Wiretap Channel," *IEEE Transactions on Information Theory*, vol. 56, no. 7, pp. 3088-3104, 2010.

[44] A. Khisti and G. W. Wornell, "Secure Transmission With Multiple Antennas—Part II: The MIMOME Wiretap Channel," *IEEE Transactions on Information Theory*, vol. 56, no. 11, pp. 5515-5532, 2010.

[45] R. J. Mceliece, "A public-key cryptosystem based on algebraic coding theory," *Jet Propulsion Lab Deep Space Network Progress report*, Tech. Rep., 1978.

[46] C. S. Park, "Improving code rate of McElieces public-key cryptosystem*," Electronics Letters*, vol. 25, no. 21, pp. 1466–1467, 1989.

[47] P. Gaborit, "Shorter keys for code based cryptography," in WCC 2005, Oyvind Ytrehus, Springer, Lecture Notes Computer Science, volume 3969, 2005, pp. 81–90.

[48] A. Payandeh, "Adaptive secure channel coding based on punctured turbo codes," *IEE Proceedings - Communications*, vol. 153, pp. 313–316(3), April 2006.

[49] A. Nerri, D. Blasi, L. Gizzi, and P. Campisi, "Joint security and channel coding for OFDM communications," *in EUSIPCO 2008*, Aug. 2008.

[50] A. A. Sobhi Afshar, T. Eghlidos, and M. R. Aref, "Efficient secure channel coding based on quasi-cyclic low-density parity-check codes," *Communications, IET*, vol. 3, no. 2, pp. 279–292, 2009.

[51] M. Baldi, M. Bianchi, and F. Chiaraluce, "Security and complexity of the McEliece cryptosystem based on quasi-cyclic low-density parity-check codes," *IET Information Security*, vol. 7, no. 3, pp. 212-220, 2013.

[52] E. Arikan, "Channel Polarization: A Method for Constructing Capacity-Achieving Codes for Symmetric Binary-Input Memoryless Channels," *IEEE Trans on Information Theory*, vol. 55, no. 7, pp. 3051–3037, 2009

[53] D. M. Abbasi and V. T. Vakily, "Enhanced secure error correction code schemes in time reversal UWB systems," *Spring Wireless Personal Communication*, vol. 64, no. 2, pp. 403-423, 2012.

[54] H. Shi and A. Tennant, "Secure physical-layer communication based on directly modulated antenna arrays," in *Loughborough Antennas and Propagation Conference (LAPC)*, Loughborough, 2012.

[55] H. Shi and A. Tennant, "Enhancing the security of communication via directly modulated antenna arrays," *IET Microwaves, Antennas & Propagation*, vol. 7, no. 8, pp. 606-611, 2013.

[56] H. Shi and A. Tennant, "Covert communication using a directly modulated array transmitter," in *European Conference on Antennas and Propagation (EUCAP)*, Hague, Netherlands, 2014.

[57] H. Shi and A. Tennant, "Secure communications based on directly modulated antenna arrays combined with multi-path," in *Loughborough Antennas and Propagation Conference (LAPC)*, Loughborough, 2013.

[58] J. G. Proakis, Digital communictions, New York: McGraw-Hill, 1995.

[59] G. J. Foschini, "Layered space-time architecture for wireless communication in a fading environment when using multi-element antennas," *Bell Labs Tech. Journ.*, vol. 1, no. 2, pp. 41-59, 1996.

[60] J. Winters, "On the Capacity of Radio Communication Systems with Diversity in a Rayleigh Fading Environment," *IEEE Journal on Selected Areas in Communications*, vol. 5, no. 5, pp. 871-878, 1987.

[61] D. Gesbert, M. Shafi, S. Da-shan and P. Smith, "From theory to practice: an overview of MIMO space-time coded wireless systems," *IEEE Journal on Selected Areas in Communications*, vol. 21, no. 3, pp. 281-302, 2003.

[62] F. P. Fontan and P. M. Espieira, Modelling the Wireless Propagation Channel: A simulation approach with Matlab, Vigo, Spain: Wiley Publishing, 2008.

[63] H. Shi and A. Tennant, "Simultaneous, Multichannel, Spatially Directive Data Transmission Using Direct Antenna Modulation," *IEEE Transactions on Antennas and Propagation,* vol. 62, no. 1, pp. 403-410, 2014.

[64] C. Balanis, Antenna Theory: analysis and design, 3rd ed., New Jersey: John Wiley & Sons, Inc, 2005.

[65] H. Visser, Array and Phased Array Antenna Basics, Chichester: John Wiley & Sons Ltd, 2005.

[66] B. Mobasseri, "Digital modulation classification using constellation shape," *Signal Processing,* vol. 80, no. 2, pp. 251-277, 2000.

[67] J. Lopatka and M. Pedzisz, "Automatic modulation classification using statistical moments and a fuzzy classifier," in *WCCC-ICSP 2000*, Beijing, 2000.

[68] A. Nandi and E. Azzouz, "Algorithms for automatic modulation recognition of communication signals," *IEEE Transactions on Communications,* vol. 46, no. 4, pp. 431-436, 1998.

[69] S. Haykin, Communication Systems, 2nd ed., New York: John Wiley & Sons, 1983.

[70] NSI-800F-10 User's Guide, Nearfield System Inc.

[71] Agilent E5071C ENA Network Analyzers Service Guide, Sixth Edition, Agilent Technologies.

[72] A. GoldSmith, Wireless Communications, 1st ed, New York, NY: Cambridge Univ. Press, 2005.

[73] J. G. Proakis and M Salehi, Digital communictions, 5th ed, New York: McGraw-Hill, 2008.

[74] G. M. Rebeiz, G. Tan and J. S. Hayden, "RF MEMS phase shifters: Design and applications," *IEEE Microw. Mag.*, vol. 3, no. 2, pp. 72-81, 2002.